AD-A277 152

ESL-TR-91-30

FROUDE SCALING OF BURIED STRUCTURES USING COAL AND COAL/LEAS AS SIMULANTS FOR SAND - VOLUME I OF II - STUDY RESULTS

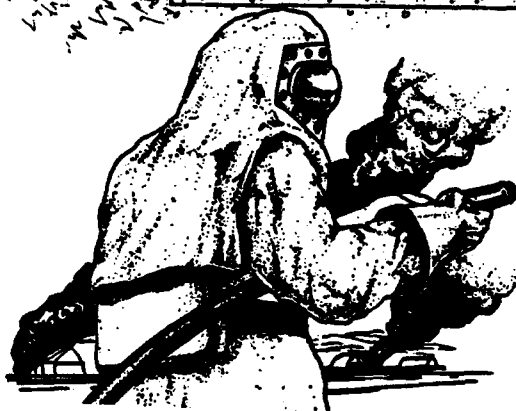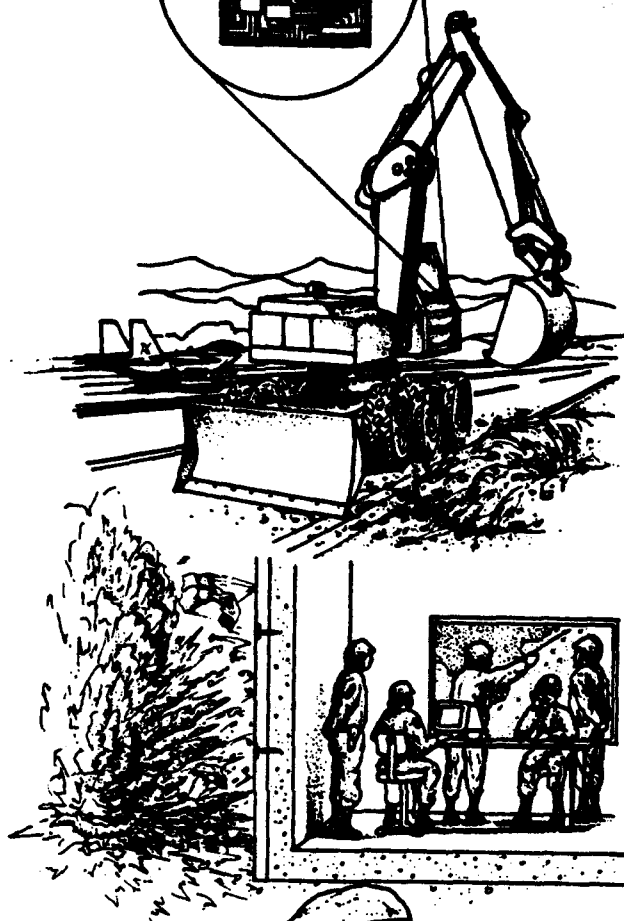**M.A. PLAMONDON, D.E. CHITTY**
R.L. GUICE

APPLIED RESEARCH ASSOCIATES, INC.
4300 SAN MATEO BLVD, N.E.,
SUITE A220
ALBUQUERQUE NM 87110

JUNE 1993

FINAL REPORT

AUGUST 1989 - MARCH 1991

DTIC
SELECTE
MAR 17, 1994
S B D

94-08531

NOTICE

PLEASE DO NOT REQUEST COPIES OF THIS REPORT FROM HQ AFCESA/RA (AIR FORCE CIVIL ENGINEERING SUPPORT AGENCY). ADDITIONAL COPIES MAY BE PURCHASED FROM:

> NATIONAL TECHNICAL INFORMATION SERVICE
> 5285 PORT ROYAL ROAD
> SPRINGFIELD, VIRGINIA 22161

FEDERAL GOVERNMENT AGENCIES AND THEIR CONTRACTORS REGISTERED WITH DEFENSE TECHNICAL INFORMATION CENTER SHOULD DIRECT REQUESTS FOR COPIES OF THIS REPORT TO:

> DEFENSE TECHNICAL INFORMATION CENTER
> CAMERON STATION
> ALEXANDRIA, VIRGINIA 22314

REPORT DOCUMENTATION PAGE

Public reporting burden for this collection of information is estimated to average 1 hour per response, including the time for reviewing instructions, searching existing data sources, gathering and maintaining the data needed, and completing and reviewing the collection of information. Send comments regarding this burden estimate or any other aspect of this collection of information, including suggestions for reducing this burden, to Washington Headquarters Services Directorate for Information Operations and Reports, 1215 Jefferson Davis Highway, Suite 1204, Arlington, VA 22202-4302, and to the Office of Management and Budget, Paperwork Reduction Project (0704-0188), Washington, DC 20503.

1. AGENCY USE ONLY (Leave blank)	2. REPORT DATE June 1993	3. REPORT TYPE AND DATES COVERED Technical 890815 to 910331

4. TITLE AND SUBTITLE

Froude Scaling of Buried Structures Using Coal and Coal/ Leas as Simulants for Sand
Volume I of II, Study Results

5. FUNDING NUMBERS

6. AUTHOR(S)

Maynard A. Plamondon, Daniel E. Chitty, Robert L. Guice.

7. PERFORMING ORGANIZATION NAME(S) AND ADDRESS(ES)

Applied Research Associates, Inc.
4300 San Mateo Blvd. N.E., Suite A220
Albuquerque, NM 87110

8. PERFORMING ORGANIZATION REPORT NUMBER

ARA - 5582

9. SPONSORING/MONITORING AGENCY NAME(S) AND ADDRESS(ES)

Air Force Civil Engineering Support Agency
HQ AFCESA/RACS
Tyndall AFB, FL 32403-6001

10. SPONSORING/MONITORING AGENCY REPORT NUMBER

ESL-TR-91-30

11. SUPPLEMENTARY NOTES

12a. DISTRIBUTION/AVAILABILITY STATEMENT

Approved for public release.
Distribution unlimited.

12b. DISTRIBUTION CODE

13. ABSTRACT (Maximum 200 words)

This technical report is divided into two volumes. Volume I presents the results of the study, while Volume II contains the Appendices. This study describes the development of the Froude scaling relationships between the various parameters for the general problems of both dynamic and static loadings. The results of laboratory tests on potential simulant materials are presented. The rationale for the selection of crushed coal and a mixture of crushed coal and lead shot as simulants for sand is presented and the results of a crushed coal/cement/water mix as a simulant for concrete.

Results of proof-of-principle static tests of cone penetrometers being pushed into sand and the crushed coal and crushed coal/lead shot simulants are presented. Stress at the tip of the penetrator as a function of depth is presented for the full scale test in sand, the approximate 1/5 scale test in coal, and the approximate 1/10 scale test in the coal/lead mixture.

(Continued on back of page)

14. SUBJECT TERMS

Gravity Effects, Simulant Materials, Scaling Methods, Shallow Buried Structures, Froude Scaling

15. NUMBER OF PAGES

16. PRICE CODE

17. SECURITY CLASSIFICATION OF REPORT	18. SECURITY CLASSIFICATION OF THIS PAGE	19. SECURITY CLASSIFICATION OF ABSTRACT	20. LIMITATION OF ABSTRACT
UNCLASSIFIED	UNCLASSIFIED	UNCLASSIFIED	Same As Report

EXECUTIVE SUMMARY

The response of buried structures to the explosive affects of conventional weapons is often determined by testing scale models instead of actual full size structures. The size and material properties of the scale model structures are determined based upon scaling laws. Most scale models are based upon the Replica scaling law that reduces the linear dimensions of the structure while maintaining the same material properties. This scaling law works well when the distortions resulting the non-scaled acceleration of gravity is not important. This report presents the results of scale models that use the Froude scaling law that reduces the linear dimensions of the structure and changes the material properties to avoid distortions resulting from the use of a constant acceleration of gravity. The results indicate that using coal or a mixture of coal and lead as a simulant for sand can result in model tests that properly replicate the full-scale test conditions.

(The reverse of this page is blank)

PREFACE

This technical report has been reviewed by the Public Affairs Office (PA) and is releasable to the National Technical Information Service, where it will be available to the general public, including foreign nationals.

This technical report has been reviewed and is approved for publication.

RICHARD A. REID, Capt, USAF
Project Officer

WILLIAM S. STRICKLAND, GM-14
Chief, Engineering Research
 Division

JON B. ANDERSON
Chief, Air Base Survivability
 Branch

TABLE OF CONTENTS

TABLE OF CONTENTS
(CONCLUDED)

LIST OF FIGURES

LIST OF FIGURES
(CONTINUED)

LIST OF FIGURES
(CONTINUED)

LIST OF FIGURES
(CONCLUDED)

LIST OF TABLES

LIST OF TABLES
(CONCLUDED)

SECTION I
INTRODUCTION

A. OBJECTIVES

The objective of this study is to determine how well materials respond in selected static and dynamic tests, selected to simulate soil and concrete based upon Froude scaling requirements. Materials selected will have standard laboratory tests performed to determine stiffness, strength and density relationships. These materials will then be used in Froude-scaled static cone penetration tests to determine the adequacy of the material from static test results. The same materials will be used in Froude-scaled dynamic buried explosive tests on buried cylinders to determine the adequacy of the techniques for dynamic tests.

B. BACKGROUND

Both analytical and experimental studies are performed to determine the effects of conventional weapons on protective structures. Tests are normally performed on a few full-scale structures. However, small-scale structures are more frequently used because of cost and environmental issues. The use of small-scale structures sometimes makes it necessary to interpret the small-scale test results in light of the model distortions to the full-scale system response. One distortion normally present in Replica-scaled testing is the acceleration due to gravity. The force of gravity induces static stresses in buried structures and an increase of both the static stress and the shear strength of granular soils with increasing depth. One method to overcome this distortion is to conduct the scale test in a centrifuge whereby the appropriately scaled acceleration can be simulated. A second method for correcting the distortion is to accept the existing acceleration of gravity and to adjust the material properties as required by Froude scaling. In this method of scaling, the values of the stress/stiffness/strength scale factor (K_σ), and the density scale factor (K_ρ) are related to the length scale factor (K_l) by the relationship $K_l = K_\sigma/K_\rho$ (Reference 1).

Reference 1 presents the results of a Phase I SBIR study performed by ARA. This study included a survey of potential candidates for soil and concrete simulants. Pumice, perlite, vermiculite and Q-cell of the P-Q Corporation were recommended for investigation in more detail as simulants for sand. For concrete, a mixture of plaster, celite, sand and water was considered the most promising candidate, with

perlite concrete, and vermiculite concrete as potential simulants. It was also recommended that both simple static and dynamic small-scale experiments be performed.

The study outlined laboratory tests required to fully characterize the mechanical properties of the proposed simulants. A small-scale proof-of-principle test that was simple and inexpensive and which would demonstrate the importance of gravity effects was identified. A static experiment on piles was deemed to satisfy all the requirements. It was also recommended that small-scale dynamic experiments using explosive loadings on buried arches at three different scales be conducted and correlated with full-scale tests, if available. The anticipated low cost of each test would allow several experiments to be conducted at each scale to investigate the response at different load levels and/or structural configurations. If successful, this method could serve as the basis for a comprehensive study of the response of buried structures subjected to conventional weapon effects and the development of design criteria for these structures.

A literature seuuch on Froude scaling through the Defense Technical Information Center (DTIC) failed to identify any new work in this area since the Phase I study.

C. SCOPE AND SUMMARY OF RESULTS

The study reported in this document briefly describes the development of the Froude scaling relationships between the various parameters for the general problems of both dynamic and static loadings. The results of laboratory tests on potential simulant materials are presented. The rationale for the selection of crushed coal and a mixture of crushed coal and lead shot as simulants for sand is presented, as well as the results of a crushed coal/cement/water mix as a simulant for concrete.

Results of static Proof-of-Principle tests consisting of cone penetrometers pushed into sand and sand simulants are presented. Plots of the nondimensional stress at the tip of the penetrator as a function of nondimensional depth are presented for the full scale test in sand, the approximate 1/5 scale test in coal, and the approximate 1/10 scale test in the coal/lead mixture. A comparison of the results shows reasonable agreement.

Results of three tests involving a buried explosive loading on a buried cylinder are also presented. A 1/10 Replica-scaled reinforced concrete cylinder buried in sand was subjected to the explosive effects of a 0.39 kilogram sphere of C-4 explosive buried 0.6 meters from the edge of the cylinder. Measurements were made of the free-field acceleration and earth stresses at various ranges from the explosive charge as well as structure acceleration. A 1/5 scale test using crushed coal as the sand

2

simulant with a 0.31 kilogram C-4 charge as the explosive located 1.2 meters away from a reinforced concrete cylinder with the thickness adjusted to account for mass and stiffness effects was also tested and similar measurements made. A third test involving a test bed of a coal/lead mixture, at a scale of 1/10, using a 0.039 kilogram C-4 charge located 0.6 meters from a geometrically and mass (but not stiffness) scaled reinforced concrete cylinder was conducted.

The results scaled to nondimensional parameters demonstrate that the one Replica-scaled test and the two Froude-scaled tests appear similar when the results are nondimensionalized with the possible exception of stress attenuation with range. The two Froude-scaled tests are very similar, however, the Replica-scaled test provides a much lower result for the scaled stress at a given scaled range. If this difference can be shown to be statistically significant, this may indicate why small Replica-scaled buried structures appear to be stronger when tested than the prototype full-scale structure since the applied stress is smaller.

The results of this study are very encouraging as to the use of coal and a coal/lead mixture as simulants for sand. More studies need to be performed to develop the concrete simulant. However, it appears that mixing cement and water with the sand simulants has promise. It is believed that adjustments to actual steel/aluminum wire sizes/spacings can be made to model the steel reinforcement. Simulants for clay and rock should also be investigated. Recommendations for additional static and dynamic tests are also made.

SECTION II
SCALING LAWS

A. THEORY

The determination of the response of any protective structure to a conventional weapon detonation can be simplified to the solution of a differential equation of the type indicated by Equation (1) and Figure 1 (Reference 1).

$$\frac{\partial \sigma}{\partial x} = \rho \frac{\partial^2 u}{\partial t^2} + c_1 \rho g \tag{1}$$

In this equation, σ is the stress resulting from applied pressures or stresses at certain boundaries or the stresses arising from stiffness, strength, viscosity, or surface tensile properties of the medium in which the disturbance propagates, x is distance along the medium of interest, ρ is the density of the medium, u is the displacement of a point in the medium defined by the distance x, t is time, and g is the effective acceleration of gravity. The nondimensional constant c_1 relates the direction x to the direction of the acceleration gravity (g). In general, the solution to Equation (1) is obtained through the use of finite elements that account for the three-dimensional nature of the disturbance and the changes in the stiffness and mass density of the various materials involved. Typically, these materials are air, earth materials such as rock, sand, clay, water and entrapped air, and structural materials such as concrete and steel.

Normally, finite-element calculations are performed to predict the behavior of the medium and the structure to the weapon effects. Similarly, experiments are conducted and measurements made of the structure and media response. Comparisons of the predictions to the experimental results are made and attempts are made to identify the source of any differences. Differences are frequently attributed to uncertainties in the stiffness and strength relationship for both the earth media and the structural materials.

However, a definite explanation for the differences in calculated and observed behavior cannot always be made. The problem may actually be so three-dimensional that the current state of the art in computing resolution available is inadequate from a storage and run-time perspective. Thus, considerable reliance is placed upon the results obtained from experimental programs. However, the testing of actual full-scale structures to various weapon effects is a very expensive and time consuming

4

Soil Properties
ρ, M, η, ν, ϕ

Buried Cylinder

Explosive Location
W
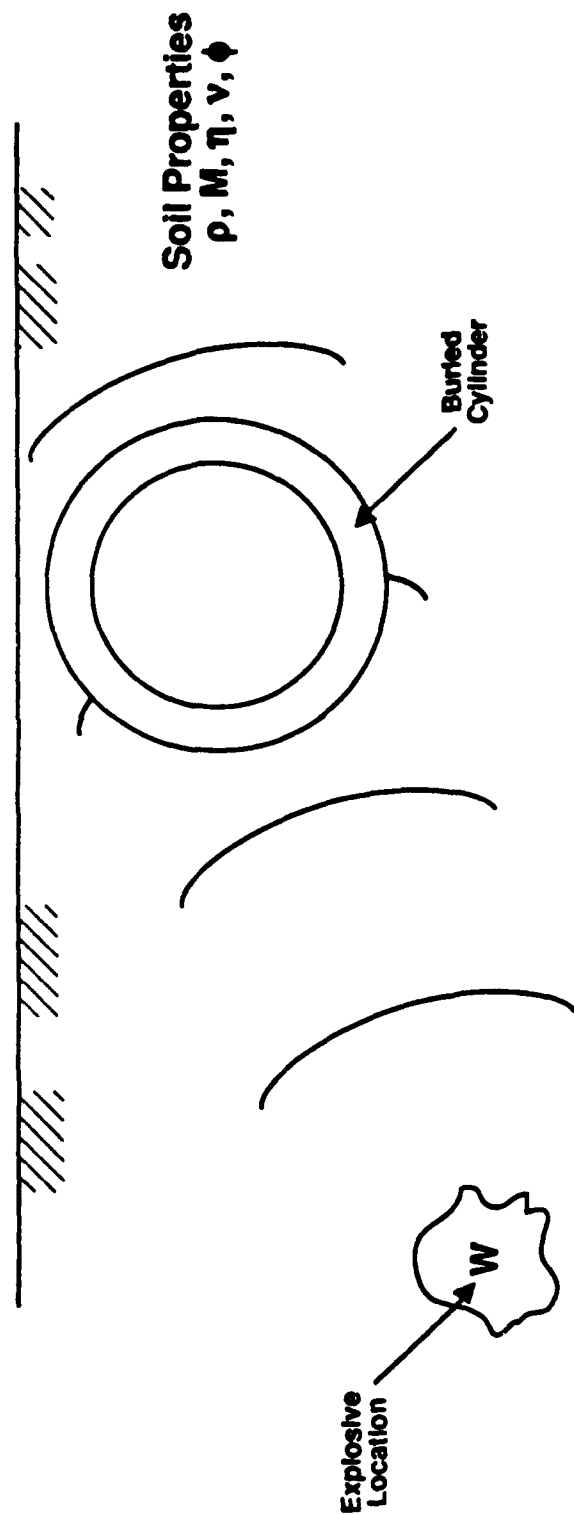
GENERAL FORM OF GOVERNING EQUATION TO DETERMINE RESPONSE:

$$\frac{\partial \sigma}{\partial X} = \rho \frac{\partial^2 u}{\partial t^2} + C_1 \rho g$$

OR IN TERMS OF SCALED PARAMETERS:

$$\frac{\partial \sigma}{\partial X} = \left[\frac{K_p K_l^2}{K_\sigma K_t^2}\right] \rho \frac{\partial^2 u}{\partial t^2} + \left[\frac{K_p K_g K_l}{K_\sigma}\right] C_1 \rho g$$

See text for definition of symbols

Figure 1. Determination of Response of Buried Structures to Conventional Weapon Effects.

5

process. To lessen the time and expenses necessary to obtain experimental data, scale models of the structural system are often used.

The use of smaller than actual size structures can result in a different behavior for the model than for the prototype if proper scaling is not used. In order to identify how the model parameters should vary with respect to the prototype values, scale factors for all the relevant parameters can be defined and inserted into Equation (1), resulting in the following expression for the model response where K_{sub} is the ratio of the value of the model value of sub to the prototype value of sub:

$$\frac{K_\sigma}{K_l}\frac{\partial \sigma}{\partial x} = K_\rho \rho \frac{K_l}{K_t^2}\frac{\partial^2 u}{\partial t^2} + c_1 K_\rho \rho K_g g \tag{2}$$

or rearranging terms:

$$\frac{\partial \sigma}{\partial x} = \frac{K_\rho K_l^2}{K_\sigma K_t^2}\rho\frac{\partial^2 u}{\partial t^2} + \frac{K_\rho K_g K_l}{K_\sigma}c_1 \rho g \tag{3}$$

If the scale factors are chosen so that:

$$\frac{K_\rho K_l^2}{K_\sigma K_t^2} = 1 \tag{4}$$

and

$$\frac{K_\rho K_g K_l}{K_\sigma} = 1 \tag{5}$$

it is apparent that Equation (1) and Equation (3) will be identical and the computed response will be identical for the model and the prototype.

Froude scaling accepts the fact that the gravity scale factor (K_g) will be equal to one. Therefore, Equation (5) may be rewritten as:

$$K_\rho K_l = K_\sigma \tag{6}$$

6

or

$$K_I = \frac{K_\sigma}{K_\rho}$$ (6a)

Similarly, inserting the above relationship into Equation (4) leads to:

$$K_I = K_t^2$$ (7)

Thus, Froude scaling relationships define the relationships between the length scale factor K_I, the time scale factor K_t, the stress (stiffness/pressure/strength) scale factor K_σ and the density scale factor K_ρ.

The scale factor for energy can be shown to be (Reference 1):

$$K_E = K_\sigma K_I^3$$ (8)

or

$$K_E = K_\rho K_I^4$$ (9)

B.   APPLICATION TO THIS STUDY

To investigate the applicability of Froude scaling to the response of buried structures, a full scale experiment indicated by Figure 1 was visualized. Investigations discussed in Section III identified that the use of coal as a simulant for sand resulted in a K_σ of about 1/10 and a K_ρ of about 1/2. Use of coal as a simulant would result in a K_I of 1/5 and a K_t of $1/\sqrt{5}$ from Equations (6) and (7).

It was also found that the addition of lead particles to the coal would not appreciably change K_σ but could raise K_ρ to a value of about 1. Use of the coal/lead mixture as a simulant results in a K_I of 1/10 and a K_t of $1/\sqrt{10}$. These two materials were therefore chosen for use in the test program as simulants for sand based upon the matching of stiffness characteristics as well as the fact that the nominal angles of

internal friction for the sand and the simulants were approximately equal. This would result in both the stiffness and strength properties scaling properly.

Because of the limited scope of the current contract, it was not possible to fully develop simulant materials for the concrete. The objective was therefore restricted to investigating the free-field response and the rigid body response of the cylindrical structure. Exact Froude scaling requires that the scale factors for the structure properties be the same as for the soil simulant. It was determined that use of a model structure that had the correct external length scale and effective density scale factors would provide the desired check on the applicability of Froude scaling for rigid body response. The effect of not matching the scale factor for the stiffness of the structure was felt to affect only the local flexural and hoop response of the structure. It was expected that the structures would behave elastically so that the strength scale factor for the structural material would not be an issue.

To demonstrate how well Replica scaling would apply for the case under consideration when K_g, the scale factor for gravity, was not appropriately scaled as would be required from Equation (5), a 1/10 length scale K_l Replica-scaled test was also been included in the test program. Using the same materials as would be used in the prototype, the scale factors for stress K_σ and density K_ρ are 1. From Equation (4), the time scale factor K_t can be determined to be equal to the length scale factor K_l.

The main objective of the test program was to obtain motion and stress-time histories in the free-field and the velocity-time history for the structure in two mutually perpendicular directions in two tests that use appropriate Froude scaling and one test where Replica scaling is used but with the exception of scaling gravity. By using appropriate scale factors, scaling the time histories from the two Froude-scaled experiments should lead to the same prediction of a full-scale event while scaling the Replica-scaled event should result in a predicted time history for the full-scale event that would be noticeably different. If good correlation was obtained for these Froude-scaled tests, future testing, with both the structural material properties and earth properties being are simulated, will be considered. Flexible response as well as rigid body response will then be properly scaled. Failure mechanisms for the structure could also be investigated.

8

C. SUMMARY OF IMPORTANT VARIABLES

The important variables affecting the behavior of the cone penetrometer and shallow buried structures are shown with their scale factors and dimensions in Table 1. The scale factor for a variable is defined as the ratio of its model to prototype values. For example, the scale factor for length, K_l, is given by l_m/l_p where the subscripts m and p refer to model and prototype, respectively.

TABLE 1. IMPORTANT VARIABLES WITH THEIR SCALE FACTORS AND DIMENSIONS.

Variable	Scale Factor * K sub	Dimensions
length	l	L
mass density	ρ	ML^{-3}
acceleration	a	LT^{-2}
time	t	T
stress	σ	$ML^{-1}T^{-2}$
strain, porosity, void ratio	ε	-
Poisson's ratio	υ	-
friction angle	Φ	-
velocity	v	LT^{-1}
force	f	MLT^{-2}
unit weight	γ	$ML^{-2}T^{-2}$
impulse	i	$ML^{-1}T^{-1}$
energy	E	$ML^{2}T^{-2}$

*The scale factors for all the variables from Table 1 are summarized in Table 2.

TABLE 2. FROUDE SCALING FACTORS

Variable	Scale Factor K_{sub}	Froude Scale Factor	Replica Scale Factor
length	l	l	l
mass density	ρ	ρ	$\rho = 1$
acceleration	a	$a = 1$	$a = 1/l$
time	$t = \sqrt{\dfrac{l}{a}}$	$t = \sqrt{l}$	$t = l$
stress	$\sigma = \rho a l$	$\sigma = \rho l$	$\sigma = 1$
strain, porosity, void ratio	ε	$\varepsilon = 1$	$\varepsilon = 1$
Poisson's ratio	υ	$\upsilon = 1$	$\upsilon = 1$
friction angle	Φ	$\Phi = 1$	$\Phi = 1$
velocity	$v = \sqrt{al}$	$v = \sqrt{l}$	$v = 1$
force	$f = \rho a l^3$	$f = \rho l^3$	$f = l^2$
unit weight	$\gamma = \rho a$	$\gamma = \rho$	$\gamma = 1/l$
impulse	$i = \rho \sqrt{al^3}$	$i = \rho \sqrt{l^3}$	$i = l$
energy	$E = \rho a l^4$	$E = \rho l^4$	$E = l^3$

D. SUMMARY OF SPECIFIC NONDIMENSIONAL VARIABLES USED IN THIS STUDY

1. Static Tests

For the cone penetration tests, let the diameter of the tip be designated as B, and note that the actual variables measured are the stress at the tip of the penetrometer (σ) and the depth of penetration (D). The significant material property parameters are the initial constrained modulus (M), density (ρ), and initial porosity (η), Poisson's ratio (υ), and angle of internal friction (Φ). The acceleration

of gravity is also an important parameter. Combining the above parameters and ensuring that both the stiffness and density properties are included in each nondimensional term leads to the following set of nondimensional parameters:

for depth $\quad\quad\quad (\rho g D/M)$,

for tip stress $\quad\quad (\rho g B \sigma/M^2)$,

and η, υ, and Φ.

2. Dynamic Tests

The important parameters in the dynamic test series include the energy released by the explosive (E) which is obtained from a knowledge of the weight/mass of explosive and the energy released per unit weight/mass. The range of the measurement (R) from the burst is important. The soil properties, the initial modulus (M), density (ρ), or alternatively the stress wave velocity $\left(c = \sqrt{M/\rho}\right)$ could be used in place of one of the parameters, M or ρ, and initial porosity (η), Poisson's ratio (υ) and angle of internal friction (Φ). The measurements that will be made will determine the acceleration (a), the velocity (v), and the time (t). Arranging the above parameters with the requirement that the amount of explosive energy released and the soil/simulant properties be included leads to the following set of nondimensional parameters.

for range $\quad\quad\quad R/(E/\rho c^2)^{1/3}$,

for time $\quad\quad\quad\; ct/(E/\rho c^2)^{1/3}$,

for acceleration $\quad\; a(E/\rho c^2)^{1/3}/c^2$,

for velocity $\quad\quad\; v/c$,

for stress $\quad\quad\quad \sigma/\rho c^2$,

and $\quad\quad\quad\quad\;\; \eta$, υ, and Φ .

SECTION III
SIMULANT MATERIAL SELECTION

This section of the report describes the selection of Froude-scaled sand simulant materials. It includes discussions of the material selection criteria, prototype properties, candidate materials, and the laboratory testing that was conducted to determine the suitability of the various materials as simulants.

A. MATERIAL SELECTION CRITERIA

The material selection criteria were derived directly from the scaling laws presented in Section II. For complete Froude-scale similitude, the simulant material must satisfy the scaling laws for both mass density and mechanical response of the material to applied load including strength and stiffness characteristics. To limit the scope of the effort to a tractable level, it was decided early in the project to enforce the material scaling only at the macroscopic level. That is, the granular materials, both prototype and model, are considered homogeneous and no attempt has been made to scale grain sizes or distributions. Scaling relationships are considered only on the macroscopic behavior as manifested in laboratory test results.

The ratio of initial densities of the model and prototype materials defines the density ratio, K_ρ. Any change in density due to deformation under load will be correctly modeled if the deformation properties of the materials scale correctly. No specific restriction was placed on porosity or grain density. However, a material's stress-strain behavior is related to its porosity and, in practice, materials with porosity greatly in excess of the prototype porosity were eliminated because their deformation behavior does not scale properly at large strains.

Scaling of material deformation under load presents the most complex requirements. When considered in full generality, the constitutive relationships for real geologic materials are highly complex and path-dependent. In the search for Froude-scale simulants, practicality limits consideration to some approximation of the true constitutive behavior of the materials. By concentrating on the response of the materials over a strain path relevant to the problem of interest, it is possible to limit the scope of the material selection effort to a reasonable level without seriously compromising the objectives of the investigation. Thus, evaluations of the deformation properties of the prototype and model materials have been based on their behavior under uniaxial strain conditions. The uniaxial strain path approximates the initial response of a soil mass to explosive loading. Further, in contrast to a hydrostatic compression test, a fully instrumented uniaxial strain test yields measurements of both required

12

incremental elastic constants. The constrained modulus, M, and Poisson's ratio, υ, were used to define the initial elastic response the various materials.

From Section II, the stress scale factor K_σ, is defined as:

$$K_\sigma = K_\rho K_l \tag{10}$$

Once the bulk density initial constrained modulus of a candidate simulant has been determined, the length scale factor achievable with that material can be determined from the following expression where the stress ratio, K_σ, is taken to mean the ratio of constrained moduli:

$$K_l = \frac{K_\sigma}{K_\rho} \tag{11}$$

While Equation (11) gives the length ratio for a given combination of prototype and model materials, it does not assure that the other criteria or nonlinear deformation and strength will be met and further checks must be made.

In a blast loading environment, deformations beyond the material's linear range are likely to be induced. Thus, the nonlinear stress-strain curve over the *entire range* of interest must be scaled. Since strain is dimensionless, $K_\epsilon = 1$, and the stress-strain curve of any candidate simulant material can be compared with the prototype by an appropriate scaling of the stress axis only. For perfect similitude, the scaled simulant stress-strain curve must be identical to the corresponding curve for the prototype throughout the strain range of interest.

Finally, it is necessary to consider scaling of the material's strength. The prototype material of interest is sand. To a very good approximation, sand can be considered a cohesionless material. Under this assumption, the shear stress, τ, that can be supported is given by the relationship:

$$\tau = \sigma_n \tan \Phi \tag{12}$$

where

σ_n = normal stress

Φ = friction angle of the material

13

Using this model of sand strength, the only strength property that must be considered is the friction angle. Since the friction angle is dimensionless, its model ratio must be unity, implying that the prototype and simulant materials must have the same friction angle.

B. PROTOTYPE PROPERTIES

The prototype material used as the basis for simulant selection is a fine sand, known as flume sand. It was selected because it has been extensively characterized and used in field tests by the U. S. Army Engineer, Waterways Experiment Station (WES) (References 2 and 3). Properties of the prototype sand are summarized in Table 3 and its stress-strain curve in uniaxial strain is presented in Figure 2.

TABLE 3. PROPERTIES OF WES FLUME SAND AND OTHER PROTOTYPE SCALE SANDS.

	WES Flume Sand	Randolph Concrete Sand	Crushed Salem Limestone	Enewetak Beach Sand
Dry Bulk Density (kg/m^3)	1610	1850	1790	1700
Grain Density (kg/m^3)	2640	2740	2730	2310
Porosity	.39	.33	.34	.40
Initial Constrained Modulus, M$_o$ (MPa)	375	271	232	343
Poisson's Ratio	.34	.33	.30	.32
Friction Angle (deg)	30	not avail.	not avail.	not avail.

It was anticipated that the deformation properties of the candidate Froude-scale simulant materials would not exactly match those of the WES flume sand. Thus, to establish a range of expected sand
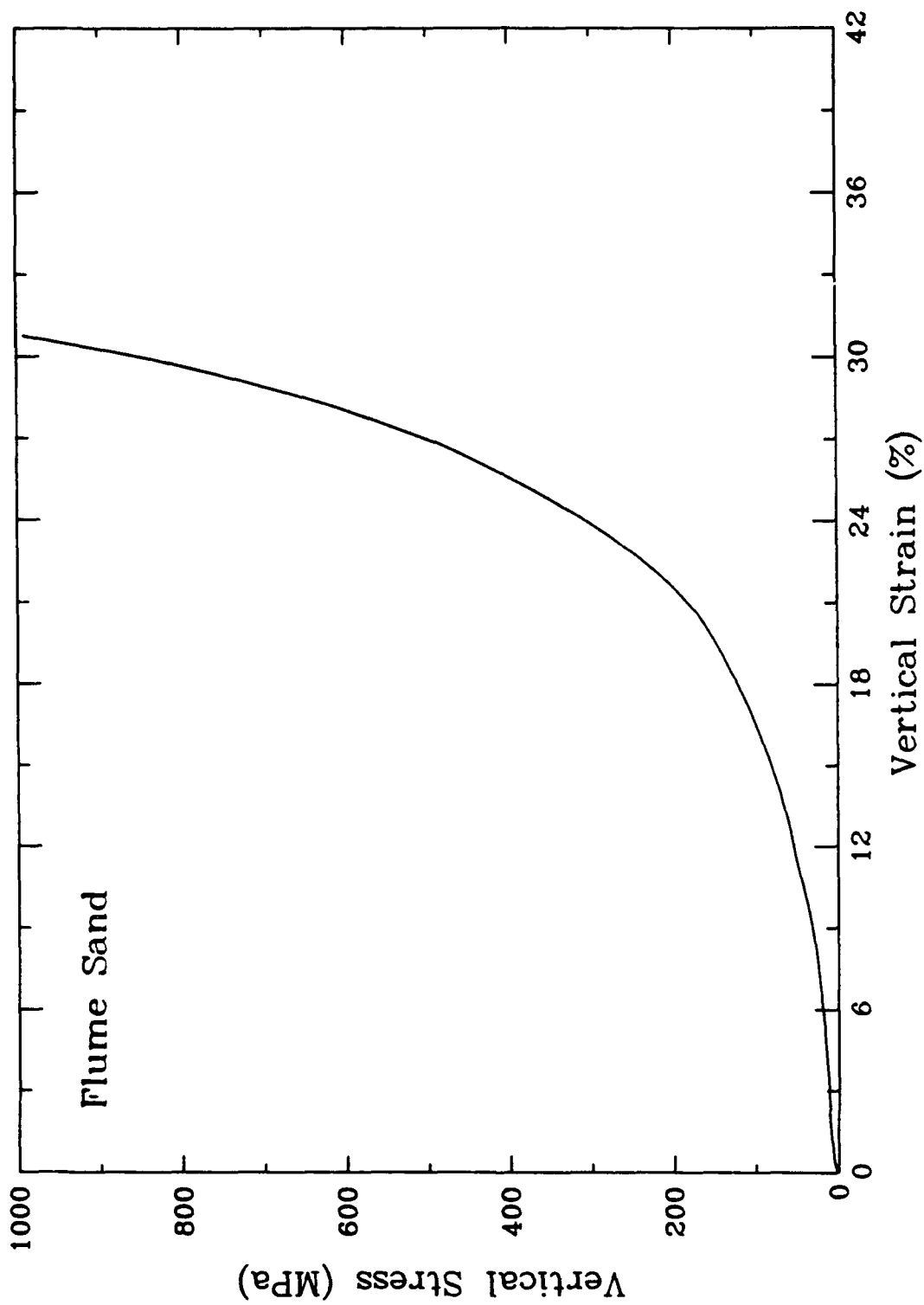
Figure 2.   Uniaxial Stress-Strain Relation for WES Flume Sand.

response, existing data on other sands were also considered. Figure 3 presents stress-strain curves for three additional sands: concrete sand from a batch plant in Randolph, Vermont, crushed Salem (Indiana) limestone, and a calcium carbonate beach sand from Eniwetok Atoll. Properties of these materials are included in Table 3. The compressibility response curves of WES flume sand and the three other sands are qualitatively similar, with moderate variation in initial modulus and more significant variation in the strain level at which the grains begin to lock up.

Figures 4 and 5 present the results of triaxial compression tests on WES flume sand at confining pressures ranging from 2 to 90 MPa from Reference 2. The friction angle of that material was determined from this data by plotting the strength points in Mohr's circle space and fitting a line tangent to the resulting curves.

C. LABORATORY TESTING FOR MATERIAL SELECTION

Over 20 candidate sand simulant materials were tested in ARA's materials laboratory located in South Royalton, Vermont. Strength and deformation properties were determined by triaxial testing. For a triaxial test, a right circular cylinder of material was prepared as indicated schematically in Figure 6. A flexible membrane, or jacket served to isolate the specimen from the confining fluid during testing. At each end, a hardened steel endcap was placed against the specimen and sealed to the jacket. Test specimens of the granular materials were prepared by carefully packing the material into a cylindrical mold lined by the jacket with one endcap in place. Upon completion of the packing, the other endcap was put in place and sealed to the jacket. Careful measurements were made of the mass of material and volume in each test specimen. Linear Variable Differential Transformers (LVDTs) were used to measure the deformation of the specimen under load. Two LVDTs in the axial direction and one in the radial direction were affixed to the jacketed specimen as shown in Figure 7. The specimen, thus prepared, was then secured in position inside the pressure vessel of the triaxial test apparatus. The triaxial apparatus can apply two independently controllable components of load, confining pressure that acts uniformly in all directions, and an incremental axial load applied by a piston to the ends of the specimen.

In the course of the simulant material evaluations, two different types of loading were employed. Uniaxial strain tests were used to determine the deformation properties of the candidate materials. In this test, compressive axial strain is imposed on the test specimen while controlling the confining pressure to maintain zero radial deformation. The uniaxial strain test provides a measure of the nonlinear stiffness (modulus) characteristics of the material under strain conditions that approximate those imposed by explosive loading. Typical uniaxial strain test results are presented in Figures 8 and

16
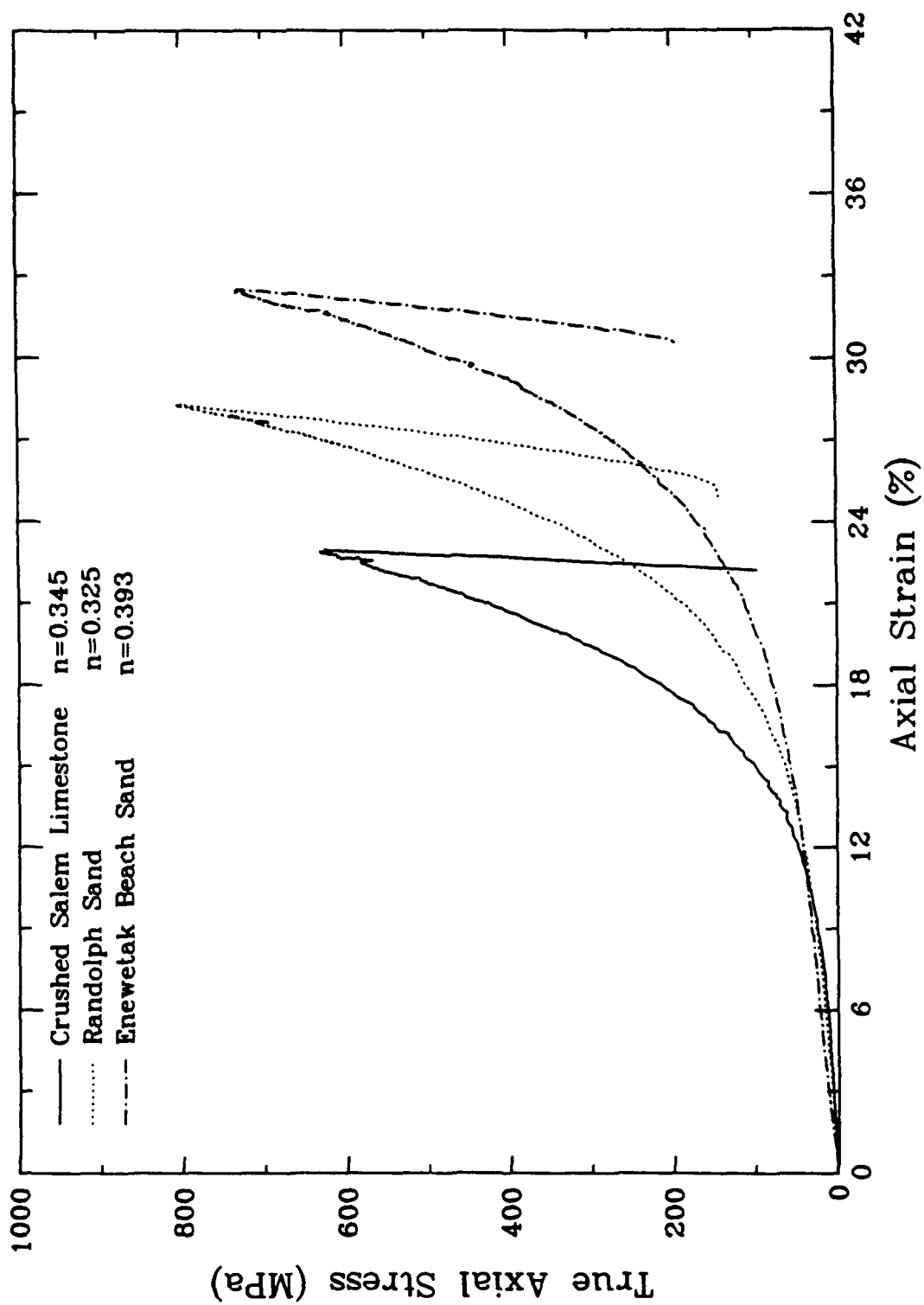
Figure 3. Uniaxial Stress-Strain Relations for Three Sands.

17
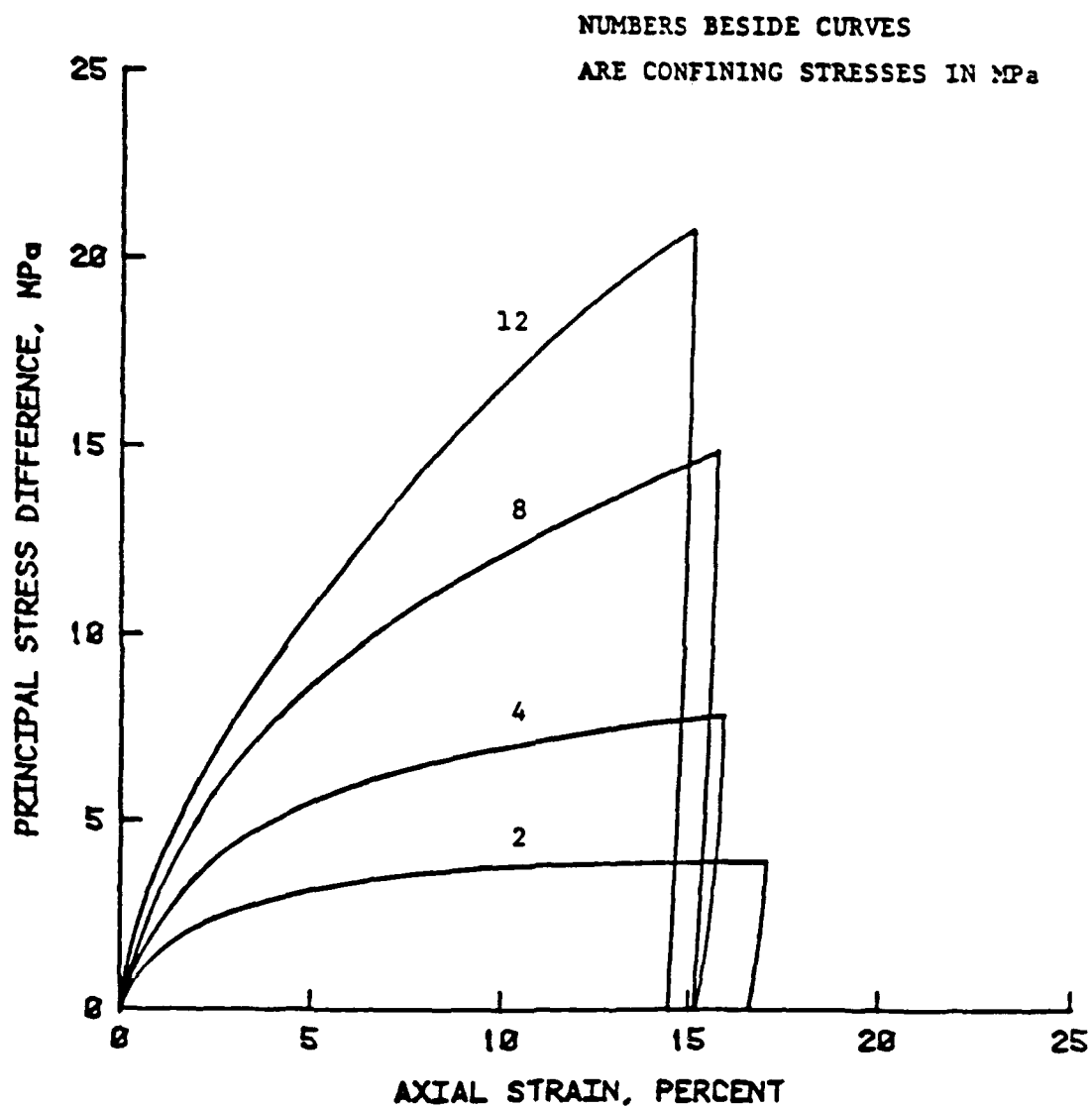
Figure 4. Triaxial Compression Test Data for WES Flume Sand at Confining Pressures Less Than 12 MPa. (From Reference 2)
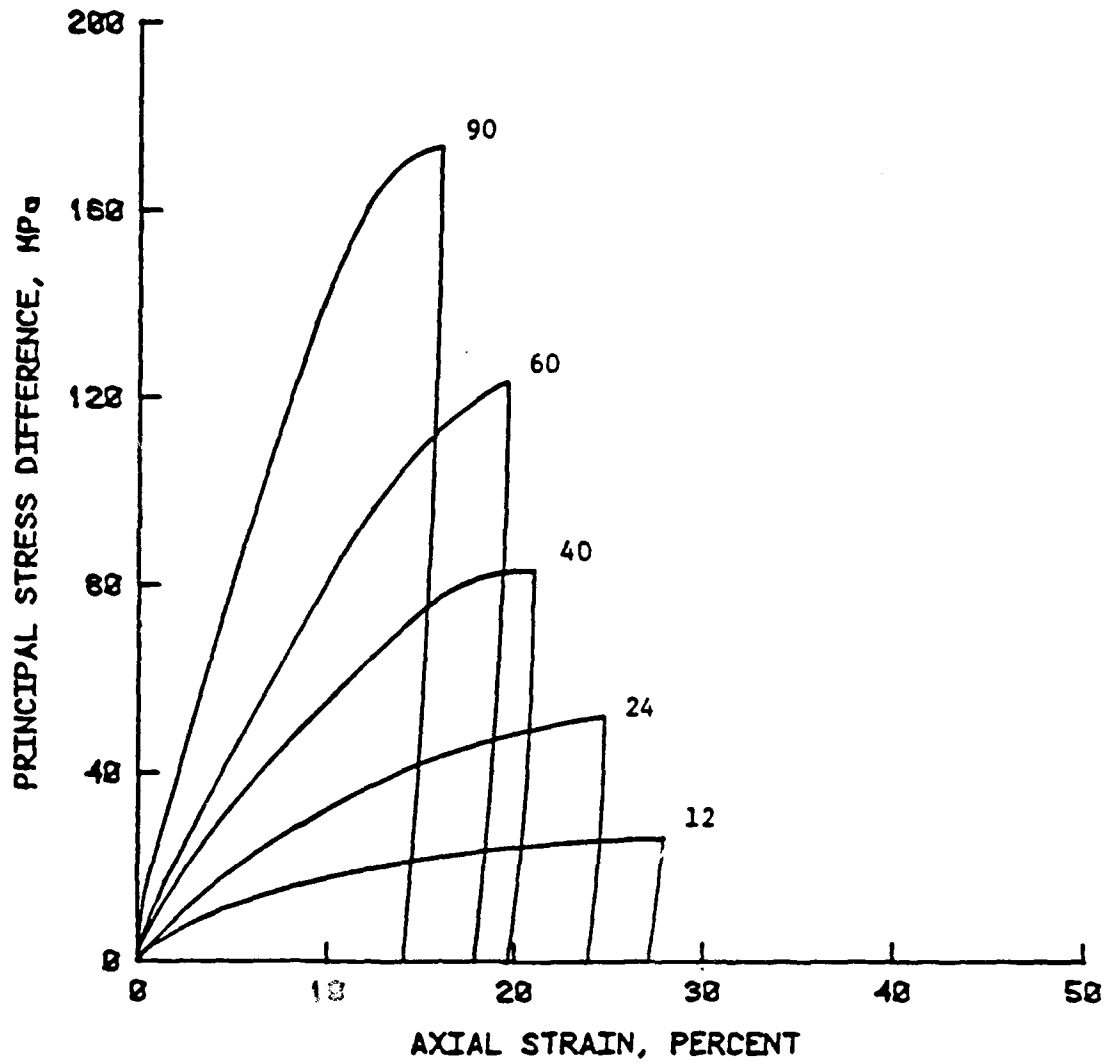
Figure 5. Triaxial Compression Test Data for WES Flume Sand at
Confining Pressures Greater Than 12 MPa. (From Reference 2)
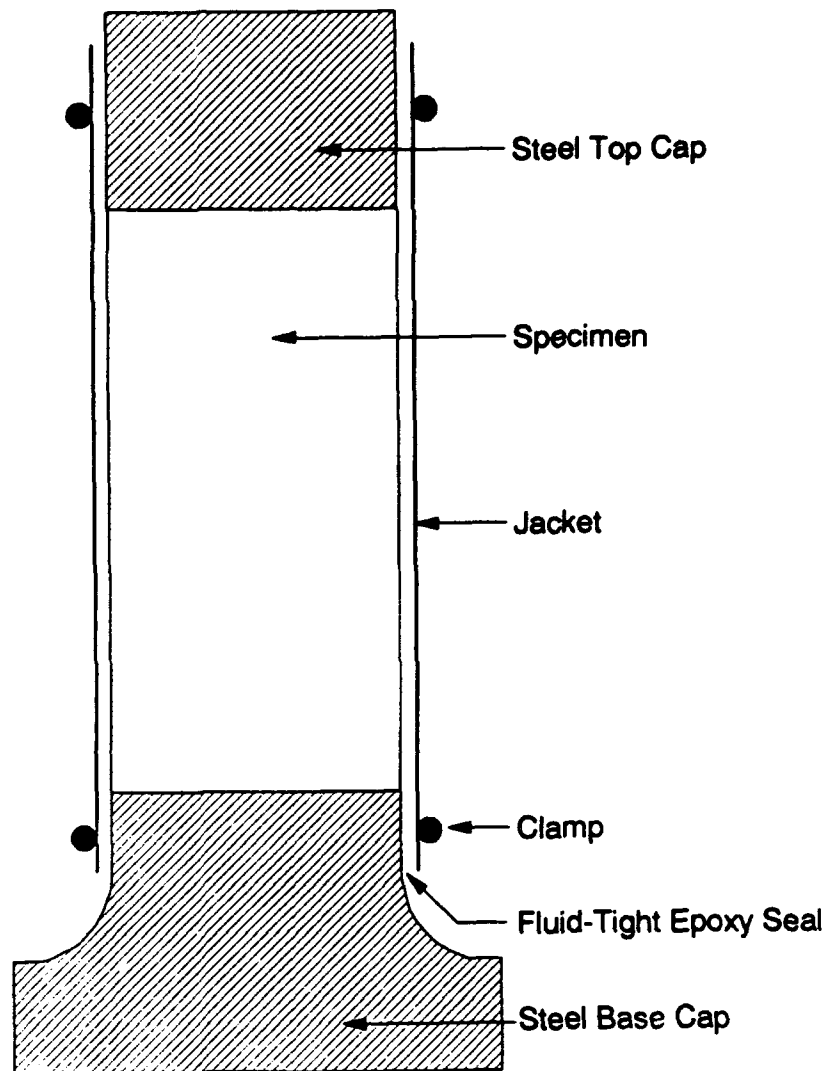
Figure 6. Cross-section of a Typical Jacketed Test Specimen.

20
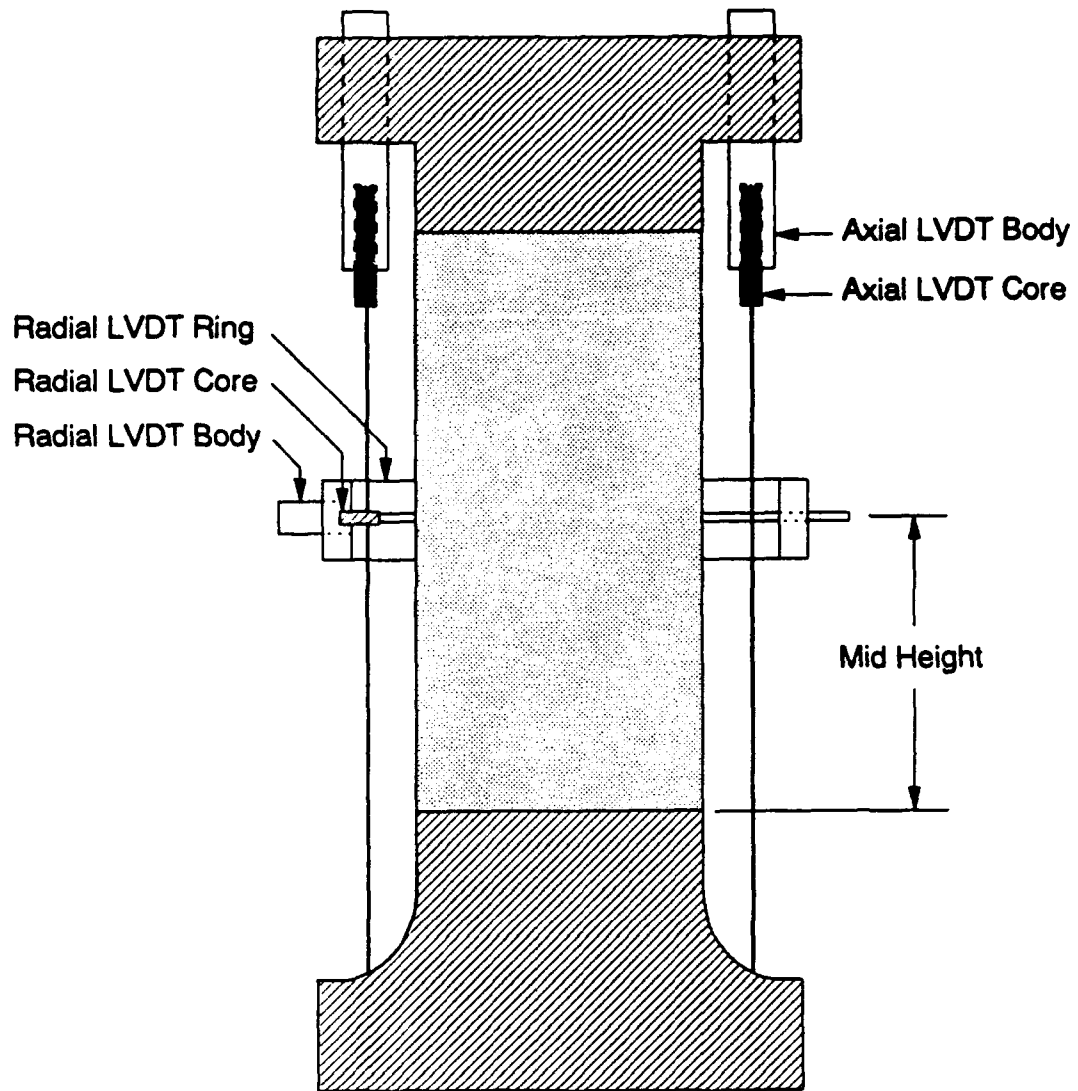
Figure 7. Typical Instrumentation for Laboratory Material Property Tests.

9. An axial stress-strain curve is shown in Figure 8. The slope of the initial linear portion of the curve is the initial constrained modulus, M. Figure 9 shows the relationship between axial stress and radial stress (confining pressure). The inverse of the slope at any point on this curve is the incremental coefficient of lateral earth pressure, Δk_o, i.e.

$$\Delta k_o = \frac{\Delta \sigma_r}{\Delta \sigma_a}$$

(13)

where $\Delta \sigma_r$ = incremental change in confining pressure

$\Delta \sigma_a$ = incremental change in axial stress

and the apparent Poisson's ratio is defined by:

$$v_a = \frac{\Delta k_o}{1 + \Delta k_o}$$

(14)

In the practice, only the value of Poisson's ratio for the initial linear portion of the loading was used for material selection.

For materials that passed initial screening based on modulus and density measurements, triaxial compression tests were performed to determine their strength properties. In a triaxial compression test, the confining pressure is increased to a pre-selected value and then held constant while compressive axial strain is imposed . The maximum axial stress reached is a measure of the strength of the material at that confining pressure. Figure 10 shows results of a typical triaxial compression test. In this plot, stress difference represents the difference in axial stress and the confining pressure at the imposed axial strain. The figure shows that loading in the test was terminated prior to reaching a peak in stress. In this case, the stress difference at 15 percent axial strain was arbitrarily taken as the strength value. At that level, the rate of increase in stress with increasing axial strain is greatly reduced from its initial level. While this is an imperfect approximation, it is consistent with common engineering practice and it is consistent with the method of processing of the test data used to define the prototype properties. Under the assumption of a cohesionless material, the friction angle of the material, Φ, can be estimated from a single triaxial compression test using the expression:

22
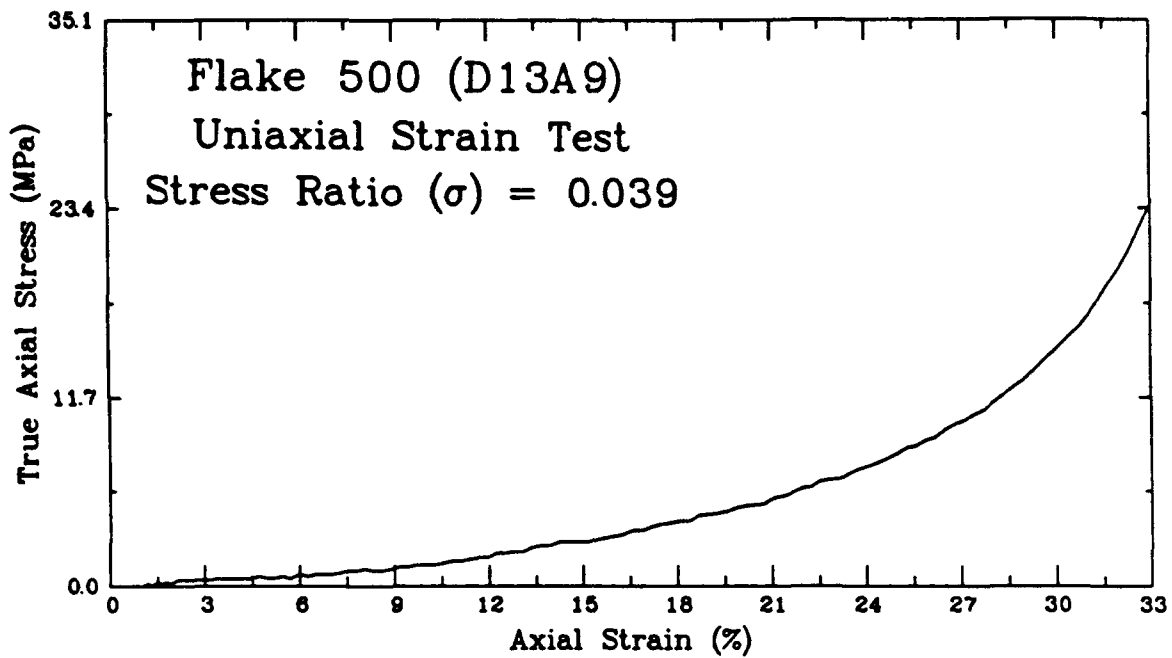
Figure 8. Typical Uniaxial Stress-Strain Data from a Test of a Candidate Simulant.
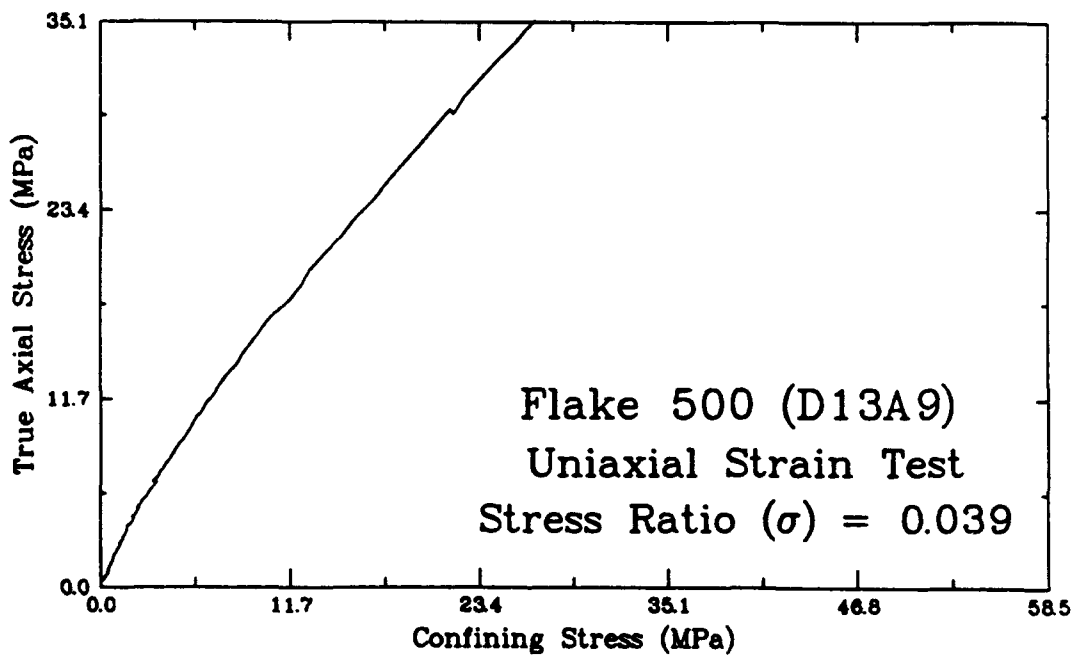
Figure 9. Typical Relationship Between Axial Stress and Confining Pressure
for the same Uniaxial Strain Test as Shown in Figure 8.

23
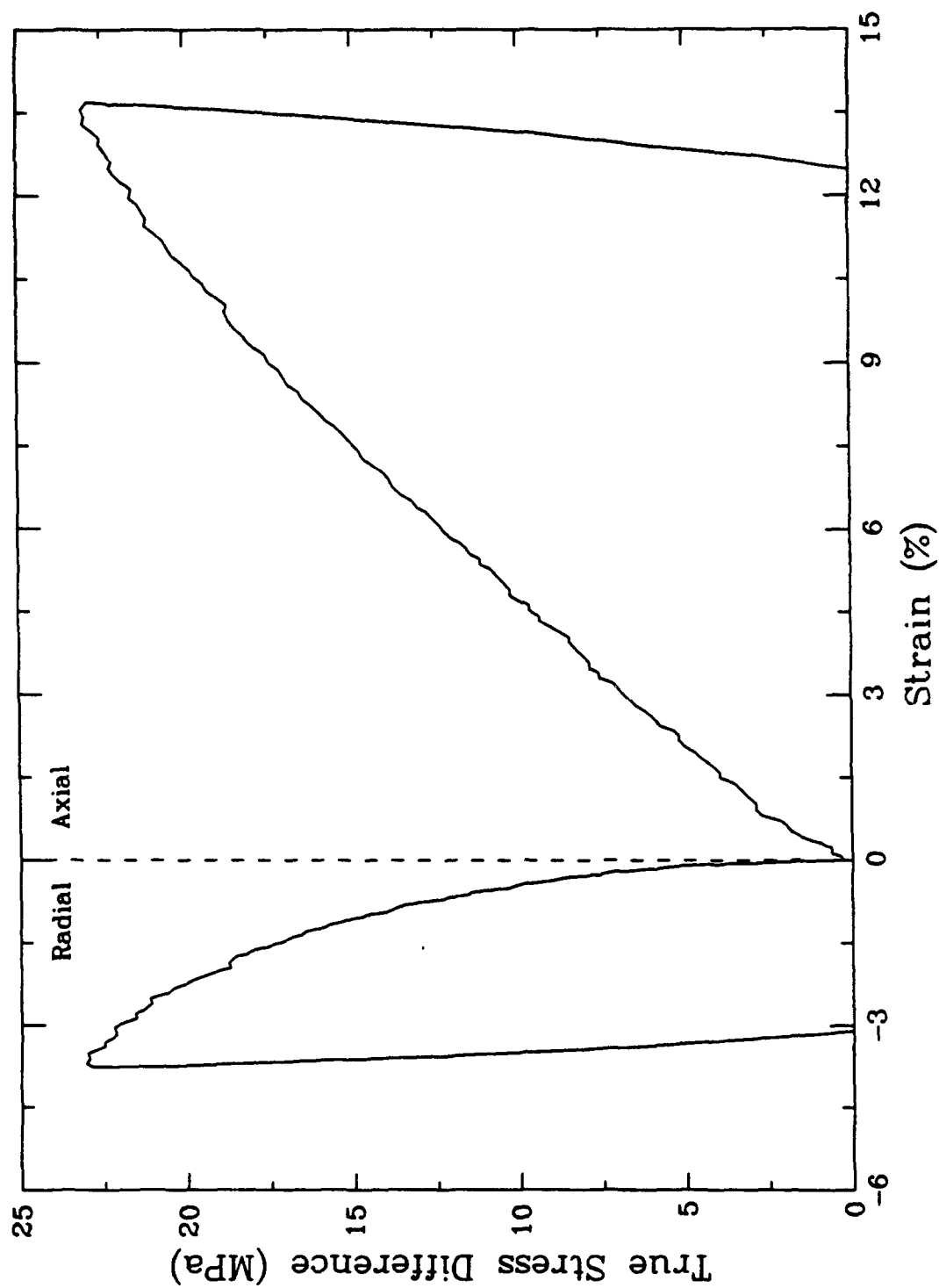
Figure 10. Axial and Radial Stress-Strain Results from a Triaxial Compression Test on Crushed Bituminous Coal at 10 MPa Confining Pressure.

$$\Phi = \sin^{-1} \frac{\sigma_d}{2\sigma_r + \sigma_d} \tag{15}$$

where σ_d = maximum stress difference

  σ_r = confining pressure

D. IMPLEMENTATION OF THE SELECTION CRITERIA

Primary screening of candidate materials was done on the basis of the length scale factor. Rearrangement of Equation (11) and substitution of the definitions of the model ratios and yields the following relationship for determination of the length scale factor:

$$K_l = \frac{M_m \rho_p}{M_p \rho_m} \tag{16}$$

where M_p, M_m = initial constrained modulus of the prototype and model, respectively

  ρ_p, ρ_m = bulk density of the prototype and model, respectively

Additional criteria which can be evaluated based on uniaxial strain test results are the Poisson's ratio and the shape of the nonlinear portion of the stress-strain curve. Poisson's ratio was computed for the initial loading portion of the curve as described earlier and compared against the prototype value. To assess the material's suitability in terms of nonlinear stress-strain behavior, plots were made of both the model and prototype stress-strain curves. Since the strain scale factor is unity, both model and prototype data were plotted to the same strain scale. The model stress data is scaled by the stress scale factor, K_σ, derived from the initial loading slopes of the two sets of test data. When plotted in this manner, the initial loading portions of the model and prototype curves overlay each other. If the two curves are identical for the remainder of the loading, then that aspect of the model material behavior is perfectly Froude-scaled to the prototype. It was recognized that it would probably not be possible to obtain even a near-perfect match with the prototype WES flume sand. Thus, axial stress-strain curves from uniaxial strain tests of the other three sands described earlier were used to define a range of acceptable nonlinear stiffness behavior.

The selection criteria described in the previous paragraph can all be evaluated based on the results of a uniaxial strain test and simple density measurements. The final criterion that can not be assessed with that limited set of test data is the friction angle. For the materials that met the scale factor and stiffness criteria, a series of triaxial compression tests were performed to evaluate the friction angle. It was computed and compared with the required prototype value.

25

E.   CANDIDATE MATERIALS

Over 20 materials were subjected to laboratory testing to determine their suitability as Froude-scale simulants for sand. Initially, the objective was to locate two or three different materials with length scales in the range of 1/10 to 1/50. Substitution of these values into Equation (16) results in a requirement that the model material either be much denser than the prototype sand or much softer (lower modulus), or a combination of the two. The search began with the materials that were identified in the Phase I effort 1. The fact that some of the Phase I materials were organic polymers (plastics) in granular form raised the possibility of finding other plastics with the required properties. In an effort to make the material selection more systematic, a search was made of a two plastics databases (References 4 and 5). Since the prototype material properties and the desired scale factors were known, Equation (16) was rewritten to determine the required numerical value of the ratio of modulus to density for the simulant material. It was necessary to modify this value because the modulus and density properties are given for solid materials in the published plastics data. Known relationships between solid grain properties and bulk properties of granular materials were used to derive a modified criterion ratio for use in the database search.

In addition to the materials identified in Phase I and those selected from the plastics database, the search encompassed various other materials suggested by individuals associated with the project. It was from this group that the simulants were eventually selected. Two simulant materials were chosen for use in the static and dynamic proof of principle (POP) tests. At a length scale of approximately 1/5, finely crushed bituminous coal is the simulant. To obtain a more extreme scaling, fine lead particles are added to the coal, resulting in a material about twice as dense with approximately the same stiffness. A 60/40 mixture (lead/coal by weight) produces a length scale of approximately 1/10. The sand simulants used in the POP testing are discussed in more detail later in this section.

Since the materials that were not selected as simulants do not effect the outcome of the POP tests, detailed descriptions of those materials and the results of their mechanical property tests are not included in the main body of the report. Instead, their test data are summarized in Table 4. Additional information on those materials, including origins, descriptions, test results, and deselection rationale are included, in Appendix A. For each of the materials, Appendix A contains a single page with a description of the material and summary of the test results followed by a page presenting stress-strain curves and axial vs. radial stress plots from the uniaxial strain tests. The plot scales were selected for the stress-strain curves to facilitate comparison with the prototype sand data presented in Figures 2 and 3.

MATERIAL	TEST ID	Grain Density (kg/m^3)	Bulk Density (kg/m^3)	Porosity	Constr. Modulus (MPa)	Poisson's Ratio	Density Ratio $K\rho$	Modulus Ratio $K\sigma$	Inverse Length Scale Factor $1/K_1$
Candidate Simulants									
MAGNETITE	N3A7	4700	2834	0.397	114	0.30	1.76	0.305	5.77
SPANTEX	D12A9	940	694	0.262	75	0.46	0.43	0.200	2.15
FLAKE 500	D13A9	2160	1445	0.331	14	0.36	0.90	0.039	23.24
DICAPERL CS-10-200	D14A9	700	482	0.311	4	0.39	0.30	0.011	28.07
THERMO ROCK	D14B9	NA	199	NA	2	0.45	0.12	0.005	23.13
Q-CEL 600	D15A9	430	298	0.307	6	0.41	0.19	0.015	12.12
STYROPOR	D15B9	NA	678	NA	97	0.42	0.42	0.257	1.63
LEAD SHOT	D18A9	11300	7101	0.372	148	0.43	4.41	0.395	11.15
BAMBERKO PURGE	D22Z9	1190	715	0.399	81	0.31	0.44	0.215	2.06
ACLON CTFE	J2A0	2130	1177	0.447	30	0.32	0.73	0.079	9.23
PTFE 50 INOX	J3B0	3250	1815	0.442	6	0.38	1.13	0.017	65.91
PTFE 25 GLASS	J4A0	2220	1165	0.475	4	0.38	0.72	0.010	75.64
FLAKE w/ FIBER	J4B0	NA	1400	NA	15	0.41	0.87	0.040	21.50
BARITE	J25A0	4480	2842	0.366	121	0.31	1.76	0.324	5.45
FLY ASH	J26A0	NA	1356	NA	82	0.36	0.84	0.219	3.85

Table 4. Summary of Screening Tests on Candidate Simulants That Were Not Selected.

The strain scales are the same and the stress scales are multiplied by the modulus ratios of the individual materials.

Several of the candidate materials were fillers, inert materials that have very low bulk density, e.g., Dicaperl, Therm-O-Rock, Q-Cell. These materials have such large voids fraction that their scaled deformation behavior does not approximate that of sand. This suggests that, to properly model the stress-strain behavior of sand up to lock-up, the simulant must be a material with the correct grain properties, not just a material with very high porosity.

Two different types of expandable polystyrene beads were tested, both yielding scale factors of approximately 2. This does not appear to be a fruitful area for further investigation.

Polytetrafluoroethylene (PTFE), also known by the trade name Teflon®, intrinsically has the correct combination of density and modulus to achieve significant scale factors. PTFE filled with a mineral or metal tends to have even higher density and lower modulus, resulting in scale factors of the order of 1/50. Unfortunately, the low coefficient of friction of PTFE results in a very high Poisson's ratio, making it unsuitable as a sand simulant. It was suggested that Polychloro-Trifluoroethylene Copolymer (PCTFE) may have properties similar to PTFE except with a higher coefficient of friction. When tested, PCTFE exhibited an appropriate Poisson's ratio, but yielded a scale factor of only about 1/10. At that scale, it would be prohibitively expensive. However, if it were possible to obtain a filled version of PCTFE with a scale factor of 1/50, its use might be practical on a laboratory scale. This has not been investigated, but is suggested as a possible area for further study.

F. SAND SIMULANT MATERIALS

Two materials were eventually selected as the Froude-scale simulants for sand, crushed bituminous coal and a mixture of crushed bituminous coal and fine lead grains. This section describes the results of the tests conducted on various specimens of coal and coal/lead mixes. These results are presented in the form of a history of the investigation that lead up to the selection of the simulant materials, including the rationale for the decisions made along the way. Table 5 presents a summary of the laboratory material property tests on coal and coal/lead mixtures. Additional information about each test is contained in Appendix B.

Candidate Simulants

MATERIAL	TEST ID	Grain Density (kg/m^3)	Bulk Density (kg/m^3)	Porosity	Constr. Mod. (MPa)	Poisson's Ratio	Density Ratio K_ρ	Modulus Ratio K_σ	Inverse Length Scale Factor $1/K_l$
ANTHRACITE COAL	D20A9	1650	956	0.420	43	0.38	0.59	0.114	5.21
BITUMINOUS COAL	J2B0	1330	988	0.257	53	0.34	0.61	0.141	4.36
BITUMINOUS COAL	J3A0	1330	857	0.356	24	0.33	0.53	0.064	8.27
ANTH. COAL w/LEAD	J5A0	NA	1946	0.326	39	0.35	1.21	0.105	11.53
40 B. COAL 60 LEAD	J5B0	NA	1810	0.360	23	0.30	1.12	0.061	18.52
50 B. COAL 50 LEAD	J9A0	NA	1514	0.364	31	0.30	0.94	0.082	11.49
DENVER COAL	F12A0	1460	828	0.433	57	0.33	0.51	0.152	3.37
DENVER COAL	F13A0	1460	820	0.438	53	0.32	0.51	0.141	3.61
60 Pb 40 D. COAL	F14A0	NA	1756	0.426	47	0.32	1.09	0.126	8.67
60 Pb 40 B. COAL	A12A0	NA	1858	0.343	38	0.31	1.15	0.102	11.29
60 Pb 40 20-50 C	A16A0	NA	1786	0.368	39	0.35	1.11	0.105	10.58

Table 5. Summary of Tests on Coal and Coal/Lead Mixtures.

29

The first coal tested in the search for sand simulants was anthracite (hard) coal intended for home heating use. For specimen preparation, a small quantity of the coal was manually crushed using a light hammer. The only material that passed a U.S. Standard No. 10 sieve was used. Further, in an effort to minimize the stiffness of the test specimen, half of the material that passed a No. 50 sieve was removed. A complete grain size analysis was not performed at that stage. The initial test of anthracite coal yielded a density ratio of 0.59 and modulus ratio of 0.114, for a scale factor of 1/5.2. Its stress-strain curve was approximately correct for simulating sand as shown in Figure 11. While this result was considered encouraging, it fell short of the desired 1/10 to 1/50 length scale factor.

A material with an even lower stiffness and/or higher density was required to obtain the desired scaling. It was reasoned that bituminous (soft) coal would have a lower modulus, and handbook values indicated only a slight decrease in density. Since there is apparently no consumption of bituminous coal in the area local to the ARA materials laboratory in South Royalton, Vermont, a small quantity of it was obtained from a coal broker in New Jersey. The test specimens were prepared in a manner similar to the anthracite specimens. The crushed bituminous coal contained fewer fine particles than the anthracite. For the first test, Test ID J2B0, no fines were removed from the specimen material. The constrained modulus measured in the first bituminous coal test was approximately 23 percent higher than the value measured on the anthracite specimen. Examination of the density and porosity values in Table 5 reveals that the specimen of crushed bituminous coal for test J2B0 was compacted to a higher density than the anthracite specimen (D20A9), in spite of its lower grain density. Apparently, due to the low strength of the bituminous coal particles, there was significant break-up of grains during preparation, resulting in a specimen with porosity significantly lower than the expected range for clean sands.

An additional test (J3A0) was performed on a specimen of crushed bituminous coal. In this test, the density was kept intentionally low by removing all material passing a No. 50 sieve and minimizing the compactive effort used in specimen construction. The initial constrained modulus was less than half that measured in the first bituminous coal test, J2B0, resulting in a scale factor of 1/8.3. In addition, this material has Poisson's ratio of 0.3, which is in the middle of the range of the sands tested, and the stress-strain curve in uniaxial strain, though slightly different than the criterion flume sand, is within the range of the sand data presented in Figure 3. A comparison of the Froude-scaled stress-strain curve for the crushed bituminous coal with the corresponding prototype data is presented in Figure 12.

The data from test J3A0 appeared to represent a lower limit on the stiffness achievable with a coal simulant. In order to push the scale factor into the desired range of 1/10 to 1/50, an increase in

30
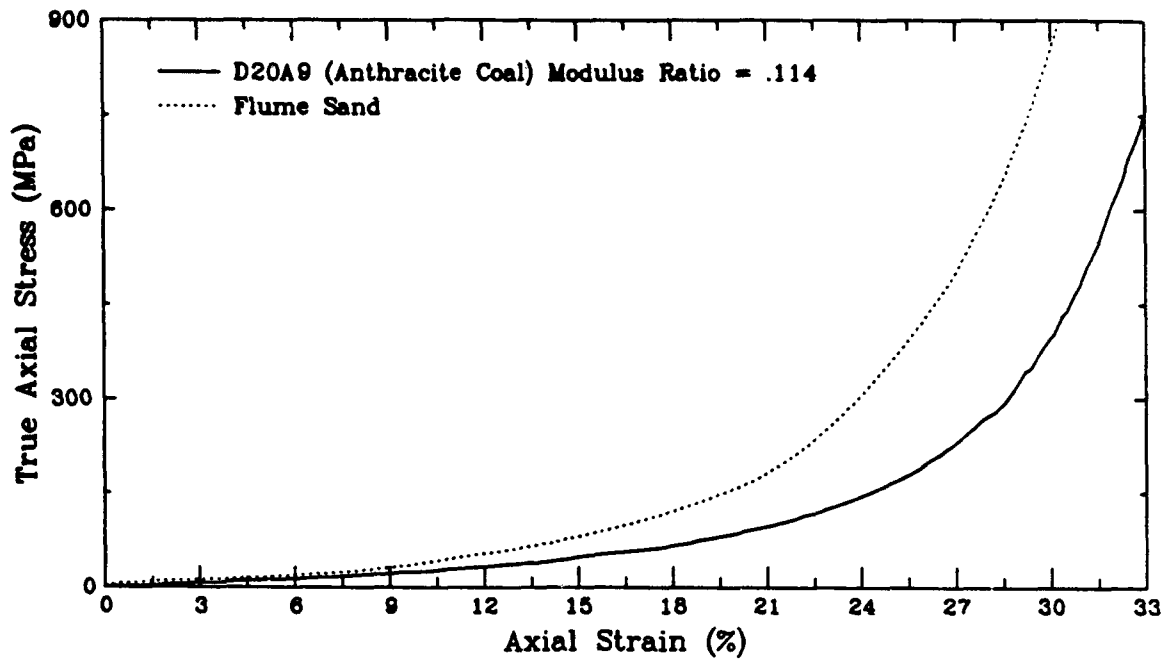
Figure 11. Comparison of Uniaxial Strain Behavior of WES Flume Sand with the
Scaled Response of Crushed Anthracite Coal.

Figure 12. Comparison of Uniaxial Strain Behavior of WES Flume Sand with the
Scaled Response of Crushed Bituminous Coal.

31

density was required. In an effort to increase the density without significantly increasing the modulus, lead shot was added to the crushed coal. Initially, 1.7 mm diameter shot was used because it was the smallest that was readily available locally. The first test of a coal/lead mixture (J5B0) contained 60 percent lead and 40 percent coal by weight. Due to the large difference in density between the two constituents (11300 kg/m^3 for lead; 1330 kg/m^3 for bituminous coal), this is equivalent to 85 percent coal and 15 percent lead by volume. Because of the high volume fraction of coal, the strength and deformation properties were expected to be approximately the same as those of plain coal. However, the high weight fraction of lead significantly increased the density. The J5B0 specimen was prepared at a density of 1810 kg/m^3, which is in the density range of well compacted natural sand. The porosity of the coal/lead mixture can be computed by the following expression:

$$n = 1 - \gamma_b \left[\frac{f_c}{\gamma_c} + \frac{f_{Pb}}{\gamma_{Pb}} \right] \tag{17}$$

where

f_c, f_{Pb} = Mass/weight fractions of coal and lead, respectively

γ_c, γ_{Pb} = grain densities/unit weights of coal and lead, respectively

γ_b = bulk density of the mixture

Using Equation (8), the porosity of the J5B0 specimen is found to be 0.360, which is in the range of the prototype sands listed in Table 3. In the first test of a bituminous coal/lead mixture, the initial constrained modulus was measured as 23 MPa. This is almost identical with the plain bituminous coal test (J3A0), and taken along with the specimen density results in a length scale factor of 1/18.5. Further, the Poisson's ratio of 0.30 is in the range of natural sands and, as shown in Figure 13, the stress-strain curve, Froude-scaled by the appropriate modulus ratio, is in excellent agreement with the prototype test data.

Based on the uniaxial strain test results, both plain crushed coal and a coal/lead mix meet the density and deformation criteria for Froude-scale simulants of sand, although not at the full desired range of scale factors. In view of the encouraging deformation test results, triaxial compression tests were preformed on both materials to determine the suitability to their strength (friction angle) properties. Three tests were preformed on plain coal and two on coal/lead mix at confining stresses ranging from 0.7 to 10 MPa. Mohr's circles representing the strength results are presented for the two material types in Figures 14 and 15, respectively. In both cases, friction angles of approximately 33 degrees are indicated. While this is slightly higher than the reported value of 30 degrees for WES flume sand, the 30 degrees value is at the low end of what would be expected for sands.
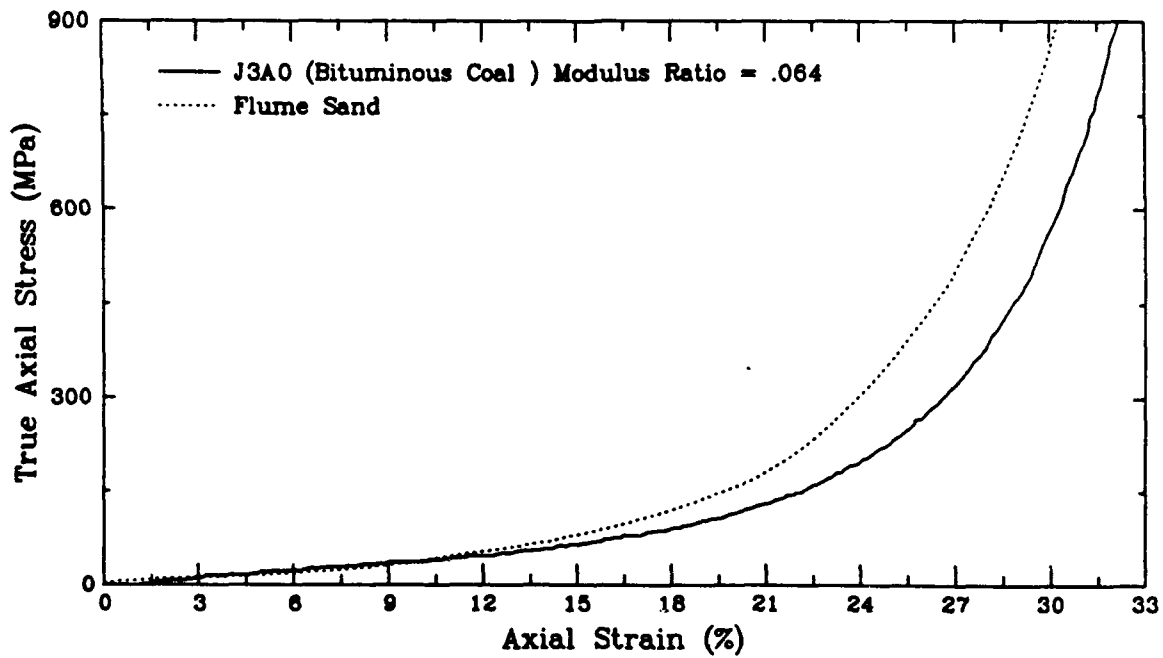
Figure 13. Comparison of Uniaxial Strain Behavior of WES Flume Sand with the
Scaled Response of a Mixture of Crushed Bituminous Coal and Lead Shot.
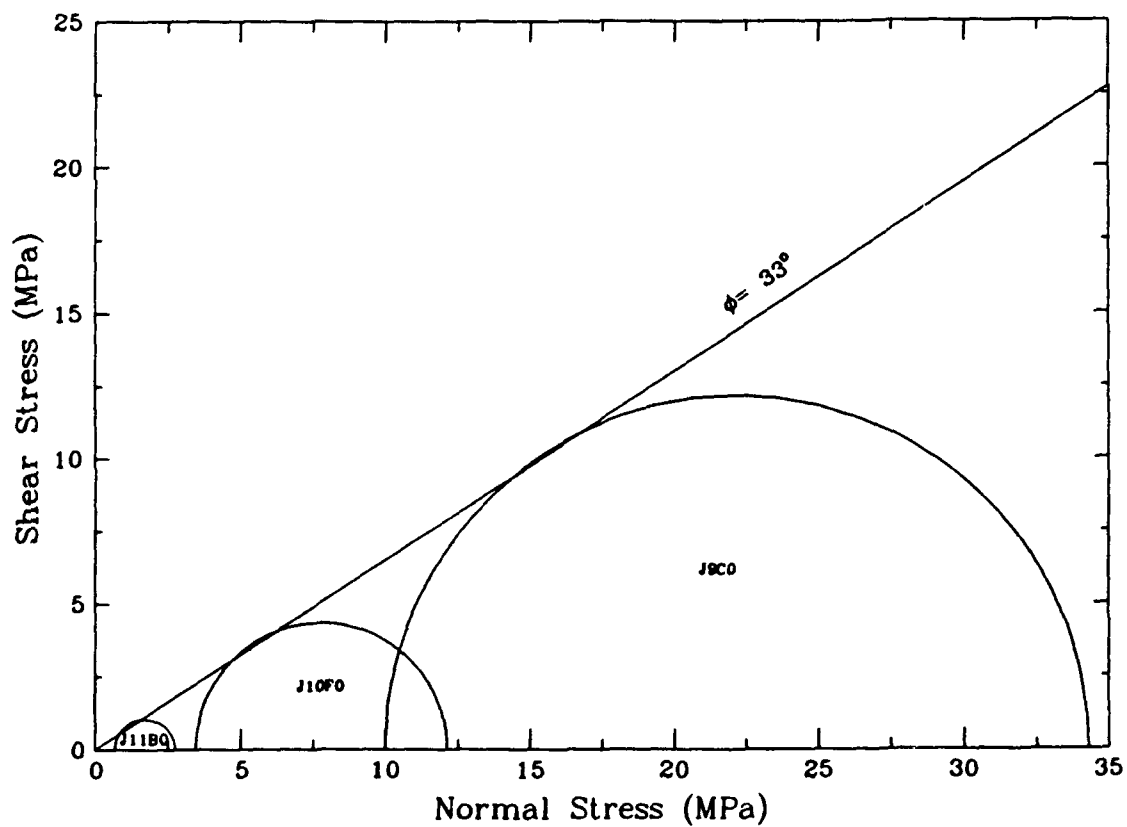
Figure 14. Friction Angle for Bituminous Coal from Triaxial Compression Tests.

33
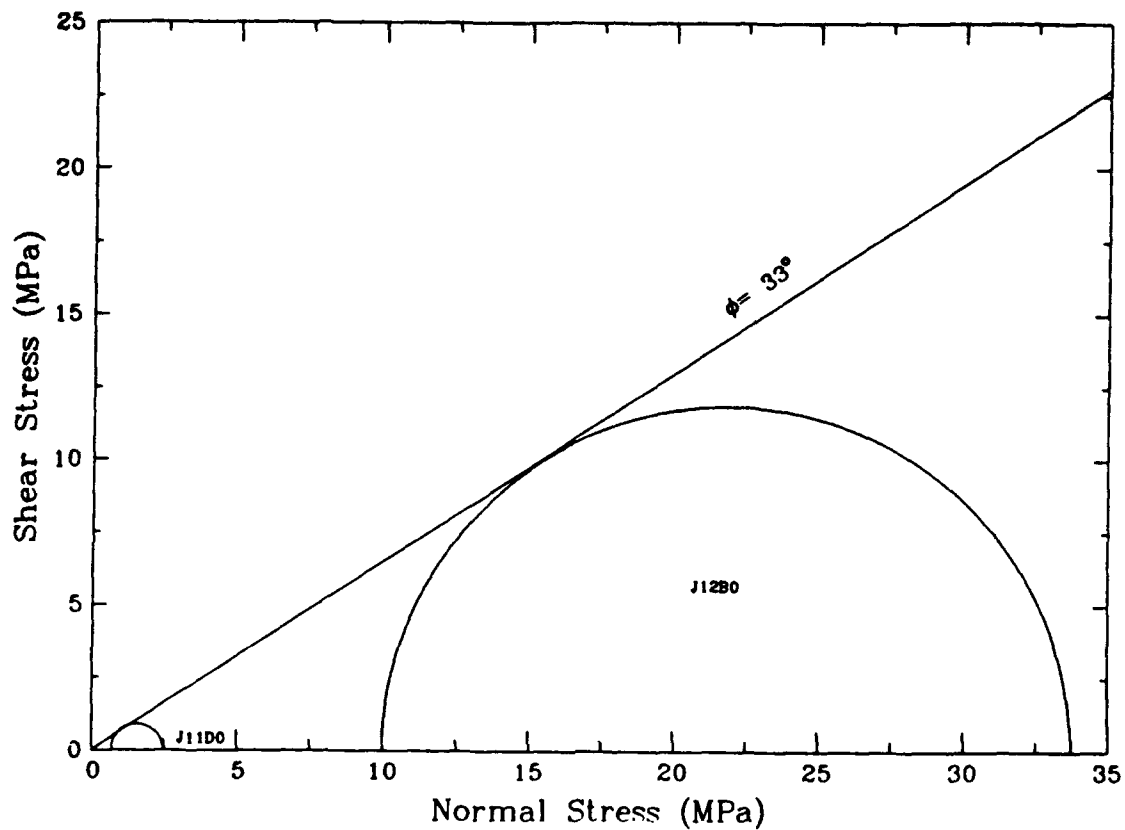
Figure 15.   Friction Angle for 40 Percent Bituminous Coal - 60 Percent Lead Shot from
                    Triaxial Compression Tests.

Thus, both crushed coal and coal/lead mixture closely satisfy all of the density, strength, and deformation criteria for Froude-scale simulants of sand at scales of at least 1/10. This fact combined with the reasonable cost of coal and the dearth of other suitable simulant materials led to the decision to compromise the requirement for three scales up to 1/50 and concentrate on coal-based simulants.

Additional tests were performed on coal and coal/lead specimens to investigate various possibilities for fielding the Proof-of-Principle (POP) tests. A mixture of 50 percent by weight each of crushed coal and 1.7 mm lead shot was tested in uniaxial strain. Its lower density combined with the

34

higher modulus measured in that test resulted in a substantially less desirable scale factor. Based on this result, the 50/50 mix was abandoned in favor of the 60/40 lead/coal mix. Since the dynamic POP tests were to be conducted at ARA's Rocky Mountain Division Test Range near Denver, Colorado, a series of tests was run to evaluate the suitability of a coal readily available in the Denver area. As shown in Table 5, the modulus values measured on specimens constructed of the Denver coal exceed all of the other coal test data with the exception of Test J2B0, in which the coal was very densely packed. This occurred in spite of the fact that the porosity of the Denver coal specimens was consistently higher than the other coal and coal/lead materials.

In view of the undesirably stiff properties of the Denver coal, and to use materials as nearly the same as possible for the laboratory materials tests and the static and dynamic tests, the decision was made to use coal from the same source for all test involving coal. Sources of supply for the materials are listed in Appendix B.

A quantity of bituminous coal was shipped to the laboratory in Vermont to support construction of the static POP test specimens. Two additional uniaxial strain tests were conducted on specimens constructed using that material. The results of those two tests, A12A0 and A16A0, are summarized in Table 5. Along with a new batch of coal, a slightly different form of lead, designated "free-flow lead shot" by the supplier was introduced. This material contains a range of grain sizes, all of which are smaller than the uniform lead shot that was initially used. Its properties are given in Appendix B. The specimen for Test A12A0 contained coal with a range of grain sizes, all passing No. 10 and retained on No. 50 serve. The initial constrained modulus measured in this test was substantially higher than in the previous test on 60 percent lead-40 percent bituminous coal (J5B0). Based on an examination of the test data, it was hypothesized that the higher stiffness was a result of a higher density (lower porosity) specimen. In order to lower the density, another specimen was prepared and tested with more nearly uniform grain size, all passing No. 30 and retained on No. 50. This specimen (A16A0) had a density less than J5B0, but the measured modulus was still substantially higher.

While some variation in test results is to be expected in geotechnical testing, the limited test data suggest that the later batch of bituminous coal actually has different, stiffer, properties than the first one. Figure 16 compares the two tests on coal/lead mixes made of coal from the shipment that was used for the static POP tests. In Figure 16, a modulus ratio between model and prototype of 1/10 has been used. It would clearly be desirable to run some additional tests to better quantify the factors that influence the variation in deformation properties of the simulant materials. However, financial considerations have precluded such additional investigations. Thus, the data presented in Figure 16 are judged to be the best available representation of the properties of the materials used in the 1/7

35
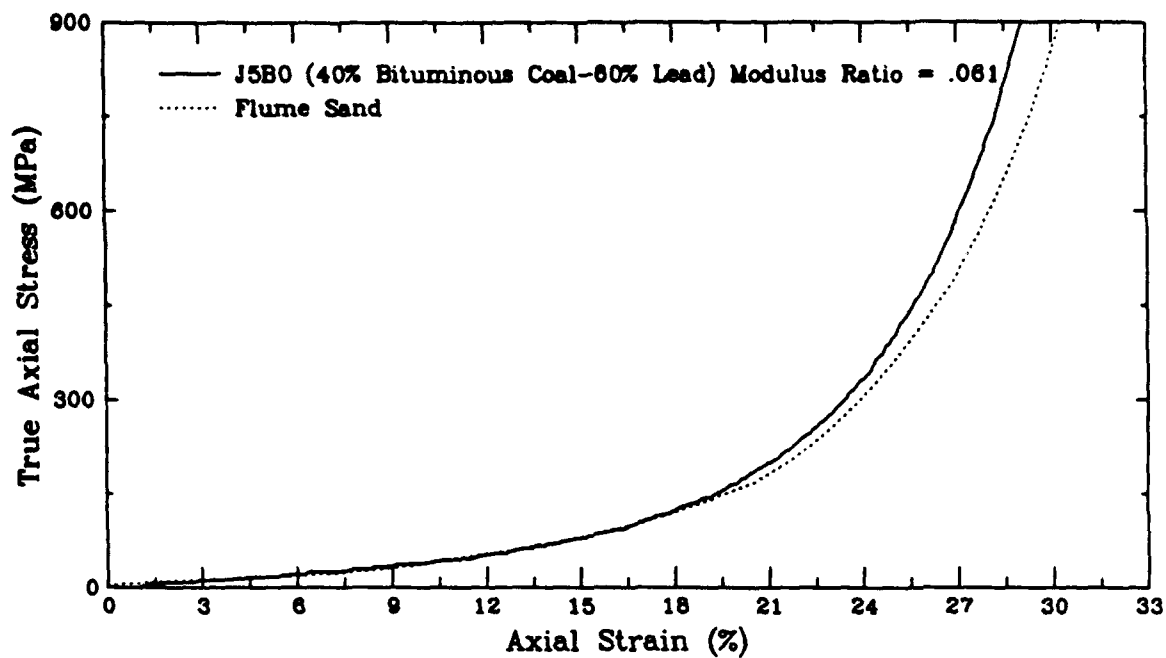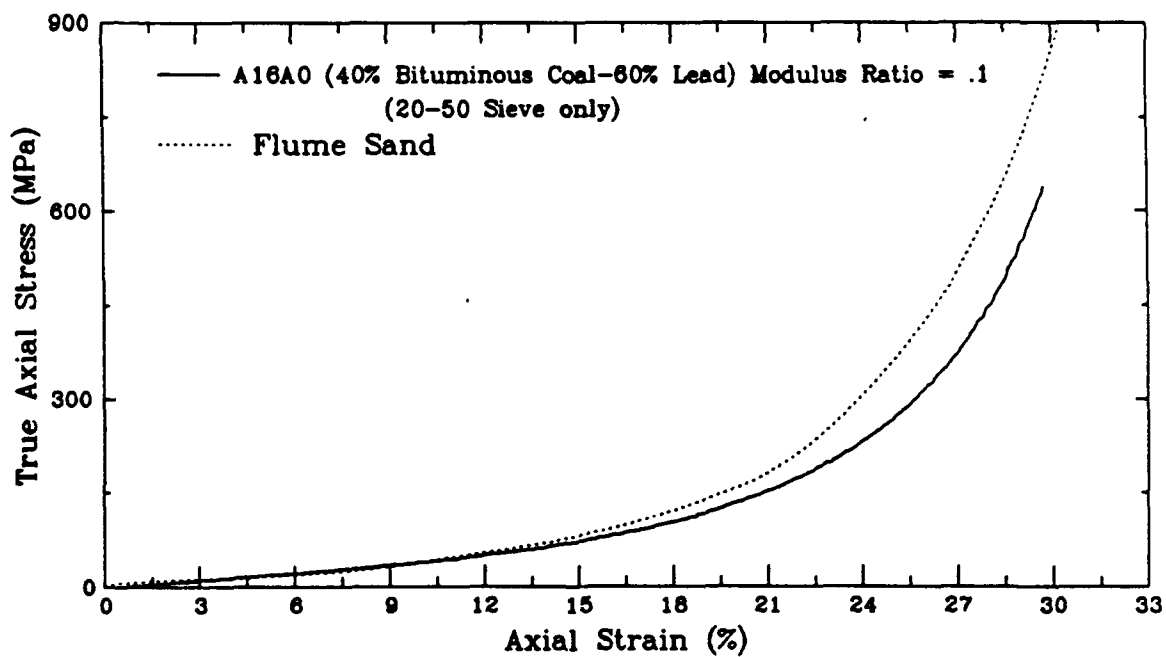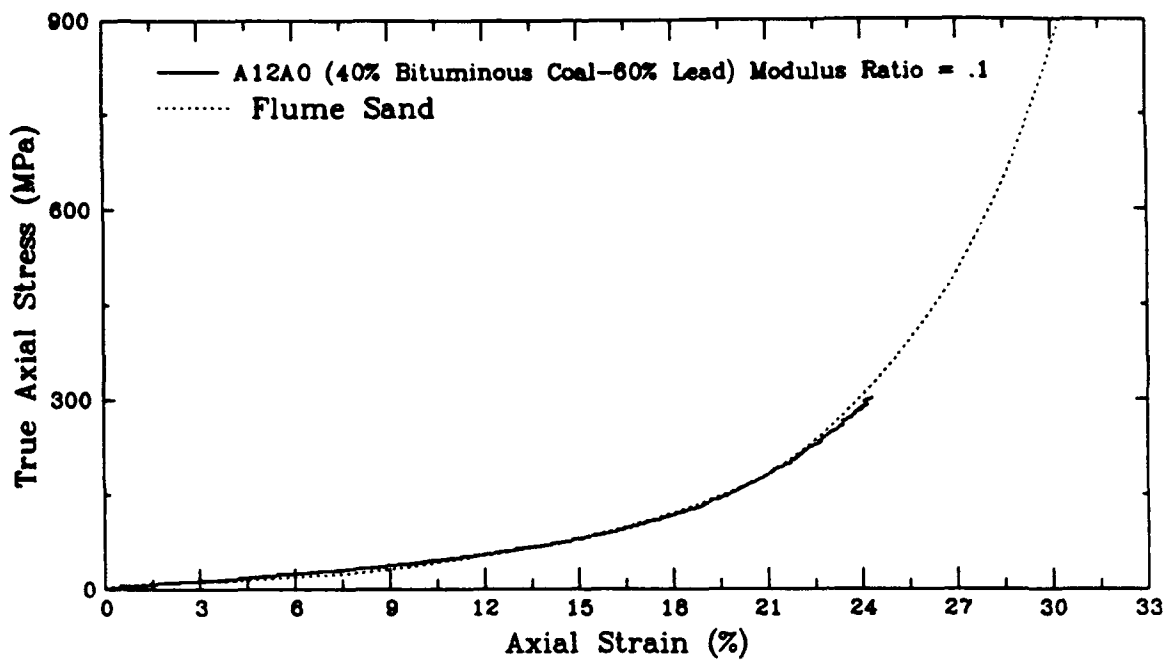
Figure 16. Comparison of Uniaxial Strain Behavior of WES Flume Sand with the Scaled
Response of Two Different 40/60 Bituminous Coal and Lead Specimens.

scale POP tests. Since similar coals with and without the addition of lead exhibit similar stress-strain behavior, the simulant data in Figure 16 are also recommended as representative of the pure coal behavior in the 1/3.5 scale POP tests. Table 6 summarizes the prototype sand and simulant material properties.

TABLE 6.   SUMMARY OF SAND AND SELECTED SIMULANT PROPERTIES
BASED ON LABORATORY TESTS

	Flume Sand	Coal	Lead/Coal 60/40 by wt.
Grain Density, kg/m^3	2640	1330	1330 (coal) 11300 (lead)
Porosity, dimensionless	0.39	0.4	0.4
Bulk Density, kg/m^3	1610	850	1850
Initial Constrained Modulus, MPa	230 - 375	20 - 40	20 - 40
Poisson's Ratio, dimensionless	0.34	0.34	0.34
Angle of Internal Friction	30°	31°	31°

G. STRUCTURE SIMULANT MATERIALS

As will be discussed in Section V, the decision was eventually made to construct the model structures of conventional concrete. For each of the three structures, the concrete section was designed such that its mass distribution correctly followed similitude. Structure stiffness was allowed to be greater than that suggested by similitude. Prior to arriving at that decision, a low-level effort was undertaken to identify appropriate simulants for concrete.

The objective of this effort was to find a concrete simulant with approximately one tenth the strength and stiffness and the same density as conventional concrete. From conventional practice, nominal values for prototype concrete are 28 MPa unconfined compressive strength, 25 GPa elastic modulus, and 2400 kg/m^3 density.

Three trial mixes, spanning a broad range of water cement ratios were tested. The mix designs are shown in Table 7. The aggregate for all three mixes was manually crushed dry bituminous coal from which all material that would not pass a No. 5 U.S. Standard sieve was removed. Type I, non-air-entraining cement was used. The trial batches were hand mixed in a bucket. Test specimens 77 mm in diameter by 127 mm long were cast in waxed cardboard molds, and tested after eight days.

TABLE 7. MIX DESIGNS FOR TRIAL CONCRETE SIMULANT BATCHES.

	Mix 1	Mix 2	Mix 3
Crushed Coal	9.53	9.54	11.5
Portland Cement	2.10	.954	.573
Water	2.34	2.33	2.98

Quantities shown are masses in kilograms of the respective material required to make approximately 0.01 m^2 of coal concrete.

The resulting strength and elastic modulus values are presented in Table 8. Of the three trial batches, the one that comes closest to the scaled criteria of 2.8 MPa strength, 2500 GPa stiffness, and 2400 kg/m^3 density is Mix 1. Its strength is approximately 50 percent high, the modulus is 8 percent low and the density is roughly half of the required density. This mix could possibly be used for 1/5 scale structures. Based on these test results, it appears likely that a mix could be devised which would much more nearly satisfy the design criteria. A denser aggregate, possibly lead or sand, would be substituted for some fraction of the coal aggregate. The water/cement ratio would be adjusted using the existing test data for guidance to obtain a mix of the required strength.

TABLE 8. TEST RESULTS FROM TRIAL CONCRETE SIMULANT MIXES.

	Mix 1	Mix 2	Mix 3
Unconfined Compressive Strength (MPa)	4.43	.690	.097
Elastic Modulus (MPa)	2324	116	10
Density (kg/m^3)	1262	1124	1107

No work beyond the first three trial mixes was performed under the current project. However, the results obtained thus far provide a good starting point for further investigation of concretes with coal and possibly coal/lead aggregates for Froude-scaled structures.

SECTION IV
STATIC PROOF-OF-PRINCIPLE TESTS

This section describes a test series designed to demonstrate the implementation of the Froude-scale concept under static loading conditions in which the response is sensitive to the influence of gravity. Electric cone penetrometer tests (ECPT) were conducted in specially prepared uniform test beds at three different scales, using three different materials. An existing set of data from full scale (1.4-inch (36 mm) diameter) ECPT work at the Misty Port III (MP III) field test site was used as the prototype. Two sets of Froude-scale tests were preformed in the laboratory, one with a length scale of 1/3.5 using crushed coal as the sand simulant, and the second in a coal/lead mixture at a length scale of 1/7.

The following paragraphs present the rationale for the experiment design, descriptions of the laboratory test apparatus and test procedures, and the results of the tests.

A. TEST DESCRIPTIONS

The electric cone penetrometer is a geotechnical exploration tool consisting of an instrumented probe and associated forcing and data recording equipment (See Figure 17). For the static Proof-of-Principle (POP) testing, three geometrically similar cone penetrometers of different sizes were used. Each has a 60° conical tip and is fastened to the bottom of a string of hollow push rods through which it is forced into the ground (or test bed) at a constant velocity. A section of each penetrometer is instrumented with strain gages in a full bridge configuration to form a load cell that measures only the force applied to the conical tip of the probe. Most cone penetrometers in common usage have an instrumented sleeve to measure frictional forces on the side of the probe and many penetrometers include additional instrumentation for other purposes. However, due to size limitations of the smallest cone, only the tip forces from all of the different sized cones were used in this application.

Electronic signals from the instruments located in the probe are transmitted to recording equipment at the surface by means of cables running through the push rods. Ectron signal conditioning amplifiers provided excitation voltage and amplification for the load cells. Spool type linear potentiometers were used to monitor the depth of penetration. Both the force and depth signals were recorded at close intervals using a Metrabyte DASH 16F analog to digital conversion board in a 80286-based computer where they were stored on disks for further processing and presentation. The digitization interval was approximately every 2 cm of depth in the prototype testing and correspondingly smaller in the subscale tests, providing an essentially continuous record of forces required to penetrate

40

F

Force Mechanism

Instrumentation
Cables

Test
Material

Depth

Instrumented
Cone
Penetrometer
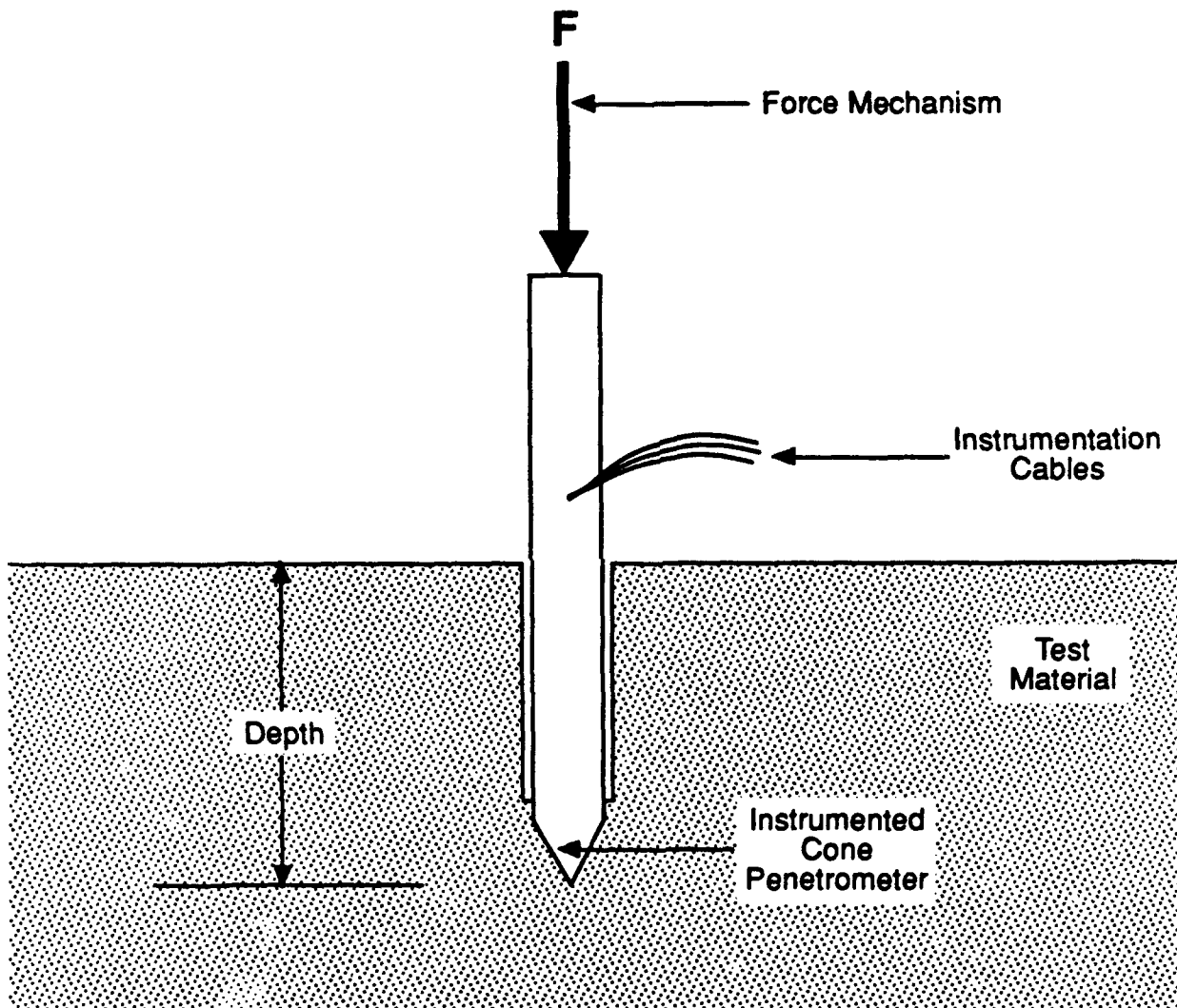
Figure 17. Simplified Proof-of-Principle Test Arrangement.

the soil strata. The tip load data are presented as tip stress which is defined as the axial load on the conical tip divided by the cross sectional area of the base of the cone.

For the static POP experiments, three scales were obtained by using three different sizes of cones in three different materials. Table 9 summarizes the dimensions and approximate properties of the materials used in the three tests. Since the equipment and materials used for the three scales of testing were significantly different, they are described individually in the following subsections.

TABLE 9. SUMMARY OF CONE PENETROMETER TEST CHARACTERISTICS.

Nominal Scale	Cone Diameter (mm)	Sand/Simulant Material		
		Type	Density (kg/m³)	Initial Constrained Modulus (MPa)
Prototype	35.7	Sand	1746	316
1/3.5	10.2	Coal	852	40
1/7	5.1	Coal/Lead	1845	40
Prototype	$n = 0.37$ $\upsilon = 0.22$ $\phi = 35° - 43°$ $w = 5\%$ (water content)			

1. Prototype Tests, Sand

An existing test data set was used to define prototype behavior. These prototype tests were conducted at the Misty Port III preevent test bed using ARA's standard size ECPT which is illustrated in Figure 18. This penetrometer has a diameter of 35.7 mm, conforming to ASTM D3441. It is mounted on a ten-wheel truck which has a total mass of approximately 23,000 kilograms and serves as a reaction mass for forcing the cone into the ground. The forcing is accomplished with a hydraulic load frame which transfers force to the push rods by means of a hydraulic head clamp. The push rods are 3 meters long, and a rod is added to the top of the string at the end of each 3 meters of push.

Figure 18. Illustration of the Prototype Scale Cone Penetrometer.

43

Misty Port III was conducted at the Phenomenology Test bed of the Defense Nuclear Agency Permanent High Explosive Test Site, located at White Sands Mi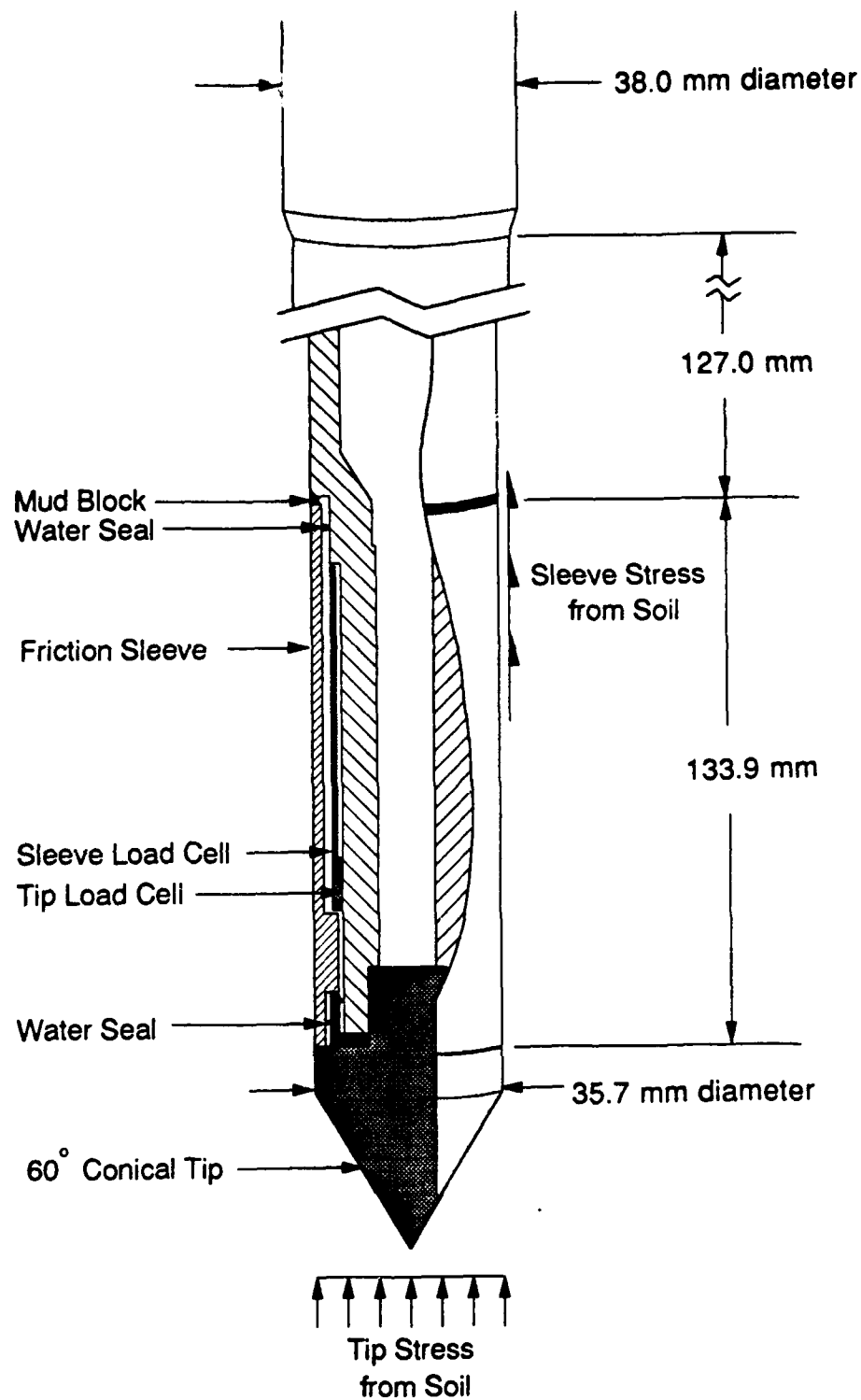ssile Range, New Mexico. The portion of the test bed from which the prototype data was taken was excavated to a depth of 7 meters then backfilled with a compacted fine-grained sand identified as Socorro Plaster Sand (Reference 6). Care was taken in test bed construction to achieve a density as uniform as possible. The approximate properties of the sand test bed are given in Table 9.

Four cone penetrations were made through the nominally uniform test bed. The individual records of the four tests are contained in Appendix C. Figure 19 presents the average of the four tests and the bounds at plus and minus one standard deviation.

2.   1/3.5 Scale Tests, Coal as Simulant

The first laboratory test of the static POP series was conducted using a specially constructed 10.2 mm diameter cone penetrometer in a test chamber filled with crushed bituminous coal. Figure 20 presents a disassembled view of the cone penetrometer. For use, the sleeve slips loosely over the load cell and the tip screws into the end of the penetrometer body. Since the narrow section of the penetrometer body is slightly longer than the sleeve, all the load on the tip is transferred through the load cell. Also, the frictional load on the sleeve is transferred to the shoulder above the load cell and thus does not influence the load cell measurement. Push rods fabricated from 1/4 inch nominal size (13.7 mm diameter) pipe with internal couplings were used to force the cone penetrometer into the test chamber. The push rods were 280 mm long, corresponding to the stroke of the hydraulic cylinder providing the force. As with the full scale ECPT system, a push rod was added to the load string at the end of each cylinder stroke. A special slotted fitting was used between the top of the push rod string and the hydraulic cylinder to allow for cable egress. The hydraulic cylinder used to force the penetrometer into the sand simulant was mounted on a load frame which was attached directly to the walls of the test chamber. The depth measurement, signal conditioning, and recording systems were the same as used in the prototype test.

The sand simulant in the test chamber was prepared from bituminous coal obtained from the same source as the material used in the laboratory material property tests and the dynamic field test. In preparation for placement in the test chamber, the coal was crushed to obtain an appropriate grain size distribution. As an objective, it was considered desirable to keep the grain size less than one tenth of the cone diameter. The coal was crushed in a mill consisting of two counter-rotating 76 mm diameter rollers set 1.6 mm apart. The resulting material had over 90 percent passing a U.S. Standard No. 16
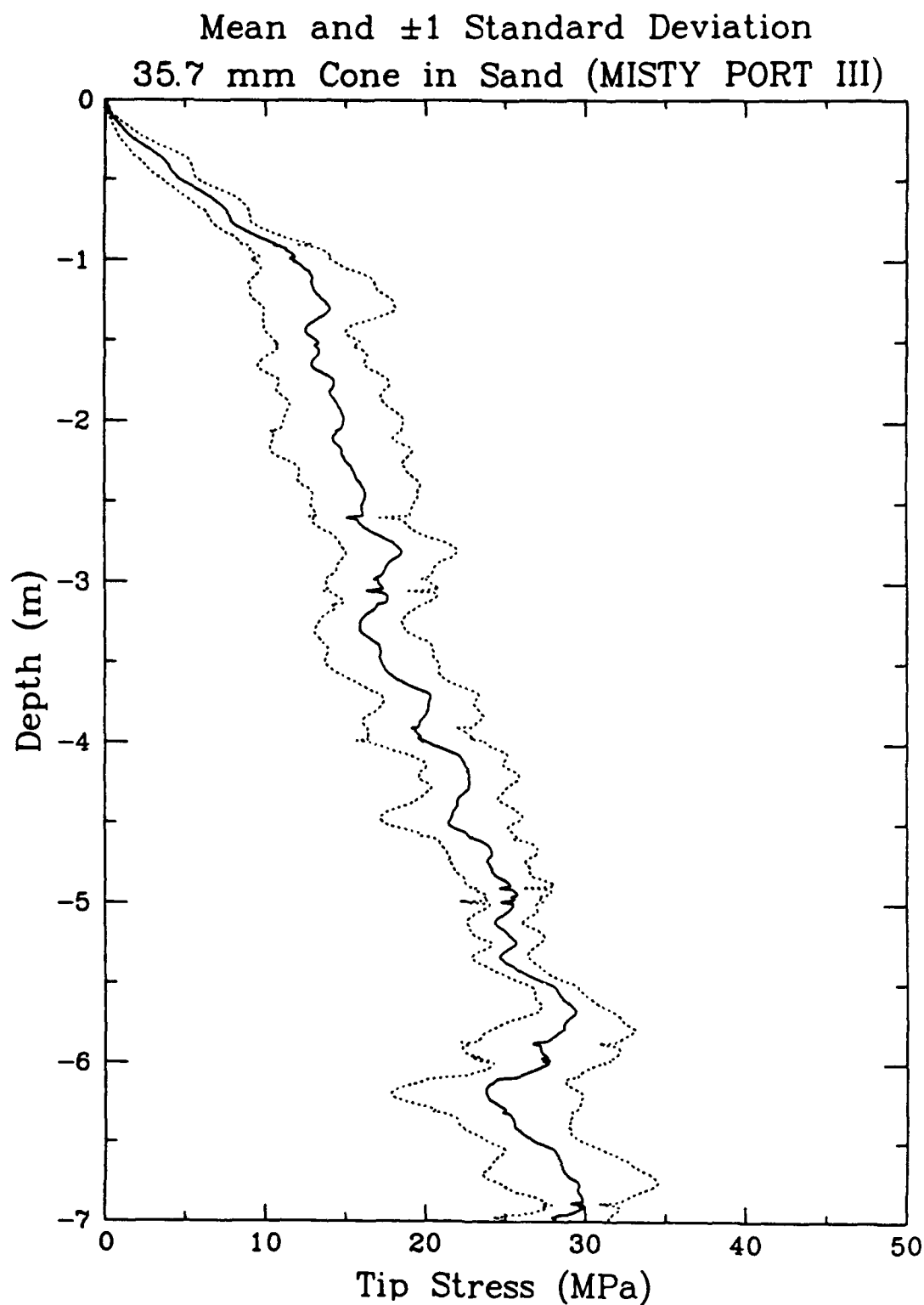
Figure 19. Mean and 1 Standard Deviation Bounds of Tip Stress Data from Prototype Scale Cone Penetrometer Tests in a Prepared Sand Testbed (MISTY PORT III).

10.2 mm Diameter Cone
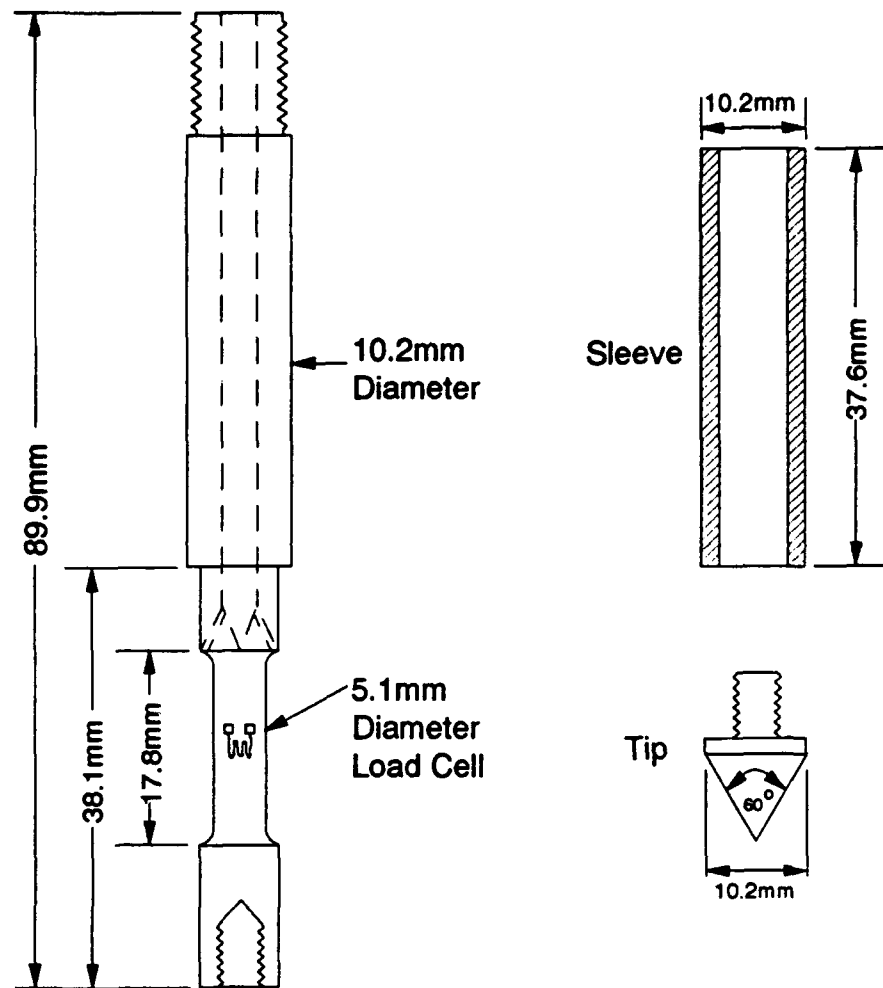

Figure 20. Disassembled View of the 10.2-mm Cone Penetrometer used in Laboratory Testing.

46

(1.0mm) sieve. On the fine end of the grain size distribution, 10 percent passed a No. 140 sieve (0.11 mm).

Previous research (Reference 10) indicates that the results of a cone penetrometer test in a test chamber are not affected by the chamber walls if the diameter of the chamber is 50 to 60 times the diameter of the cone. The test chamber was constructed of two 55-gallon drums with tops removed. The bottom was removed from one drum and fastened to the top of the other one. The drums have a diameter of approximately 575 mm, giving a diameter ratio of 56. To be consistent with the laboratory material property tests, a target density for the material in the test chamber was as 857 kg/m^3. To control the density, crushed coal was placed in the chamber in 100 mm lifts. For each lift, the required mass of the sand simulant was weighted and placed in the chamber. It was then lightly tamped to the required depth in the chamber. It was not always possible to achieve the desired density without crushing the coal, and thus the final average density was 852/kg/m^3, slightly below the desired value but well within the range of the laboratory tests. The final depth of coal in the chamber was 1.55 meters.

Four cone penetrometer tests were conducted in the simulant material thus prepared in the test chamber. The test holes were located so that each was well separated from the others and from the chamber walls. The tip stress records as a function of depth are presented in Appendix C. The mean tip stress for the four tests is presented in Figure 21, along with lines indicating the mean plus and minus one standard deviation. The variations in tip stress with depth at a frequency of one per 100 mm are apparently related to variations in density within the individual lifts of material that were placed in the container.

3. 1/7 Scale Tests, Coal/Lead as Simulant

The final static POP tests were conducted in a test chamber filled with a mixture of crushed bituminous coal and lead particles using a 5.1 mm diameter electric cone penetrometer. The penetrometer is illustrated in Figure 22. As with the larger penetrometers, the sleeve slips over the load sensing portion of the penetrometer body, isolating the load cell from all but the load on the conical tip. The load cell was formed by internally strain gaging a 2.6 mm diameter hole in the thinnest section of the penetrometer body. The internal strain gaging was performed by Strainsert of West Conshohocken, Pennsylvania. Push rods were fabricated from 6.4 mm diameter stainless steel tubing. The push rods were fabricated in 280 mm lengths, corresponding to the stroke of the hydraulic cylinder used to load the cone. It was originally intended that sections of rod would be added at the end of each push rod stroke as was the case with the larger penetrometers. However, due to the extreme fragility of the fine gage wires connected to the internal strain gage installation, this operation was judged to be impractical.
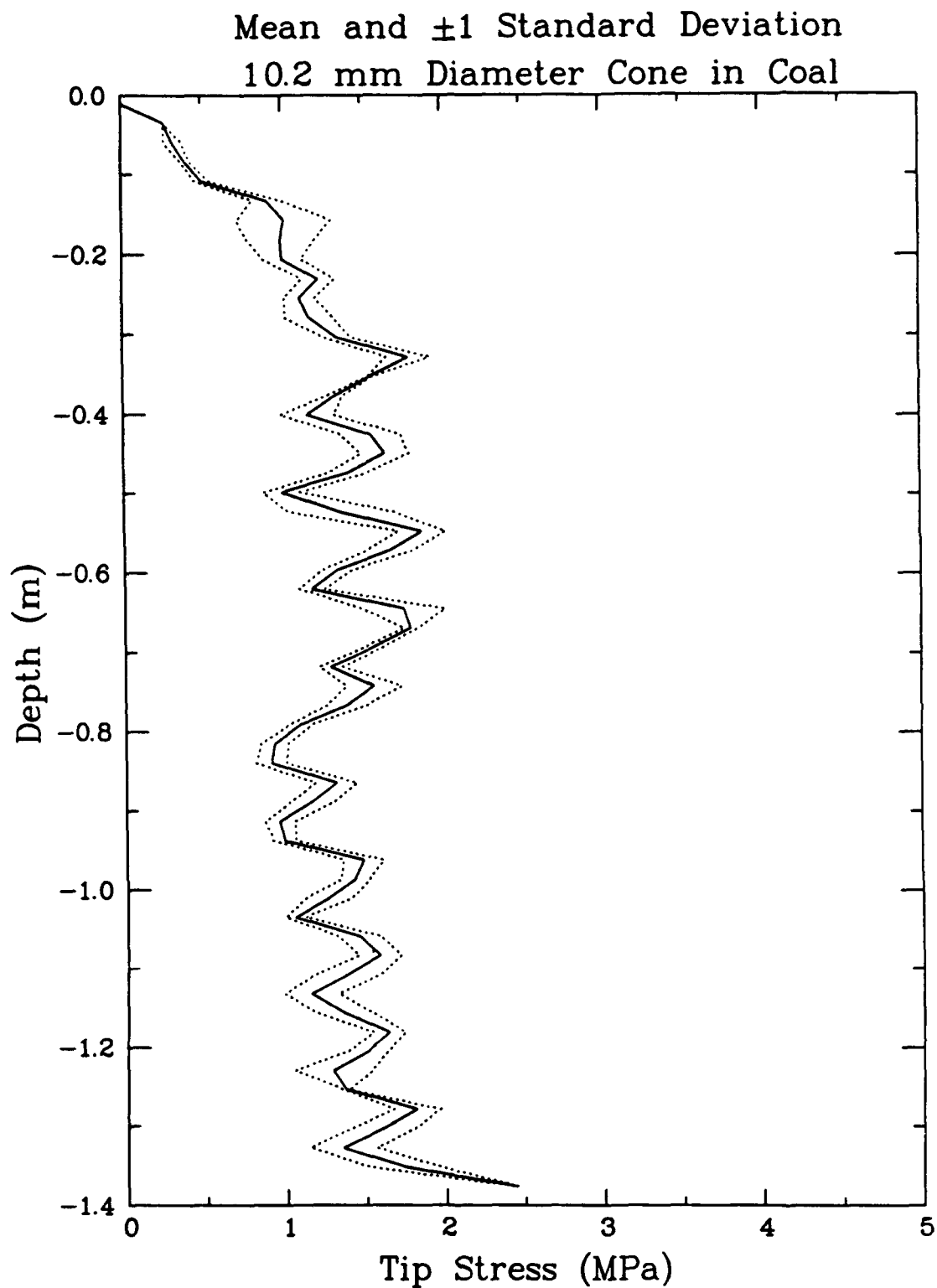
47

Figure 21. Mean and 1 Standard Deviation Bounds of Tip Stress Data from 1/3.5 Scale Cone Penetrometer Tests in a Laboratory Test Chamber Using Crushed Coal as the Sand Simulant.
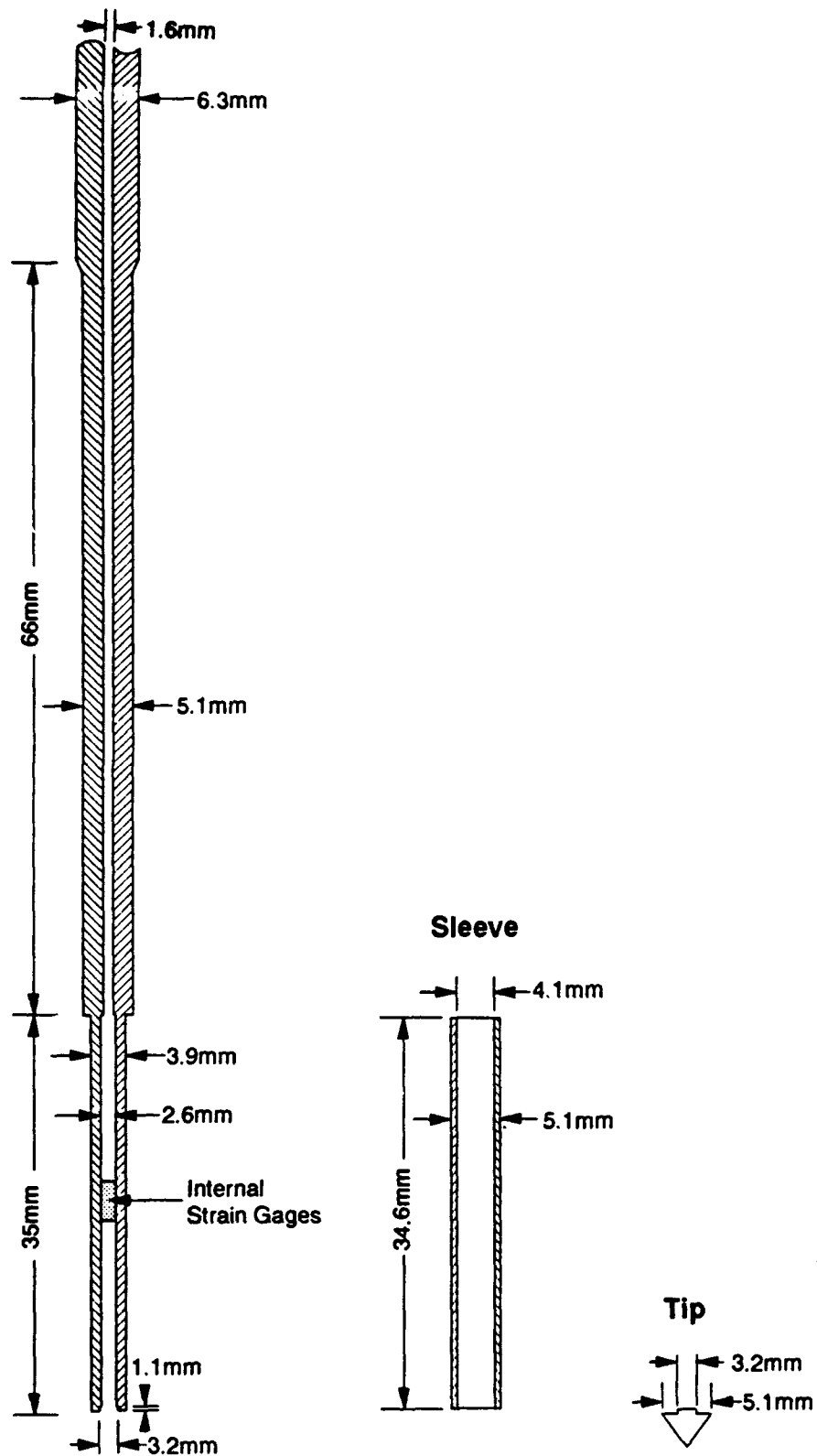
48

Figure 22. Disassembled View of the 5.1-mm Cone Penetrometer used in Laboratory Testing.

49

Since the full length of the push rod string was only about 1 meter, it was possible to conduct the test without disassembling it. A slotted fitting at the top of the rod string allowed for cable egress. As in the 1/3.5 scale test, a load frame was attached to the walls of the test chamber. In this case, it included a provision for height adjustment so that the tests could be performed without adding rod sections. Since the push rods were assembled and pushed as a single unit, it was necessary to employ a system of braces to maintain stability of the slender rod assembly during forcing. The depth measurement, signal conditioning, and recording systems were the same as in the prototype and 1/3.5 scale tests.

The sand simulant for the 1/7 scale static POP tests consisted of a mixture of crushed bituminous coal and fine lead particles, as described in Section III. The bituminous coal was first crushed as described earlier. The output of the crusher was passed through a U.S. Standard No. 20 sieve (0.71 mm), and everything that would not pass was discarded. In preparation for placement in the test chamber, the coal was then mixed with Free-Flow lead shot at a ratio of 40 percent coal to 60 percent lead, by weight.

The test chamber for the 1/7 scale test was made of a 305 mm diameter cardboard tube of the type used to form concrete columns. The ratio of diameters of the test chamber and penetrometer is 60, which is slightly larger than in the 1/3.5 scale test. The target density for preparation of the sand simulant in the test chamber was 1810 kg/m^3. Based on this density, quantities of lead and coal sufficient to form 25 mm lifts were weighed out and mixed together. This procedure was designed to insure that, on average, the coal and lead were distributed properly over the depth of the test chamber, even though there might be some non-uniformity of mixing within individual 25 mm layers. The final depth of material in the test chamber was 930 mm. The actual density achieved was 1845 kg/m^3. While this density is somewhat higher than desired, it corresponds to a porosity of 0.35 which was considered acceptable.

Four penetrometer tests were conducted in the coal/lead mixture with the 5.1 mm diameter cone. As with the 1/3.5 scale laboratory test, the test holes were located so that each was well separated from the walls of the test chamber and from the other test holes. Tip stress records as a function of depth are presented in Appendix C. Figure 23 presents the mean of three of the four tip stress profiles along with lines indicating the mean plus and minus one standard deviation. In one of the four tests, data were lost for a small segment of the test, making it impossible to include this test in the average.
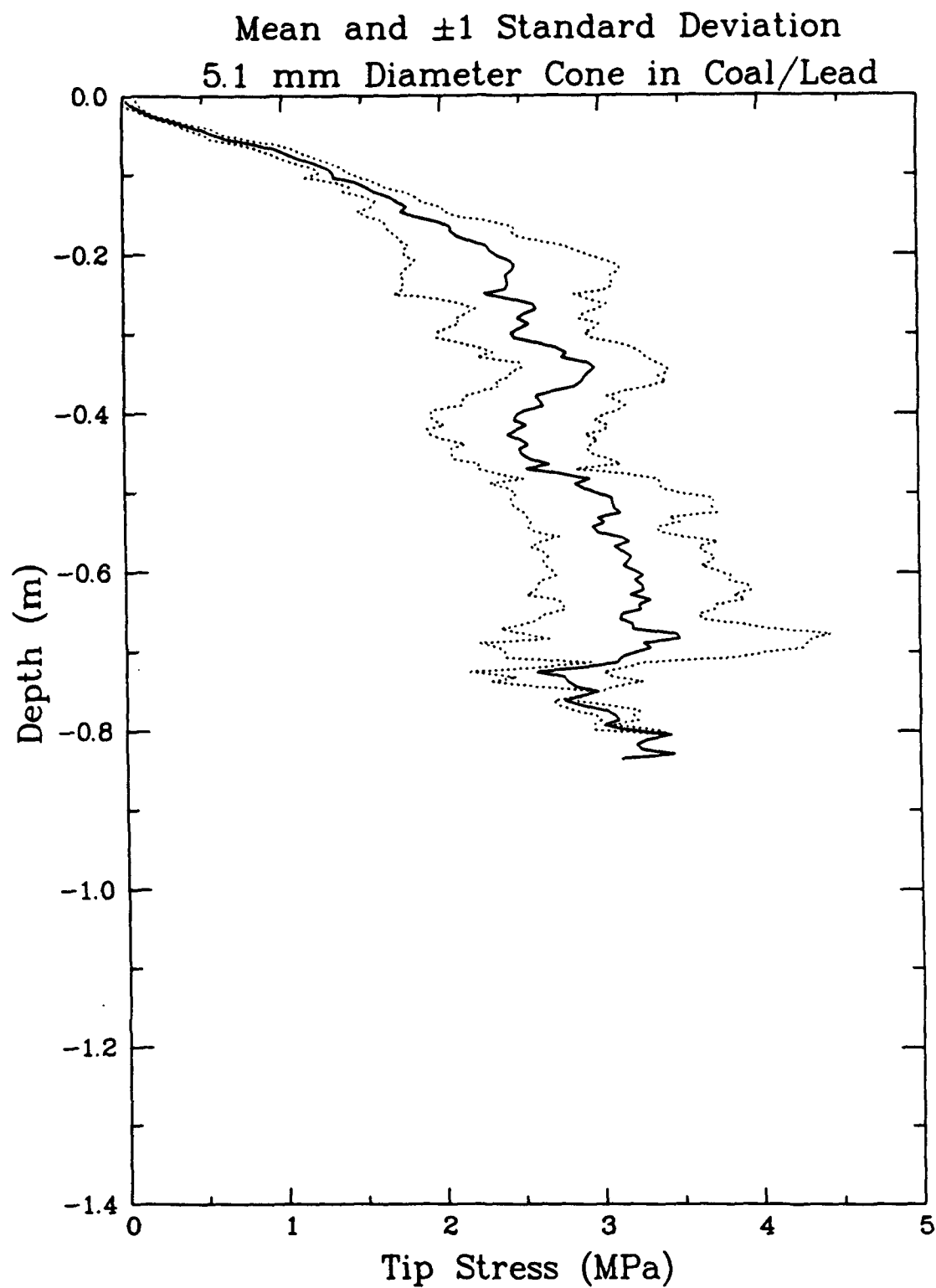
50

Figure 23. Mean and 1 Standard Deviation Bounds of Tip Stress Data from 1/7 Scale Cone
Penetrometer Tests in a Laboratory Test Chamber using a Mixture of Crushed
Coal and Lead as the Sand Simulant.

B. COMPARISON OF TEST RESULTS

If these tests had been completely Froude-scaled, it would be possible to compare the results by simply scaling the depth and stress data by their respective scale factors. However, the length scale factors of the cone penetrometers were somewhat different than the length scale factors derived from the material properties. The cones in the two model tests length scale to the prototype by factor of 1/3.5 and 1/7. The best estimate of the simulant scale factors based on incomplete knowledge of the material properties as they existed in the actual test beds is 1/3.9 and 1/8.3. In order to compare the results of the three tests as accurately as possible, they have all been converted to nondimensional quantities using the following expressions:

$$\text{Nondimensional Depth} = \frac{\rho g D}{M}$$

$$\text{Nondimensional Stress} = \frac{\sigma B \rho g}{M^2}$$

where:

B = penetrometer diameter

D = depth

M = initial constrained modulus

g = acceleration of gravity

ρ = dry bulk mass density of sand or simulant

σ = tip stress on cone penetrometer

The above nondimensional values were chosen because simpler nondimensional ratios such as D/B for depth and σ/M for stress are inappropriate since the tip diameter was not precisely scaled.

The mean tip stress data from the prototype tests in a prepared sand test bed, and the scale model test in chamber containing sand simulants are presented in nondimensional form in Figures 24 through 26. Figure 27 is a comparison of tests at the three different scales. The agreement among the three data sets is quite good. Comparison with the one standard deviation bounds shows that the variation among the tests at different scales is of the same order as the scatter in nominally identical tests.

The results of these static Proof of Principle tests provide encouragement for the use of coal and the coal/lead mixture as materials to simulate sand when applying the Froude scaling techniques. This approach can be used for static problems wherein the strength and stiffness characteristics of the material are determined primarily by the stress in the material, resulting from density, acceleration, and

52
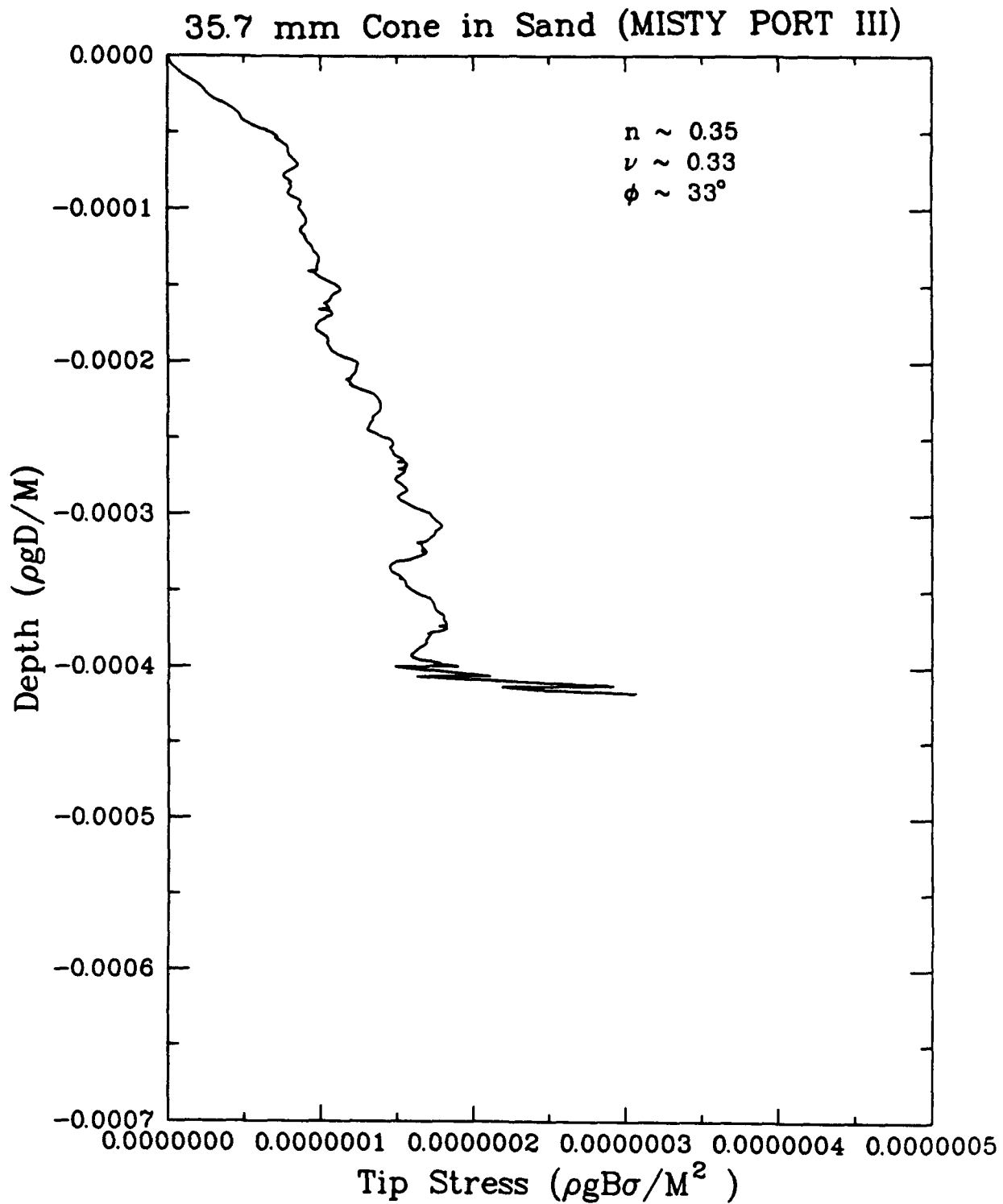
Figure 24. Tip Stress Data Plotted in Nondimensional Form from Prototype Scale Cone
Penetrometer Tests Conducted in a Prepared Sand Testbed (MISTY PORT III).

53
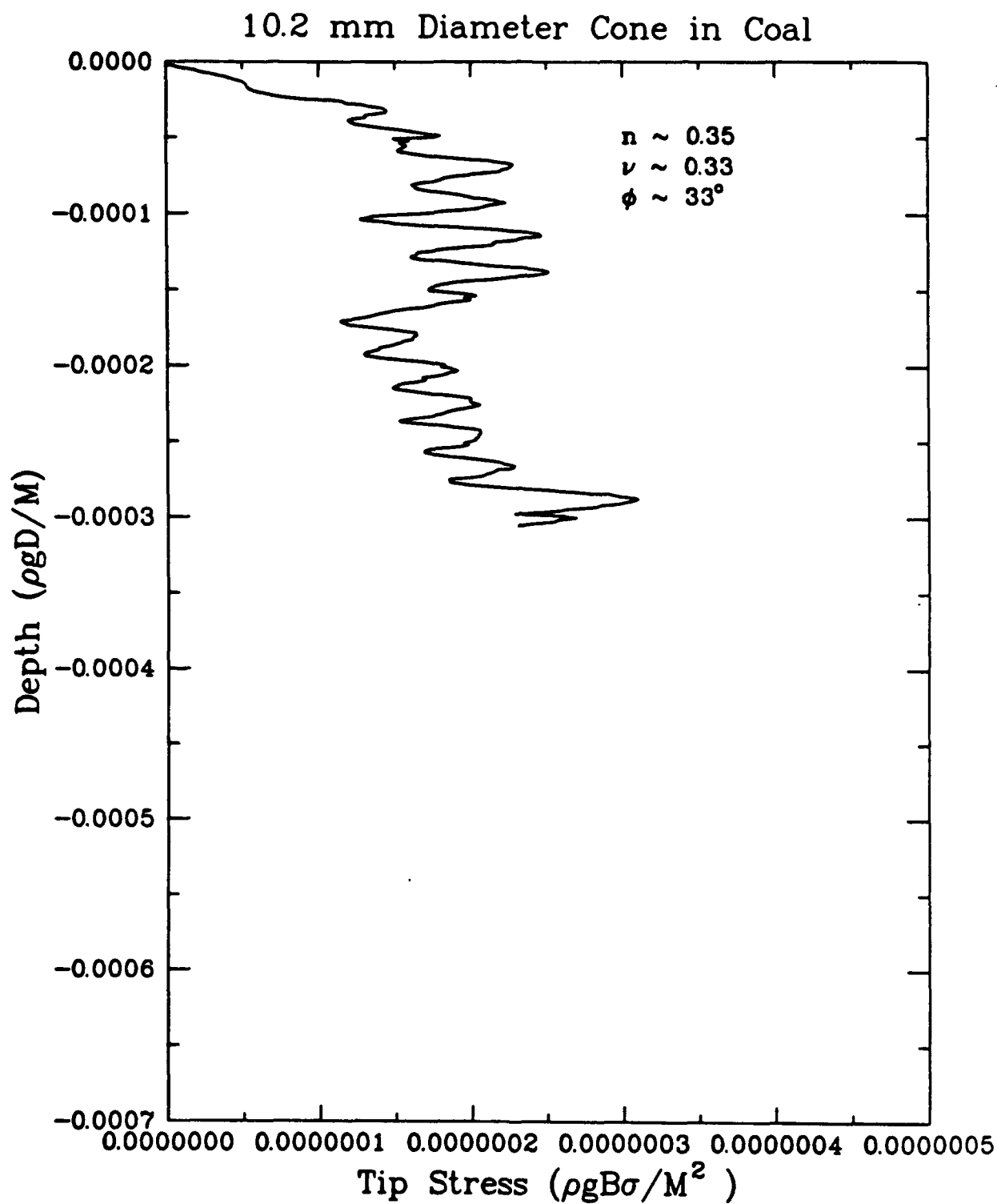
Figure 25. Tip Stress Data Plotted in Nondimensional Form from 1/3.5 Scale Cone Penetrometer
Tests Conducted in a Laboratory Test Chamber using Crushed Coal as the Sand Simulant.

54
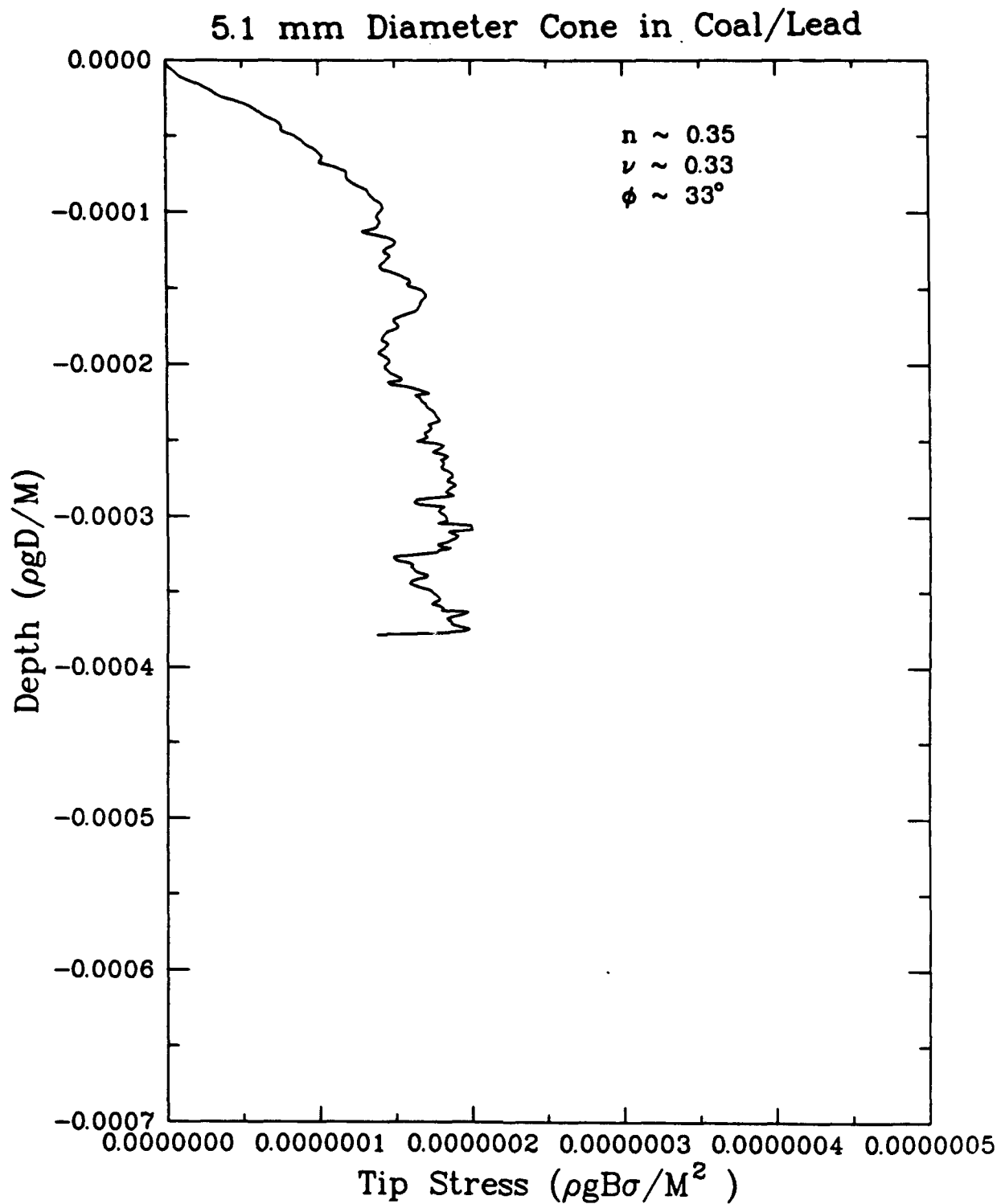
Figure 26. Tip Stress Data Plotted in Nondimensional Form from 1/7 Scale Cone Penetrometer Tests Conducted in a Laboratory Test Chamber using a Mixture of Crushed Coal and Lead as the Sand Simulant.
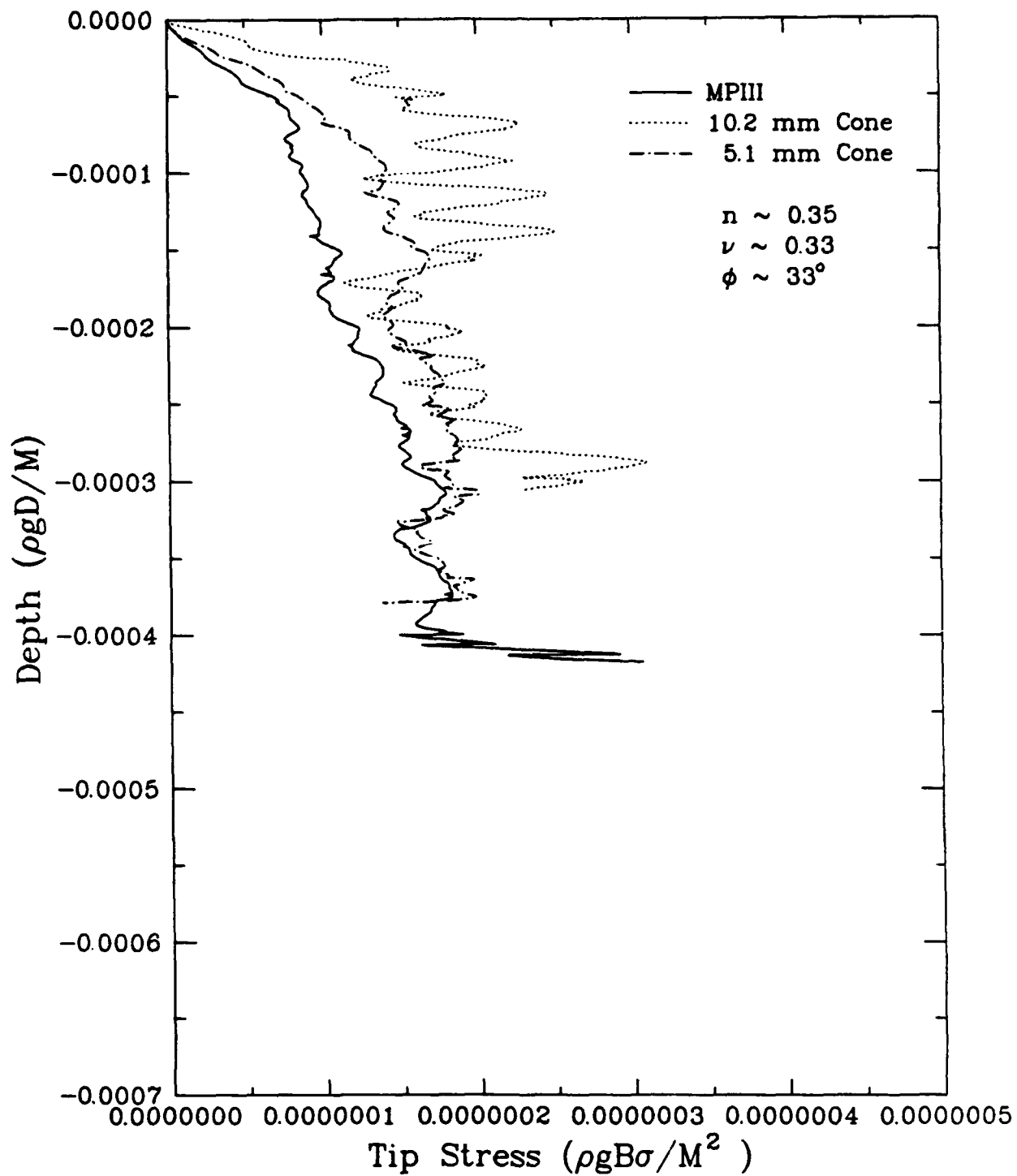
Figure 27. Comparison of Nondimensional Tip Stress Data from Cone Penetrometer
Tests at Prototype Scale and Two Reduced (Froude) Scales.

56

depth effects. Although the test was not performed, a Replica-scaled test using sand and subjected to the nominal acceleration of gravity would not have provided scaled results that compared favorably with the other scaled test results.

SECTION V
DYNAMIC TESTS ON BURIED CYLINDERS

A. TEST CONFIGURATION

1. Prototype System

Figure 28 describes the full-scale prototype system selected to be the basis for the scaled tests. The actual system consists of a buried reinforced concrete cylinder having an internal diameter of 2.5 meters and a wall thickness of 0.25 meters. This structure is a simplified version of a French designed Survivable Collective Protection Shelter (SCPS) that has been tested to conventional weapons effects. The prototype attack that was considered was a penetrating weapon that consisting of 500 kilograms of TNT detonated at a depth of 4.2 meters from the surface at a distance of 6.0 meters from the outer edge of the SCPS. The structure and weapon detonation are located in a sand material.

The explosive was chosen to be buried rather than placed on the surface because of the inability to Froude-scale the appropriate properties of air. The amount of explosive and distance from the SCPS were chosen to avoid damaging the structure. The depth of the explosion was chosen to allow essentially all of the energy to be deposited in the sand before venting to the atmosphere occurred (fully buried condition). Also the relative depth of the structure and the explosive allows for an approximately constant gravity stress to exist in the region where the peak stress is propagated from the explosion to the structure. The slightly higher elevation of the center of mass of the structure relative to the location of the explosion results in an upward component of structure motion that may prove to be beneficial when investigating the effect of gravity.

Use of this system as the basis for the experimental program will allow future comparisons of the response of various scaled systems to the observed behavior providing that adequate scaling parameters can be satisfied through the use of appropriate simulant materials for Froude-scaled tests and appropriate gravity effect adjustments for Replica-scaled test.

2. Scaled Systems

The initial Phase I effort investigating various materials that could possibly be used to Froude-scale earth and structural materials concluded that scale factors as low as 1/50 could be used when
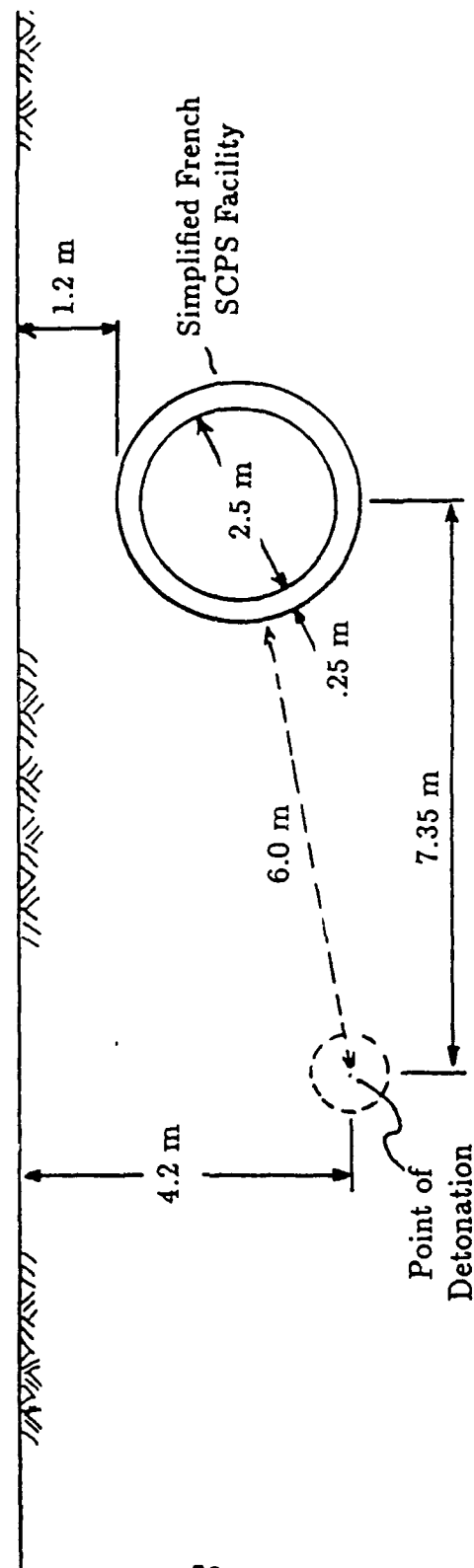
Figure 28. Full-Scale Prototype System, 500 kg TNT (Elevation View).

Simplified French
SCPS Facility

1.2 m

2.5 m

.25 m

6.0 m

7.35 m

4.2 m

Point of
Detonation

testing buried structures to conventional weapon effects. Using such a small scale would allow for many inexpensive tests to be performed to investigate the performance of a given structure to a multitude of weapon sizes and miss distances. This belief that a wide variety of scales could be used led to a planned Phase II effort consisting of many tests at three small scales.

The reality of the number of simulants found with the proper stiffness, density, Poisson's ratio, porosity, and angle of internal friction properties led to realization that scale factors of approximately 1/5 and 1/10 were the smallest currently available. Recognizing this fact lead to the selection of Froude-scale tests of 1/5 size using coal as the simulant for sand and of 1/10 size using the mixture of coal and lead as the sand simulant. By not attempting to reproduce the stiffness and strength properties of reinforced concrete, it was believed that representative size structures could be constructed to place in these tests.

The structure for the 1/10 Froude-scale event was geometrically scaled by 1/10 from the prototype and was constructed of reinforced concrete. Thus, the mass of the structure was approximately correct but the stiffness was about ten times too large.

The structure for the 1/5 Froude-scale event required some compromises. By choosing to use reinforced concrete as the cylinder material, consistent Froude scaling required that the mass of the structure be about 1/2 (same as coal/sand density ratio) and the stiffness be 1/10 (same as the coal/sand stiffness ratio). Choosing the external diameter to be scaled by 1/5, the thickness was halved from the scaled value. This results in a structure having 1/2 the mass, 1/2 the stiffness on the hoop direction and 1/8 the bending stiffness of the prototype structure.

A third test was required by the contract. Rather than adjust the ratio of coal and lead to achieve another scale factor, it was decided to have the third test be a 1/10 Replica-scaled test, recognizing that gravity could not be properly scaled thus resulting in a distorted model. The results of this test could be scaled up to the prototype size as were the Froude-scaled test results and any obvious differences could be readily identified. In all tests, the length of the structure was somewhat arbitrarily taken to be 10/3 times the external diameter, a compromise between the very long length of the actual system and the economics associated with the test size.

The sizes of the test beds were also based upon economic considerations. The test bed dimensions were chosen so as to faithfully reproduce results of a prototype system to a time of 40 milliseconds. This corresponds to 4 ms for 1/10 Replica-scaled test, 17.9 ms for 1/5 Froude-scaled test and 12.6 ms for the 1/10 Froude-scaled test (see Table 2).

60

The dynamic testing was performed at the ARA test site near Denver, Colorado, by personnel of the ARA Rocky Mountain Division.

3. Equivalent Scaled Explosive Charges

True Froude scaling of explosives requires that the energy density of the explosive vary by the same ratio as the stress factor. Such explosives are not commercially available.

The required TNT charge sizes for the 1/10 and 1/5 Froude-scaled experiments and the 1/10 Replica-scaled experiment respectively are 50, 400 and 500 grams based upon the scaling laws presented earlier in Table 2 with respect to the prototype value of 500 kg. A bomb case was not simulated. C-4 was chosen as the explosive because it is moldable, does not require a container, and is a relatively safe explosive material. Changes as small as 50 grams can be successfully detonated with a single RP-2 detonator. Table 10 lists the equation of state parameters for TNT and C-4 from Reference 8.

TABLE 10. THEORETICAL EXPLOSIVE PROPERTIES

	TNT	C-4
CJ Parameter		
ρ_o, g/cm^3	1.63	1.601
P, Mbar	.210	.28
D, cm/m sec	.693	.8193
E_o, Mbar cm^3/cm^3	.07	.09
JWL Parameter		
A	3.712	6.0977
B	.03231	.1295
C	.01045	.01043
R_1	4.15	4.5
R_2	.95	1.4
W	.30	.25

The C-4 charge weight required is lower than that of TNT because of the higher energy released per unit volume (E_o) of C-4. The volume of the RP-2 detonator is approximately .0157 in^3 (.257 cm^3). The charges were molded by hand to a spherical configuration with a detonator hole made to nominally center fire the charge.

The weights of C-4 not including the detonator, and the radii of the spheres required are given in Table 11.

TABLE 11. EXPLOSIVE CHARGE SIZES

	TNT Weight	C-4 Weight	Radius
1/10 Scale, Froude	50 grams	39 grams	1.8 cm
1/0 Scale, Froude	400 grams	310 grams	3.6 cm
1/10 Scale, Replica	500 grams	390 grams	3.9 cm

The charge was molded to be in intimate contact with the detonator. The placement of the charges was critical both for the proper environment to be created at the structure and to maintain the consistent properties of the testbed material. The charges were placed after the main testbed had been constructed for safety and operational purposes. During the construction of the testbed, a PVC pipe was installed at the location where the charge is required. After the testbed construction was completed and the charge was ready to be installed, the explosive charge with the detonator installed, was lowered down the pipe. With the charge in place, the pipe was backfilled and compacted as appropriate with the simulant material. As this filling took place, the PVC pipe was slowly withdrawn to ensure a mixture as homogeneous as possible within the testbed. The charge was then armed according to normal operational procedures as outlined in the Safety Plan (Reference 7).

A concern was expressed that the hot explosive gases could potentially ignite some of the coal dust in the Froude-scaled material. While the explosive gases may be quite hot, they contain little if any oxygen and burning or detonation of the coal dust would have to proceed using the oxygen in the pore air. A study was performed that indicated that less than 0.1 percent additional energy could be added by coal dust detonation around the explosive charge even for ideal conditions.

4. Test Predictions

The objective of this experimental project was to obtain data on the propagation of shock waves in materials believed to simulate sand using Froude scaling procedures and to obtain data on the rigid bodies motion response of a buried structure. To obtain good test results, predictions of the peak values of acceleration and stress were required. Few gages could be installed and safety factors higher than normal had to be applied to prevent gage damage or data loss because of measurement system saturation.

Peak free-field acceleration and stress estimates were obtained from the equation in the AFESC Report, Protective Construction Manual: Ground Shock and Cratering (Section V) (Reference 9). The parameters used in the equations were based upon a fully coupled burst in dry sand and for the full scale, 500 kilograms burst. The predictions for the accelerations of the structure were based on the free-field value closest to the structure.

The predicted values for the specific test events were based upon the predicted values for a full scale as determined above and applying the appropriate scaling factors for each test. A summary of the prediction used for selecting and installing gages is given in Table 12. Detailed predictions for each test based upon two other methods, one assuming the free-field material to be a perfectly locking solid and the other based upon a finite-element calculation are presented in Appendix D.

TABLE 12. PRETEST PREDICTIONS

Gage *	Predicted Peaks		
	1/10th Replica	1/5th Froude	1/10th Froude
A1 (X407)	7,060 g's	706 g's	706 g's
A2 (X408)	7,060 g's	706 g's	706 g's
A3 (X406)	3,580 g's	358 g's	358 g's
A4 (X405)	3,580 g's	358 g's	358 g's
A5 (X401)	3,580 g's	358 g's	358 g's
A6 (X402)	3,580 g's	358 g's	358 g's
A7 (X403)	3,580 g's	358 g's	358 g's
A8 (X404)	3,580 g's	358 g's	358 g's
A9 (X301)	69,800 g's	6,980 g's	6,980 g's
A10 (X302)	11,100 g's	1,110 g's	1,110 g's
A11 (X303)	69,800 g's	6,980 g's	6,980 g's
A12 (X304)	69,800 g's	6,980 g's	6,980 g's
A13 (X305)	7,060 g's	706 g's	706 g's
SS1 (X501)	N/A	12.10 MPa	12.10 MPa
SS2 (X502)	17.4 MPa	1.74 MPa	1.74 MPa
SS3 (X503)	7.4 MPa	0.74 MPa	0.74 MPa
SS4 (X504)	4.1 MPa	N/A	N/A

* X = 1, 2, or 3 depending on test.

5. Test Instrumentation

Instrumentation for the true model of gravity tests consisted of free-field accelerometers, free-field soil stress gages and an instrumented structure. The selection of transducers was based on response, acceptable signal to noise ratios, and availability.

The use of both accelerometers and stress gages in the free-field will increase the probability of ensuring acquisition of some data. Gages are placed at six different ranges from the charge in order to get multiple time-of-arrival data and free-field values and within the structure. The combination of shock velocity and peak particle velocity versus range assisted in determining the validity of the measurements themselves and the proximity of the simulant material properties to the intended values. The free-field data also assisted in checking the energy released by the explosive. Endevco Model 7270 piezoresistive shock accelerometers were used for all free-field acceleration measurements. Their low mass, extremely small size, and high resonant frequency allow them to measure high shock values. Kulite's LQV-080UH soil stress gage were used for all soil stress measurements. Both of these transducers have been used successfully to make similar measurements in the past. These transducers were ranged to the maximum signal expected. The placement of the lower priority free-field accelerometers above and below the charges in each of the tests would assist in determining the magnitude of free surface effects and will also offer some degree of redundancy for the close-range accelerometer measurements.

The emphasis given to structural instrumentation is threefold. The orthogonal measurements placed at each location are in anticipation of strong upward components of the structural motion in addition to the strong radial motions from the explosive source. The strength of the upward motion will be controlled by the counteracting forces of gravity and free surface effects. Secondly, the placement at the four principle locations around the structure is to determine the relative contribution of flexural response (which should be small) and rigid body motion. Lastly, the configuration of structural instrumentation allows for some degree of redundancy.

Instrumentation for the structures required the use of eight accelerometers per structure. For measurements with predictions of 680 g's and above, Endevco Model 2264A accelerometers were used. Six of the eight structure acceleration measurements on the Froude-scale tests had predictions of 380 g's. For these measurements, Endevco Model 2262 dynamic piezoresistive accelerometers were used since these accelerometers have a much higher sensitivity than the 2264A, while still having very good frequency response.

Each structure accelerometer was hard-mounted to a 7075 aluminum mount bolted and epoxied into the structure after construction. This technique provided good coupling between the structure and gage mount. Free-field accelerometers were mounted in WES micro tapered plug canisters.

65

All accelerometers were calibrated pretest using the Endevco Model 2965C shock motion calibrator. The 2965C calibrator offers an accurate, yet simple method of calibrating piezpresistive accelerometers. It is designed to be used with a Model 2270 accelerometer standard. The calibration of the Model 2270 is traceable to the National Bureau of Standards. The operation of the calibrator involves dropping a steel ball approximately 2 feet to strike an anvil on which the Model 2270 standard and test accelerometer are attached. The two readings are then compared and a sensitivity is assigned to the test accelerometers. Comparison calibrations can be performed at accelerations from 20 to 10,000 g.

Alpha No. 1122, four conductor, shielded cable was spliced to transducer pig-tails and run approximately 50 feet to a J-Box. The first 20 feet of this cable was run through 1/8 inch stainless steel and 1/4 copper tubing. This technique allowed adequate cable protection in the testbed area. The trunkline cable from the J-Box to the I-Van consisted of 20 runs of Belden 8728, four conductor, shielded cable.

Placement of the transducers was completed during construction of the testbed. A grid was set up at the top of the testbed using string. The locations of the grid lines correspond to transducer locations. Depth to the gage location was measured using a plumb line placed at overlapping gridlines.

As the test bed was built up, the free-field transducers and canisters were placed at the proper level and position. Before placement, the quality of each transducer was verified by confirming that the polarity was correct and recording the bridge resistance. A plumb line and angle meter were also used to set the proper angle of inclination or declination as needed.

Structure placement was completed in a similar manner. The testbed was built up to the proper level. Two plumb lines were used to place the structure. The first plumb line was located at the grid location that corresponds to the center of the structure, to ensure proper x, y, z alignment. The second plumb line was located at the grid location that corresponded to one end of the structure to ensure that the proper angle of inclination with the charge was obtained.

The signals from the piezoresistive transducers were conditioned with Ectron Model 563F signal conditioners. These signal conditioners allow selection of excitation voltage levels, calibration resistors, low pass filter cutoff frequency, and gain. They feature a low-noise, high common mode rejection ratio, and a band width up to 100 kHz.

66

Two Honeywell Model 101, 14-track analog magnetic tape recorders were used for primary recording of the test data. The recorders were set up with Wide Band group II record and reproduce heads and electronics. A tape speed of 120 inches per second was used. This speed will give a 500 kHz bandwidth.

B. 1/10 REPLICA-SCALED EVENT - SAND TESTBED

Figures 29 and 30 present the testbed layout for the 1/10 Replica-scaled test event. The backfill in the testbed was mortar sand, locally procured from Pioneer Landscaping materials, Littleton, CO. The material approximately satisfied the grain size distribution determined for Flume sand. It was clean, (i.e., less than 5 percent passing a No. 200 sieve). It was fairly fine and uniform. It had at least 90 percent passing a No. 20 sieve, and its coefficient of uniformity, C_U, less than 4. C_U is defined as follows:

$$C_U = \frac{D_{60}}{D_{10}}$$

(18)

Where:

D_{60} = the size at which the grain size distribution curve shows 60 percent passing.

D_{10} = the size at which the grain size distribution curve shows 10 percent passing.

Because of the small size of the testbed, compaction was obtained by hand tamping using a metal plate about 1-foot square.

The Figures 31 and 32 show the location of the instrumentation. Figure 33 shows details of the structure which was geometrically scaled from the prototype. The explosive charge was 0.39 kilograms of C-4 explosive. On the first attempt to detonate the explosive, the RP-2 detonator only blew a cavity in the explosive and failed to detonate the C-4. On this test and subsequent tests, a booster of about 2 grams of DETASHEET was used around the detonator.

Figure 34 shows the reinforced concrete cylinders with the accelerometers mounted at the four quadrants within the cylinder. Figure 35 is an exterior view of the same structure. A free-field accelerometer package and the tubing protecting the cables (laid away from the charge) is shown being installed in the testbed in Figure 36. A view of the testbed with the structure being installed is given in Figure 37, Also note that vertical poles are located and attached at each end of the cylinder. A sloping PVC pipe has also been installed to allow the testbed to be built up to the desired elevation prior to
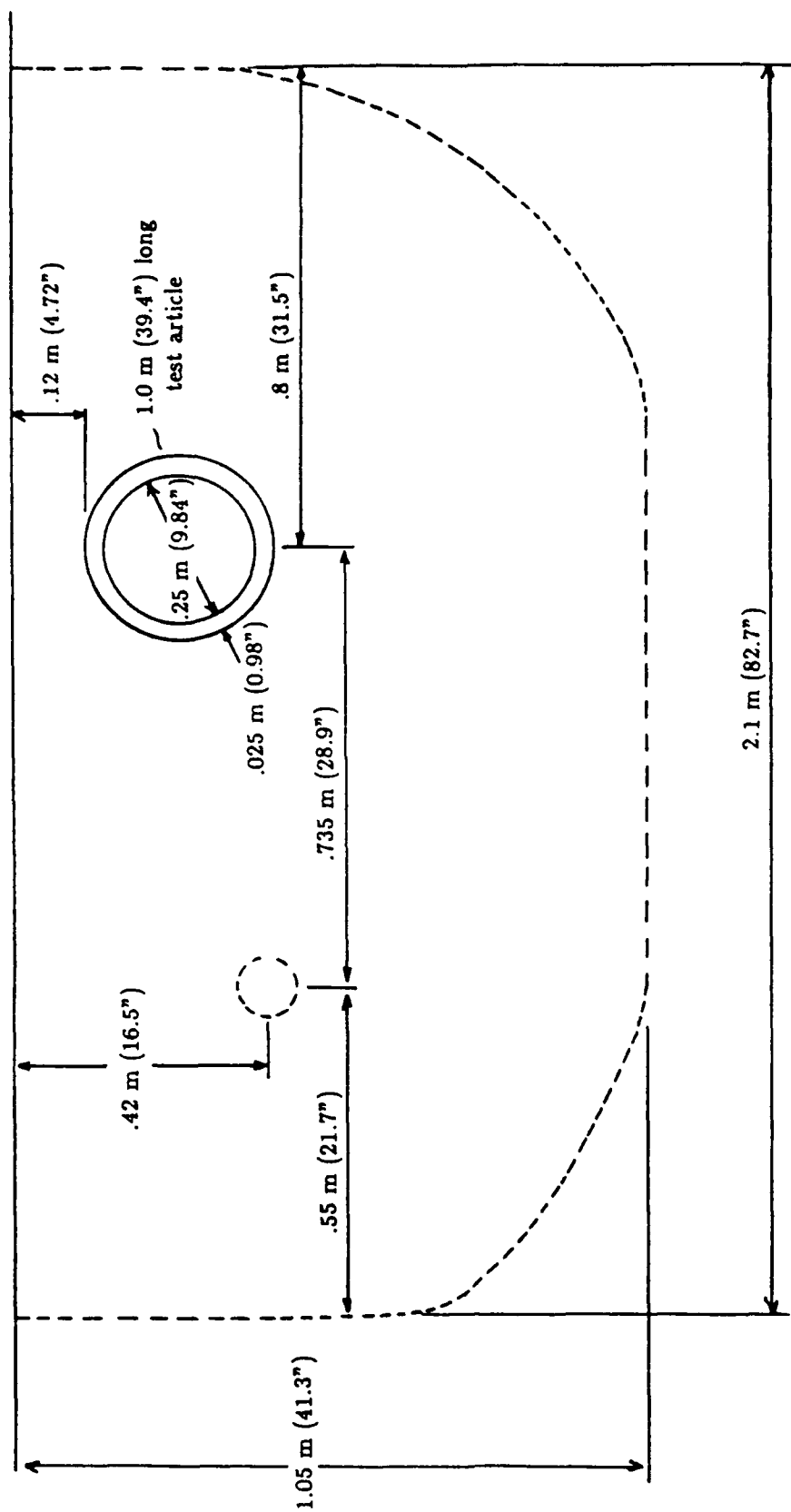
67

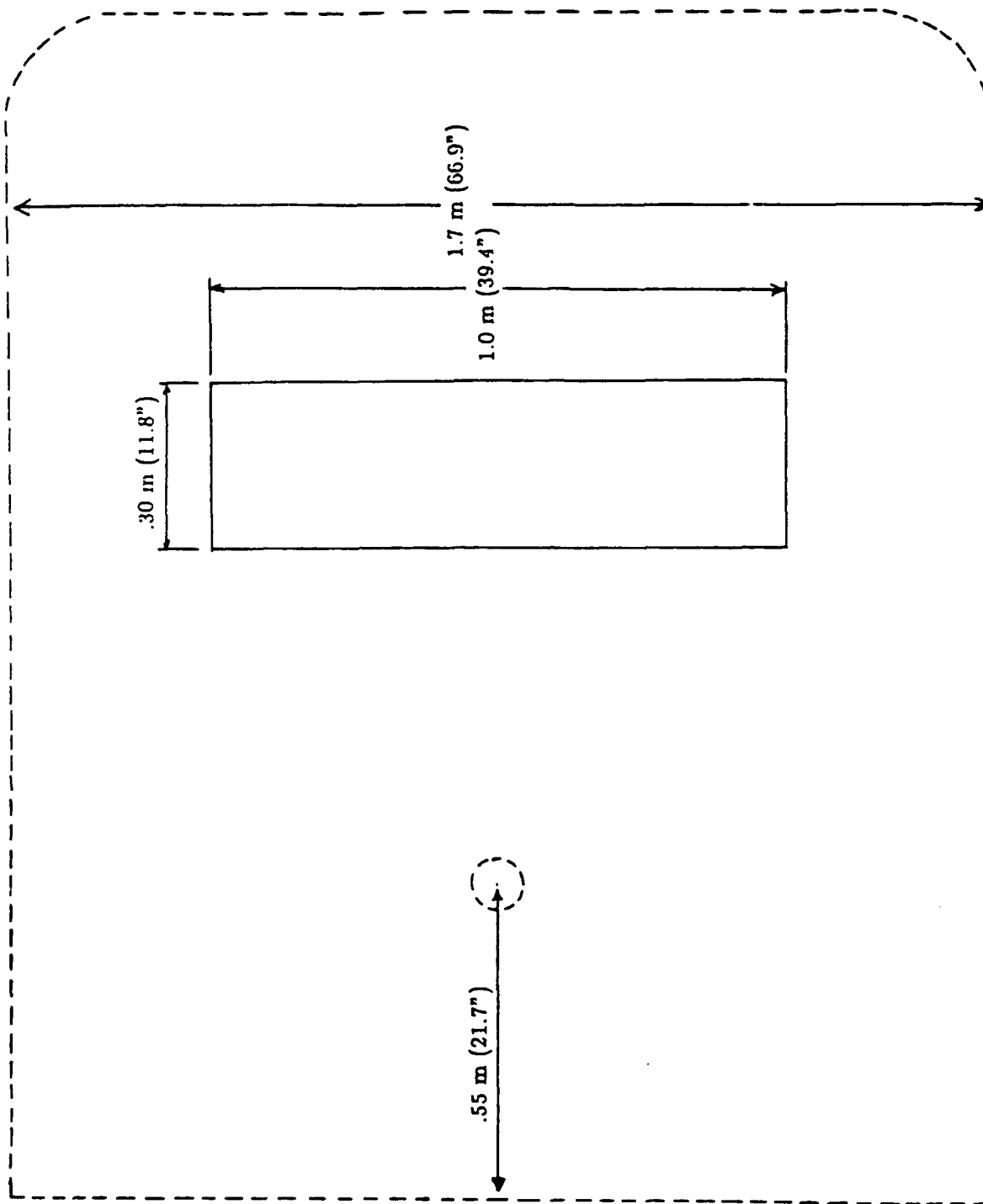Figure 29. 1/10th Replica-Scale Testbed (Elevation View).

.12 m (4.72")

1.0 m (39.4") long test article

.8 m (31.5")

25 m (9.84")

.025 m (0.98")

.735 m (28.9")

.42 m (16.5")

.55 m (21.7")

2.1 m (82.7")

1.05 m (41.3")

Figure 30. 1/10th Replica-Scale Testbed (Plan View).

1.7 m (66.9")

1.0 m (39.4")

.30 m (11.8")

.55 m (21.7")
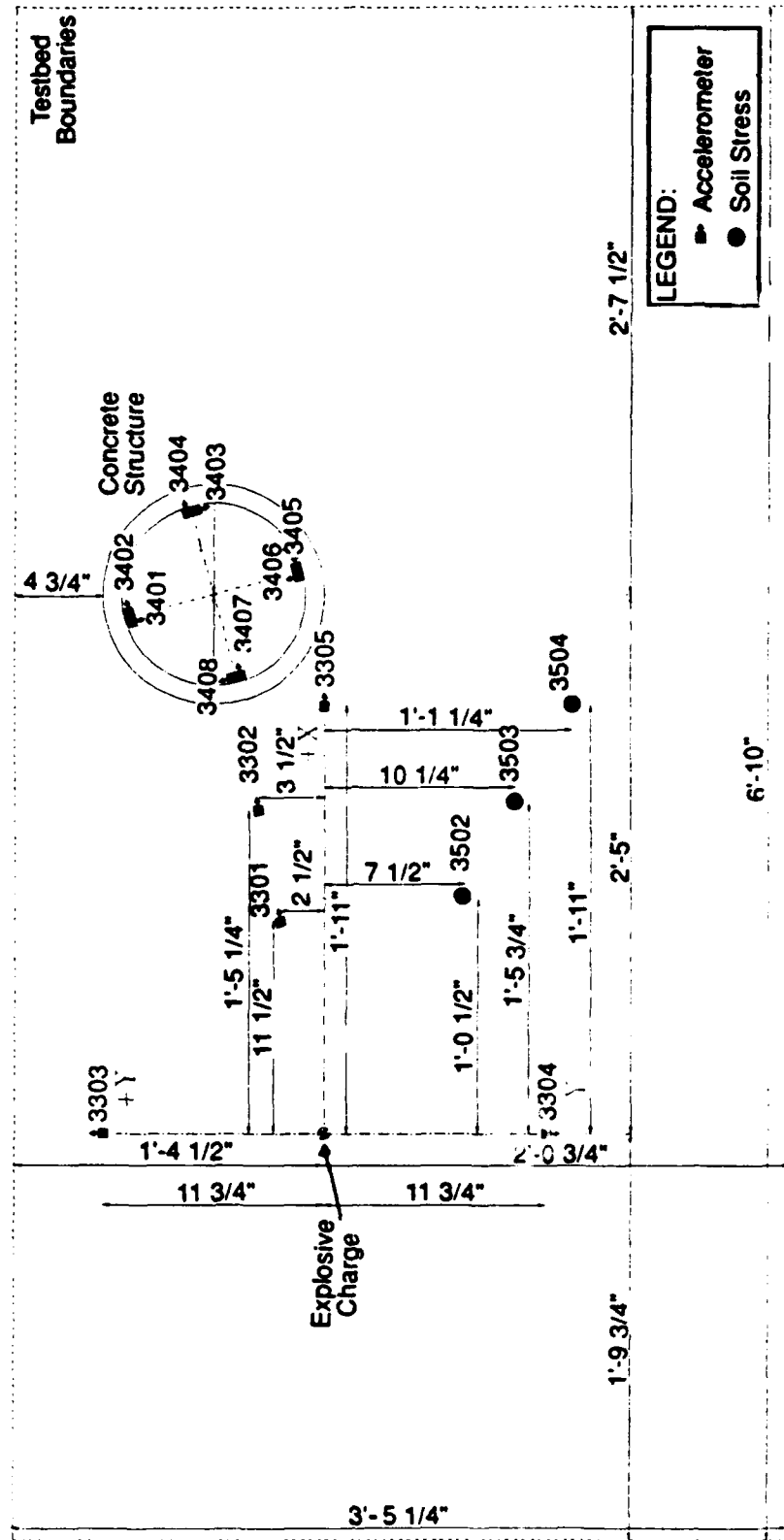
Figure 31. 1/10th Replica-Scale Testbed (Elevation View).

* Actual Location and orientation for gage 3303 uncertain.

Figure 32. 1/10th Replica-Scale Testbed (Plan View).

71
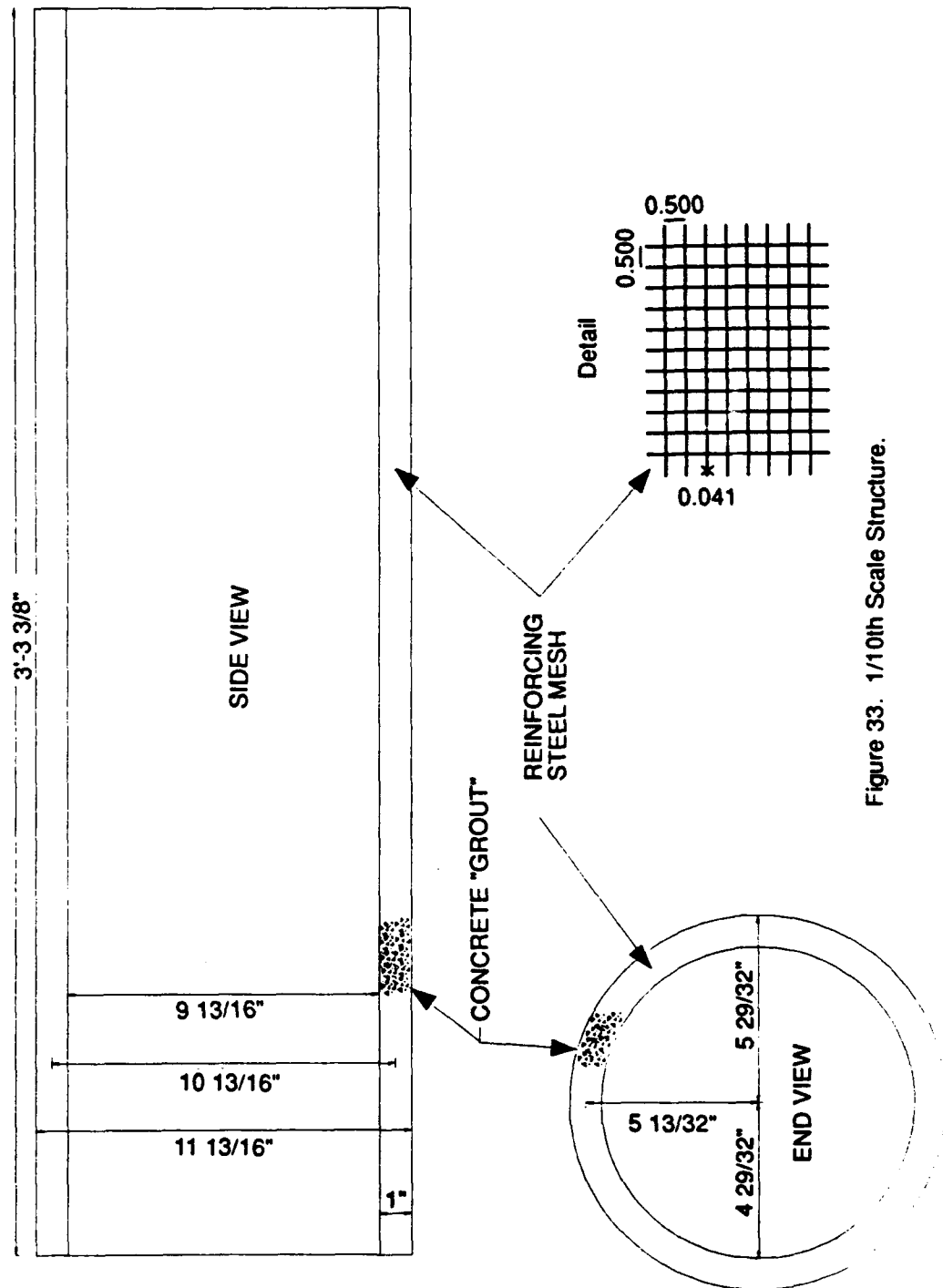
Figure 33. 1/10th Scale Structure.

72
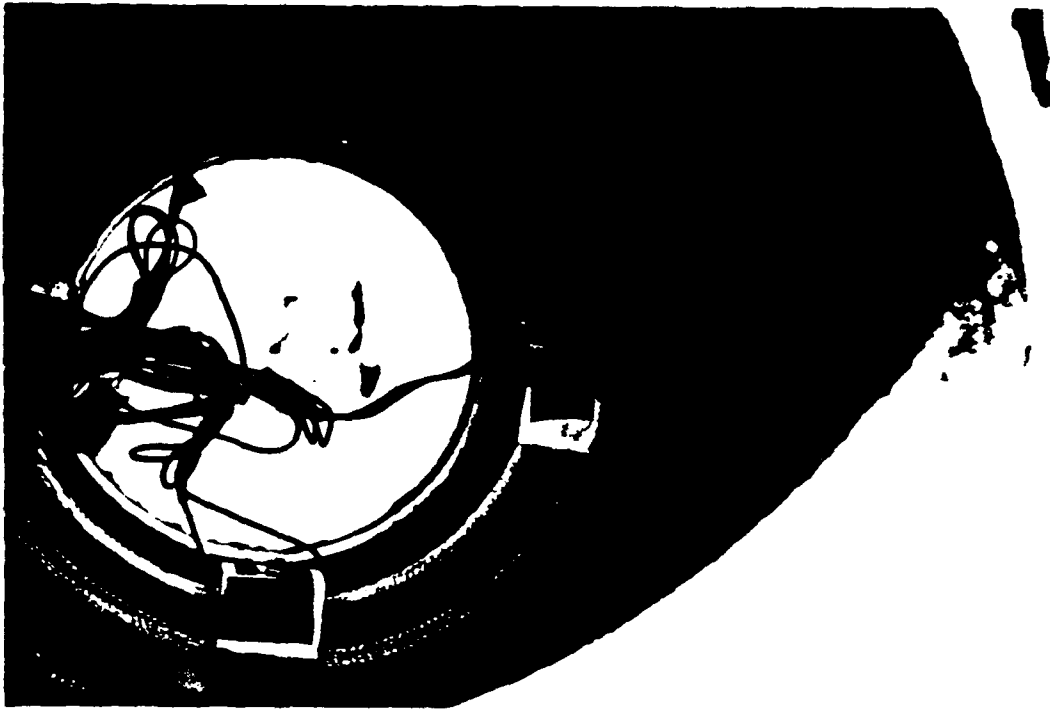
Figure 34. Test Cylinder Showing Accelerometers Installed.

Figure 35. External View of Test Cylinders.
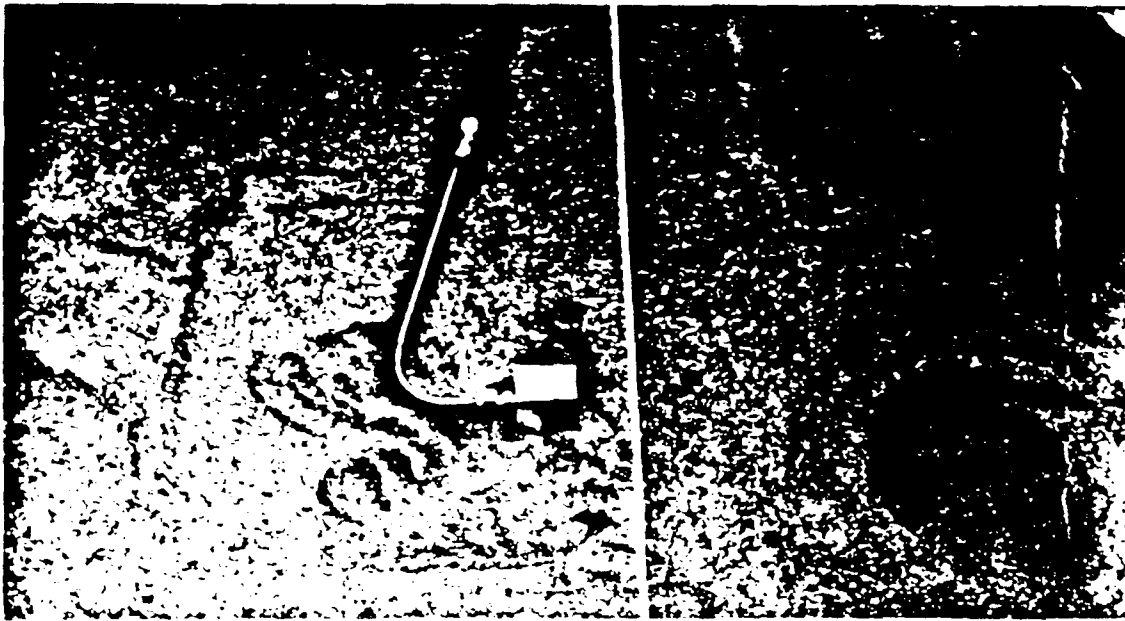
Figure 36. Accelerometer Package Being Installed in Testbed.

Figure 37. Testbed Preparation

74

installing the explosive until the desired last item, just before the test. Figure 38 shows the sphere of C-4 explosive (mass 0.39 kg, radius 39 mm) and the RP-2 detonator. Figure 39 indicates how a dummy sphere was withdrawn from the testbed through the PVC pipe, the explosive charge installed, and then the pipe was filled with sand, the sand compacted, and the PVC pipe withdrawn.

Figure 40 shows the completed testbed with markers indicating the ends of the cylinder and the location of the explosive charge (just below the short marker with the plywood base). Figure 41 is a view of the testbed after the detonation showing the crater that had a radius of about 1 meter and intersected the walls of the testbed.

Table 13 provides a summary of the measured values of sand density 1550 kg/m^3 and recorded instrumentation values. Also shown are the computed values of the stress wave propagation velocity of 280 m/s, constrained modules of 122 MPa, and the sand porosity of 0.43.

Attenuation and attenuation coefficients of peak values of acceleration, velocity, and stress with range are given in Figures 42-44. Time-of-arrival as a function of range is given in Figure 45, as well as the computed wave speed.

In locking materials such as sand, a method for determining the validity of the time history of stress and velocity for a spherically divergent wave is to plot the time histories of stress or velocity from gage located at various ranges on the same graph. If the curves overlay at later times, a large amount of confidence can be placed in the accuracy of the data. Figure 46 is such a plot for the stress data measured in the 1/10 Replica-scaled test. It is obvious that all the stress gages seem to have the same values at the times soon after 2 ms. The data are very good. Figure 47 is a plot of integrated accelerometer data. Velocities obtained from this method suffer some degree of uncertainty at later times because of a variety of reasons, most noticeably a base line shift resulting from rotation of the gage or resolution of the instrumentation system. If one disregards the upper curve, some degree of consistency in the remaining curves appears to exist during the period of 2 to 4 ms. The data again appears very good.

Detailed time histories plots of all the data are presented in Appendix E. The data obtained in this 1/10 Replica-scaled test appears to be of good quality for the desired simulation time of 4 ms.
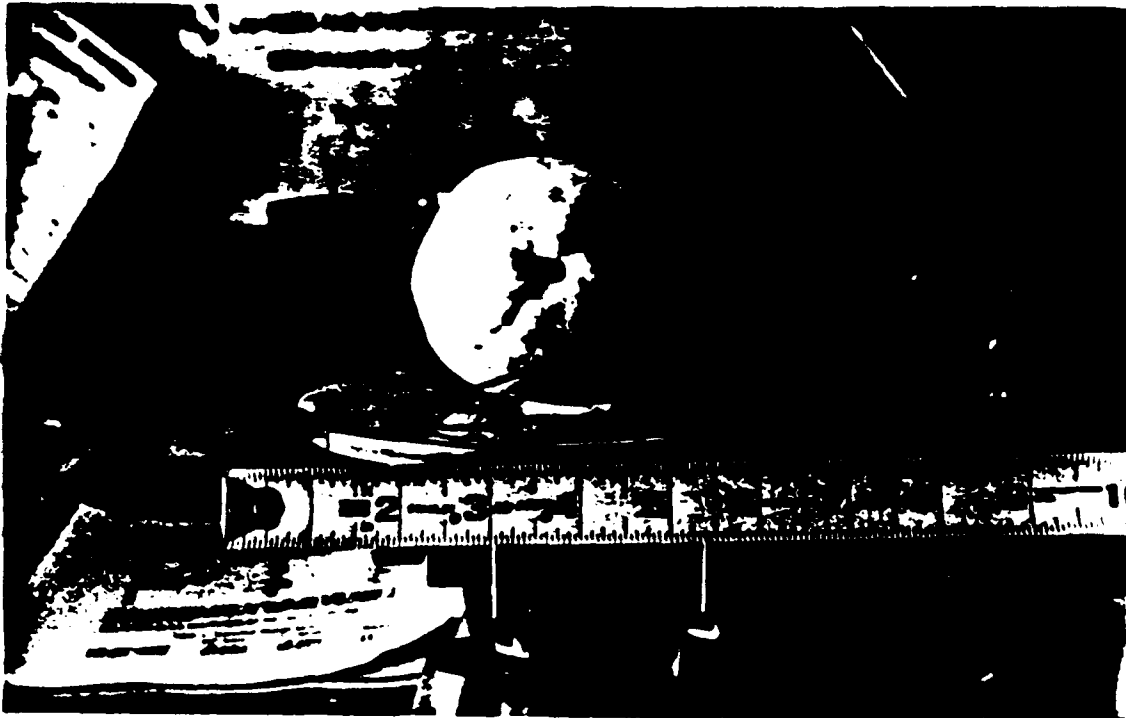
Figure 38. C-4 Explosive Charge.
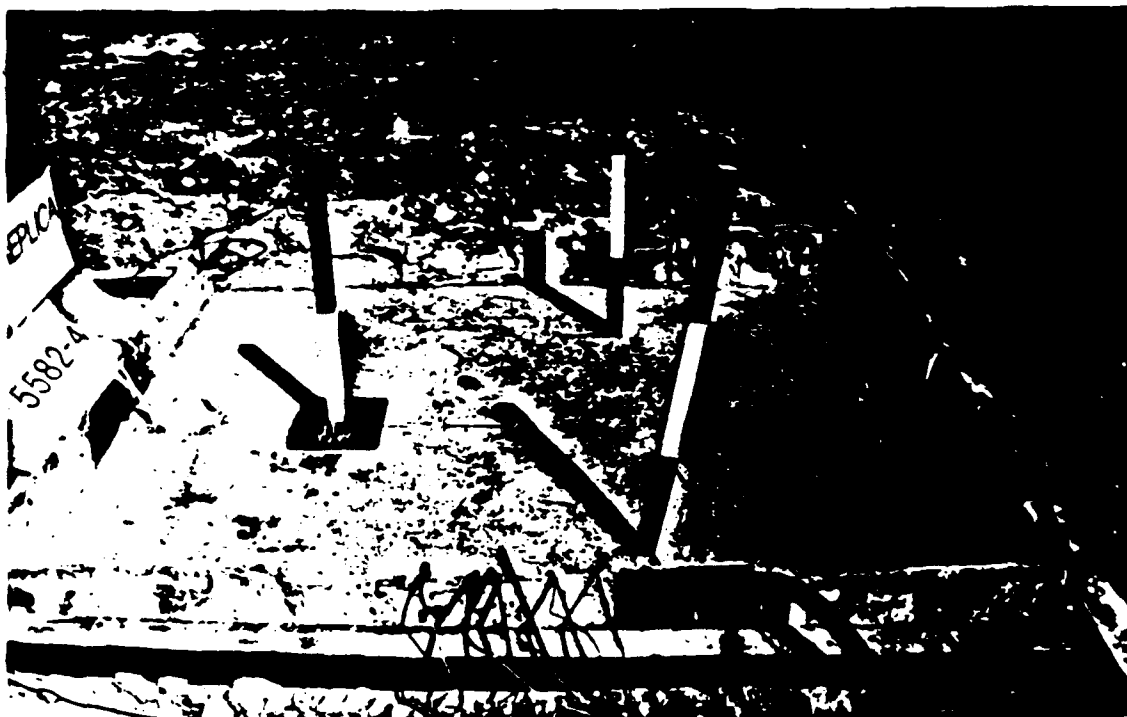

Figure 39. Installation of Explosive Charge.

Figure 40. Completed Testbed.

Figure 41. Posttest View of Testbed.

TABLE 13. SUMMARY OF 1/10 REPLICA-SCALED TEST RESULTS

Test Date: 21 September 1990

Test Bed Material: Sand
Measured Unit Weight = 97 lb/ft^3
Bulk Density = 1550 kg/m^3
n = 0.43

Explosive Charge: 0.39 kg of C4
Theoretical Energy Released, W = 2.1 MN·m

Free Field Data
Gage Number	Range, (m)	Time-of-arrival, t'(ms)	Acceleration, a(g)	Velocity, v (m/s)	Stress σ (MPa)
3303	0.12*	.355	27000	25	
3301	0.3	.69	10500	10.3	
3304	0.3	.69	9500	10.3	
3502	0.37	.965			2.8
3302	0.45	1.075	5100	5.2	
3503	0.52	1.52		3.5	1.7
3305	0.585	1.67	2000		
3504	0.67	2.02			1.0

*Gage 3303 was intended to be located at .3m, but moved as a result of misfire, location estimated from time-of-arrival.

Structural Data
3407	0.60	1.69	1200	1.8	
3402	0.75	1.79	200	1.4	
3405	0.75	1.82	400	1.6	
3404	0.90	1.865	500	1.2	
3408	0.60	1.74	900	.4	
3401	0.75	1.91	700	.8	
3406	0.75	1.86	700	1.0	
3403	0.90	1.90	500	.0	

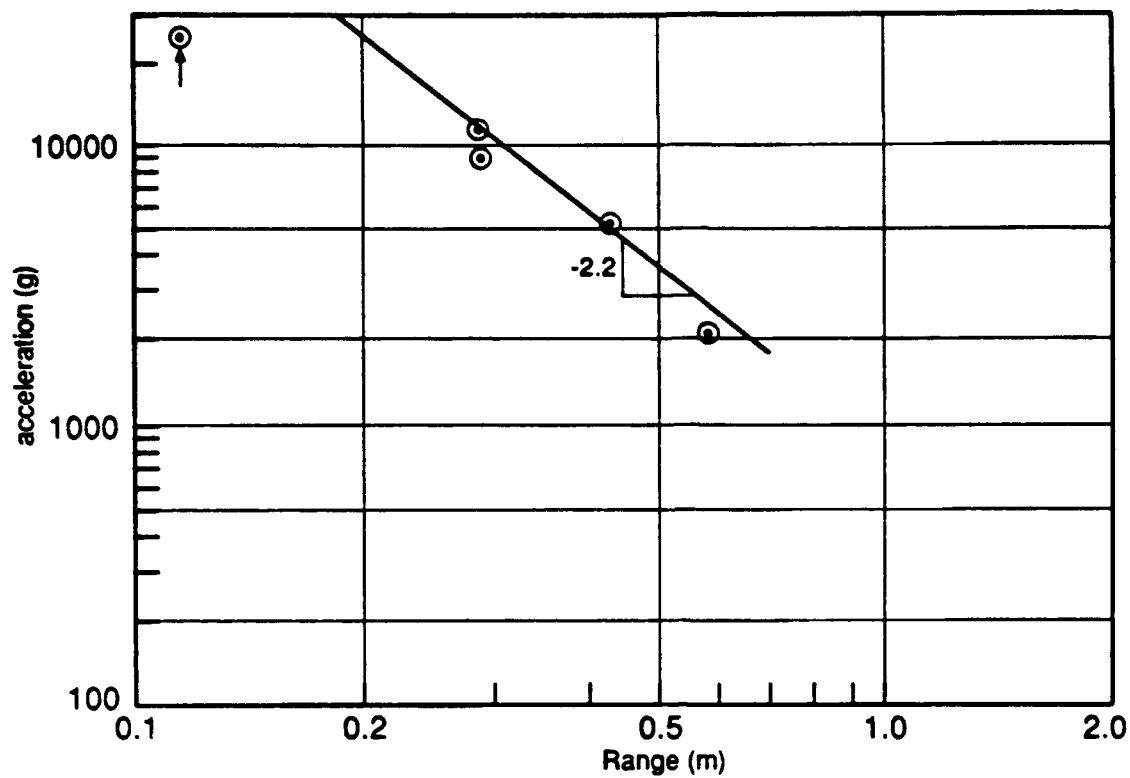Computed values: c = 280 m/s ρc^2 = 122. MPa

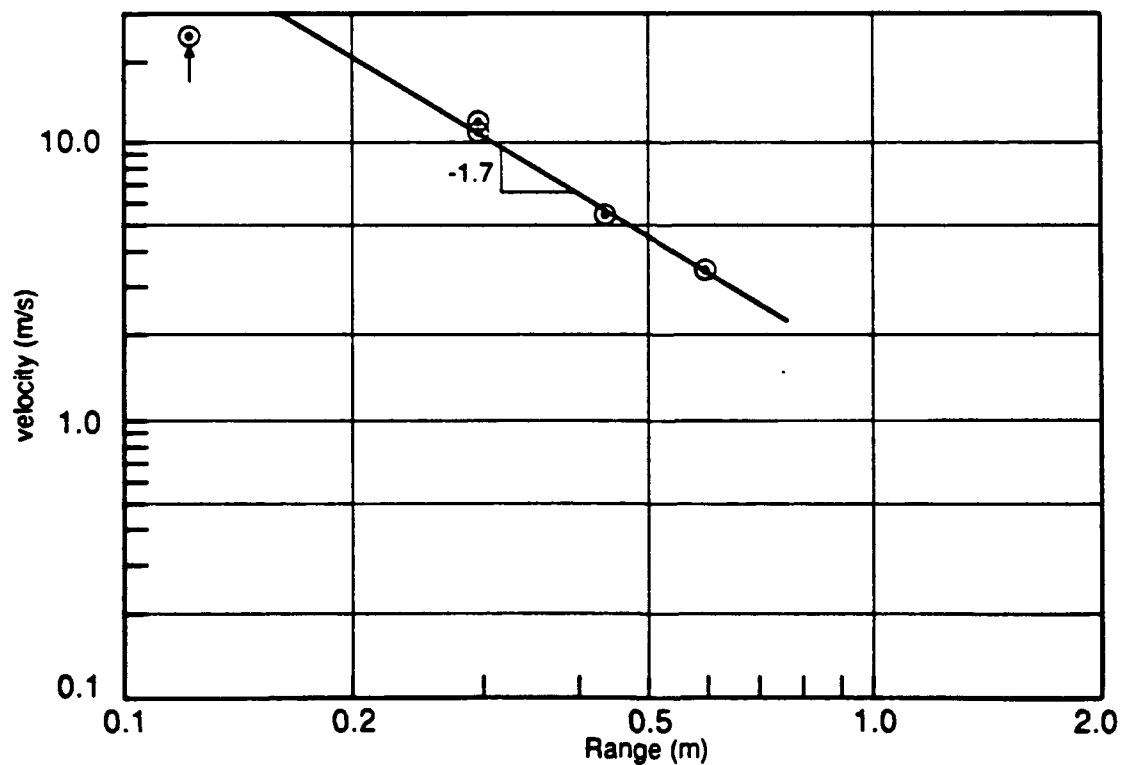Figure 42. 1/10th Replica-Scaled Test, Attenuation of Acceleration with Range.

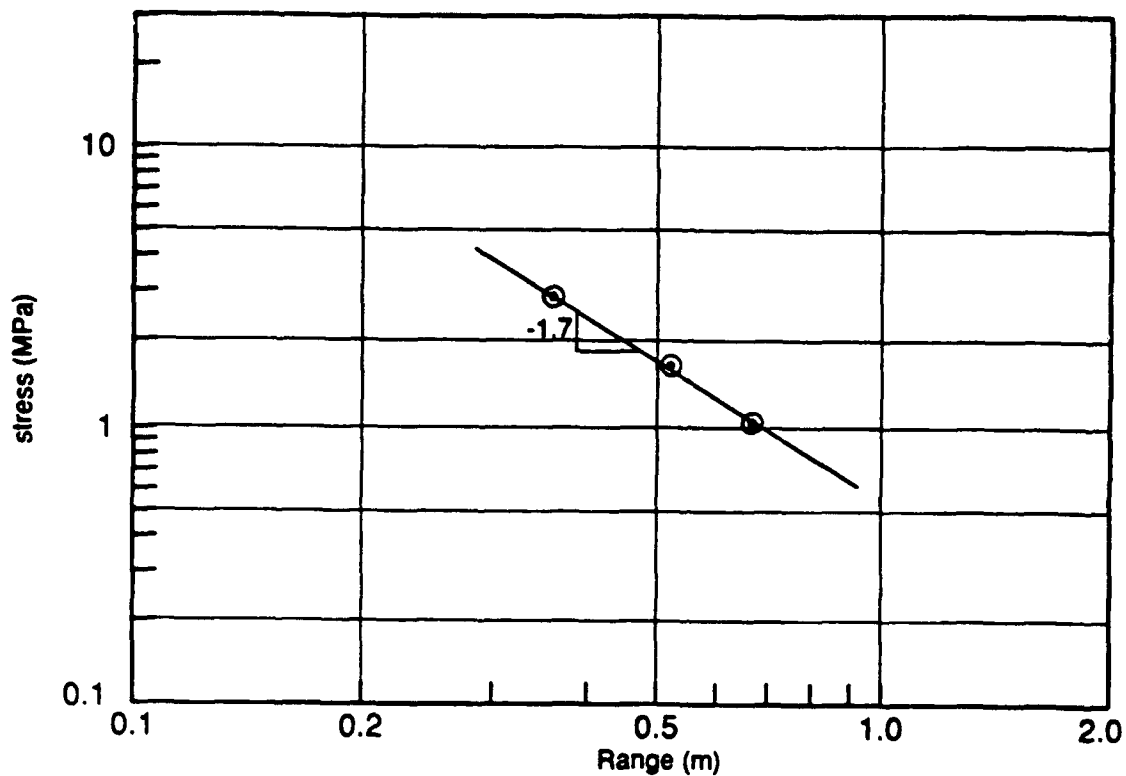Figure 43. 1/10th Replica-Scaled Test, Attenuation of Velocity with Range.

79

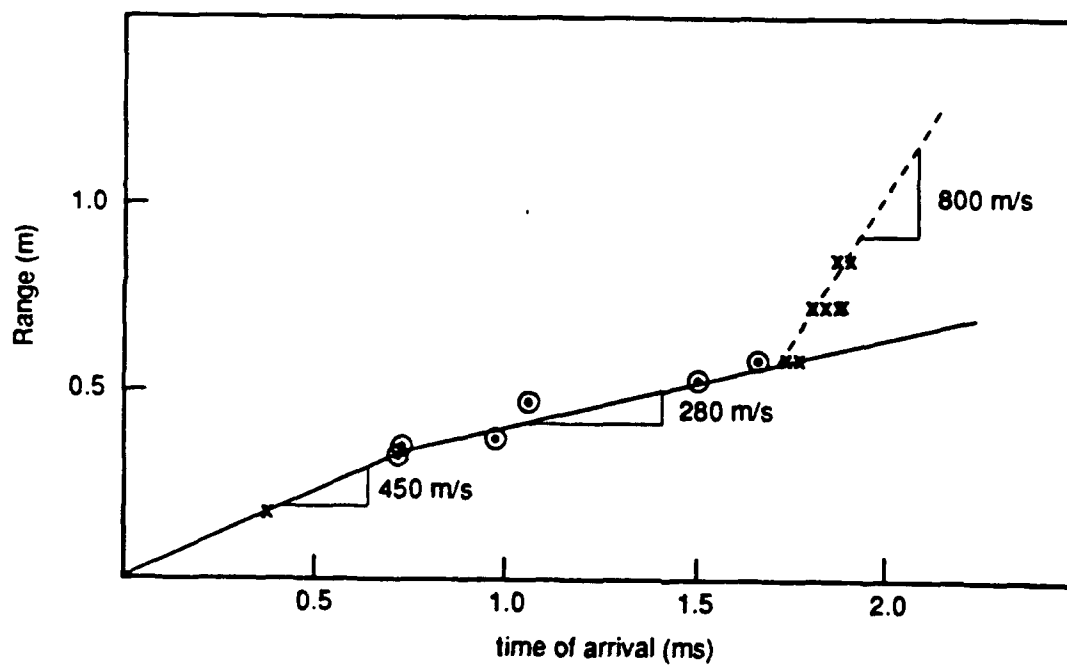Figure 44. 1/10th Replica-Scaled Test, Attenuation of Stress with Range.

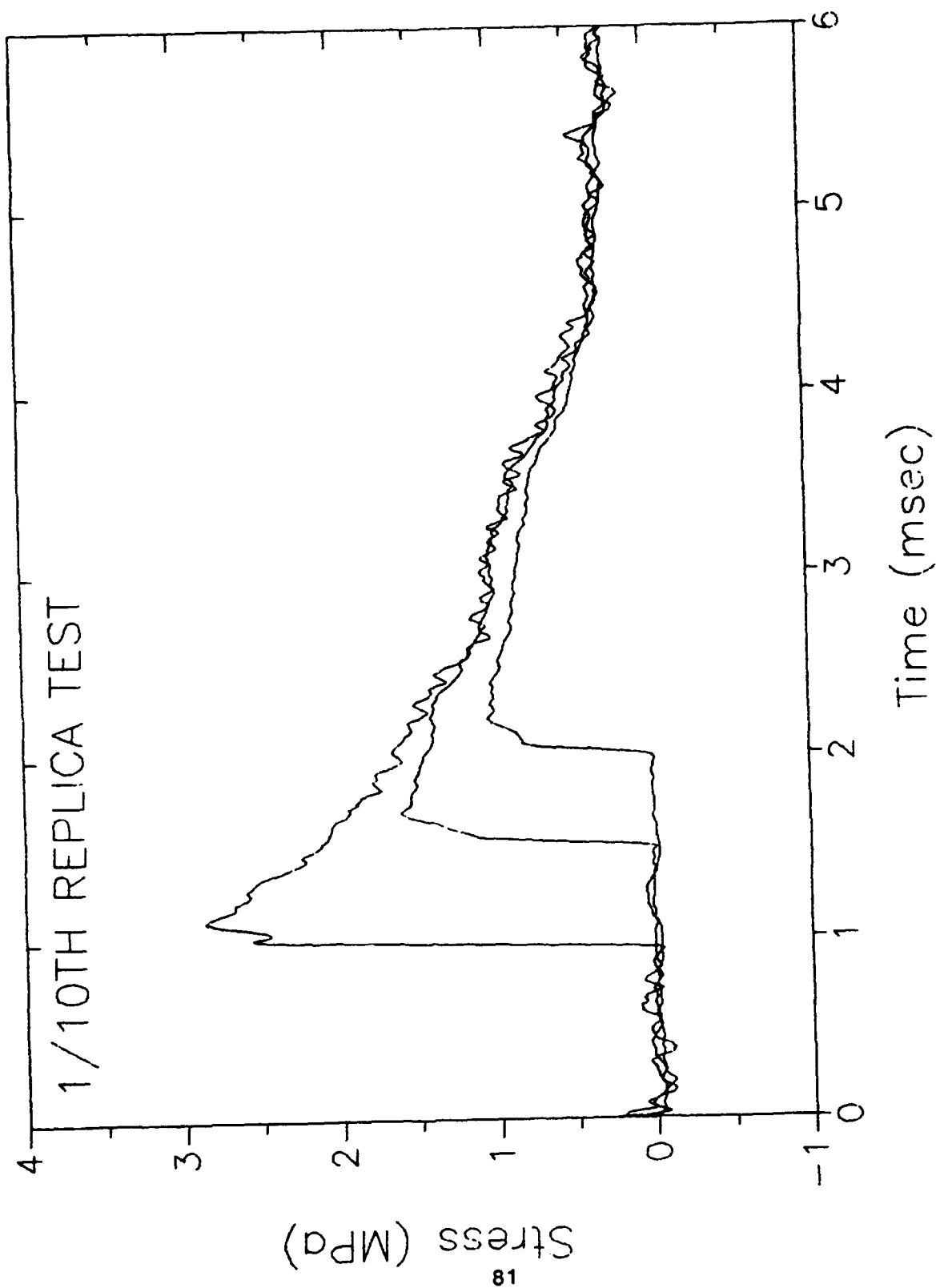Figure 45. 1/10th Replica-Scaled Test, Range vs. Time-of-arrival.

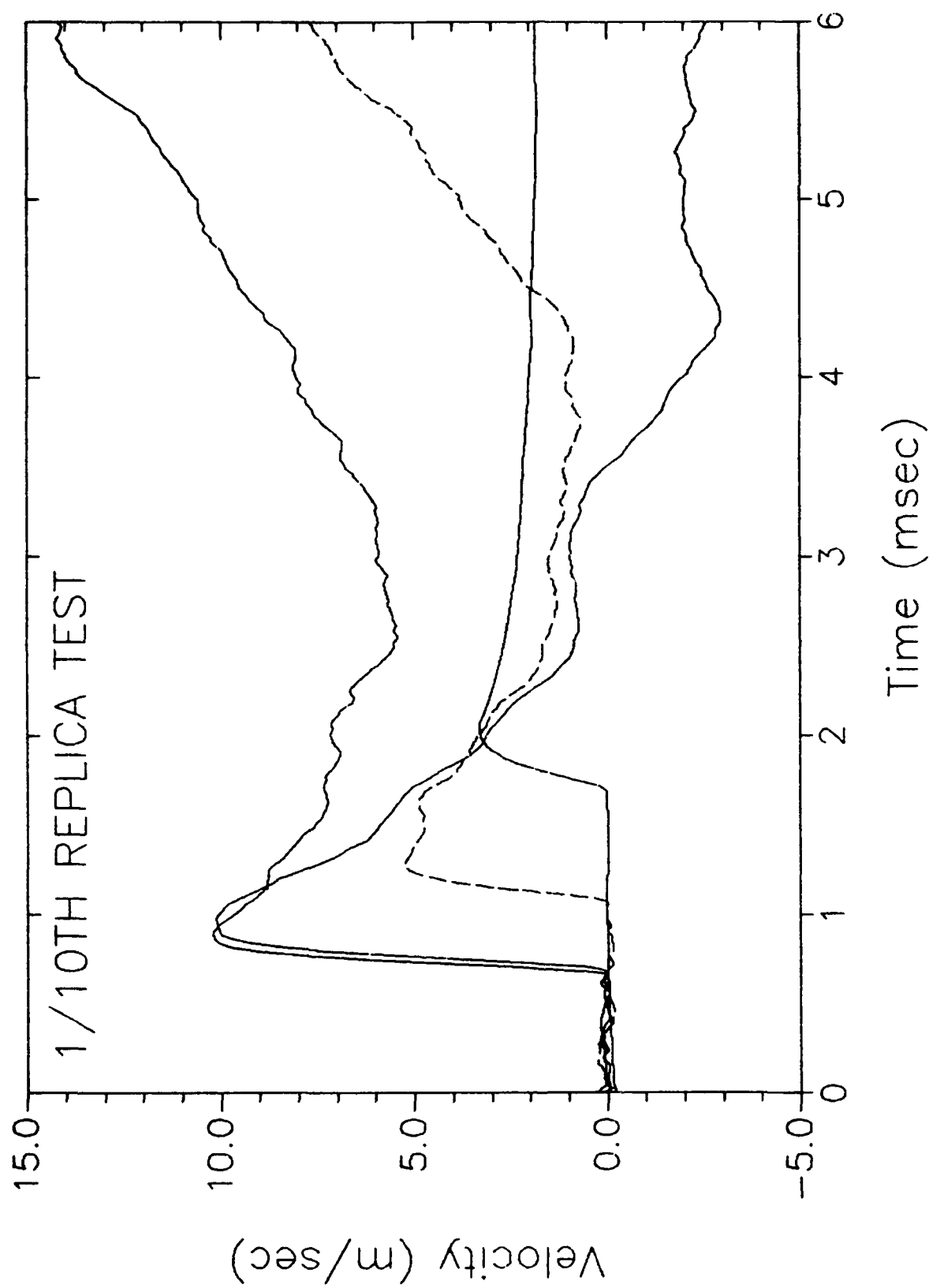**Figure 46. Comparison of Free-Field Stress Waveforms.**

81

Figure 47. Comparison of Free-Field Velocity Waveforms.

C. 1/5 FROUDE-SCALED EVENT - COAL TESTBED

Elevation and plan views for the 1/5 Froude-scaled test event are presented in Figures 48 and 49. The layout of the instrumentation for this test event is shown in figures 50 and 51. Since the density scale factor for this test was about 0.5 (density of coal to density of sand), the wall thickness for the reinforced concrete structure used in this test and shown in Figure 52 was reduced to one half that required by geometrical 1/5 scaling. This reduction in thickness resulted in the correct mass for Froude scaling, however the hoop stiffness was about 5 times too large (10 x 1/2) and the bending stiffness was about 1.25 (10 x (1/2)^3) times too large. Since the test was intended to investigate only rigid body motion of structure, the stiffness differences are acceptable. Figure 53 is a photograph of the instrumentation cable bundle and the instrumented cylinder.

The backfill in the testbed was crushed bituminous coal, procured from the same source as was used for the laboratory and the static proof-of-principle cone penetration tests and listed in Appendix B.

Thirty two tons of 1/4 inch mean diameter coal was purchased in bulk and shipped by truck to the ARA test site in Colorado. Smaller grain sizes were required to meet the grain size distribution similar to the sand which required that 90 percent pass a No. 16 sieve and 10 percent pass a No. 140 sieve. The method of crushing the coal is depicted in Figure 54. The coal was spread on a concrete pad and the bucket of a small bobcat hauler was scraped along the concrete to crush the coal. The coal was then shoveled on to a screen over a wheelbarrow as shown in Figure 55 where material that passed through the screen shown in Figure 56 was transferred to the testbed. Figure 57 shows the coal being dumped into the testbed.

The coal was compacted in the test bed using the steel plate hand compactor and a water filled roller as shown in Figure 58. Also shown in the figure is the test cylinder and the protective tubing carrying the instrumentation cable leads from the testbed to the junction box.

The explosive charge, a 0.31 kg, 36 mm radius sphere of C-4 was placed into the testbed using an arrangement of PVC pipe as shown in Figure 59.

Figure 60 is a view of the completed testbed with poles indicating location of the ends of the buried cylinder and the explosive charge. Figure 61 is a view of the testbed after the detonation showing the crater with a radius of about 1 meter.
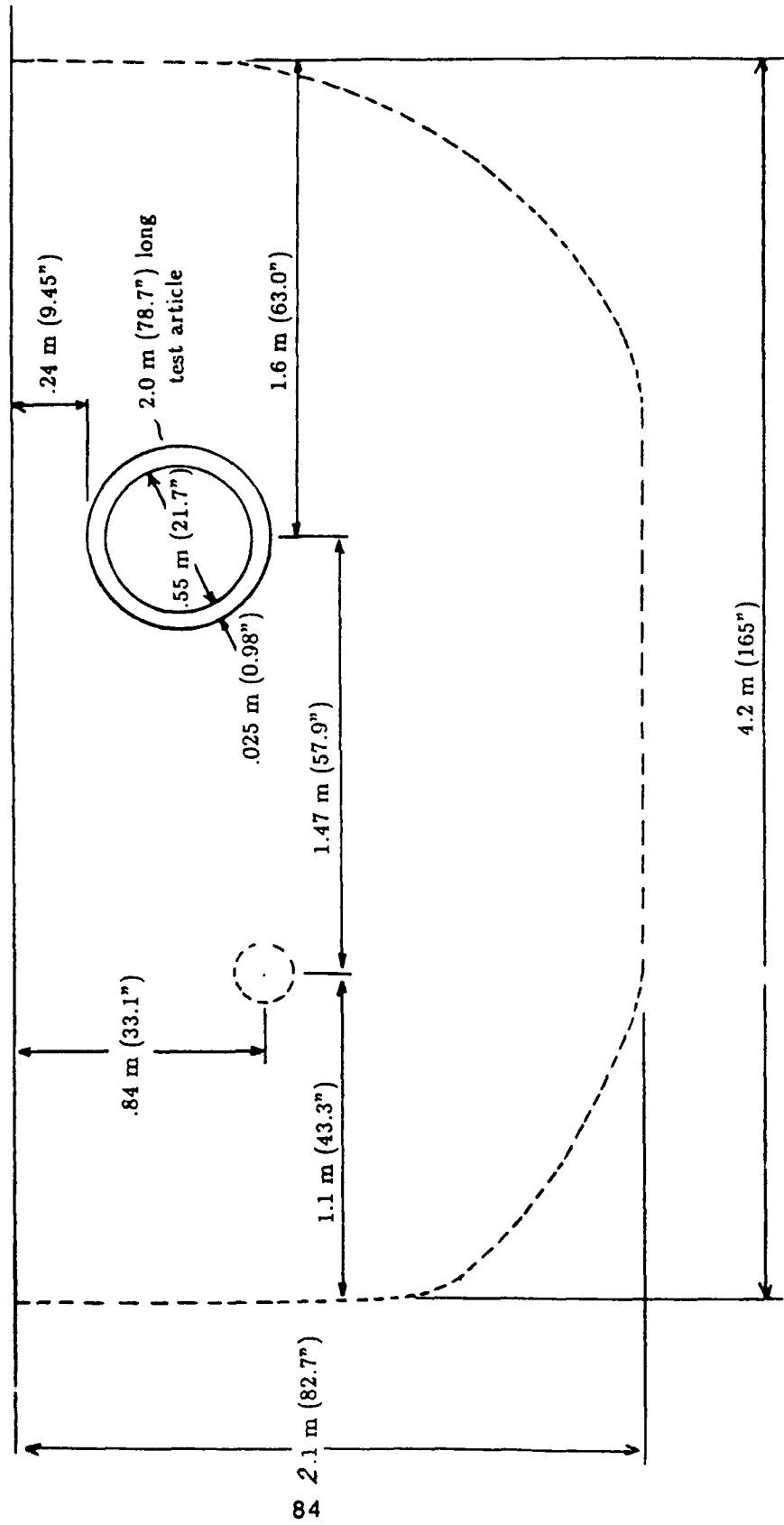
83

.24 m (9.45")

2.0 m (78.7") long
test article

1.6 m (63.0")

.55 m (21.7")

.025 m (0.98")

1.47 m (57.9")

.84 m (33.1")

1.1 m (43.3")

4.2 m (165")

2.1 m (82.7")

Figure 48. 1/5th Froude–Scale Testbed (Elevation View).

84
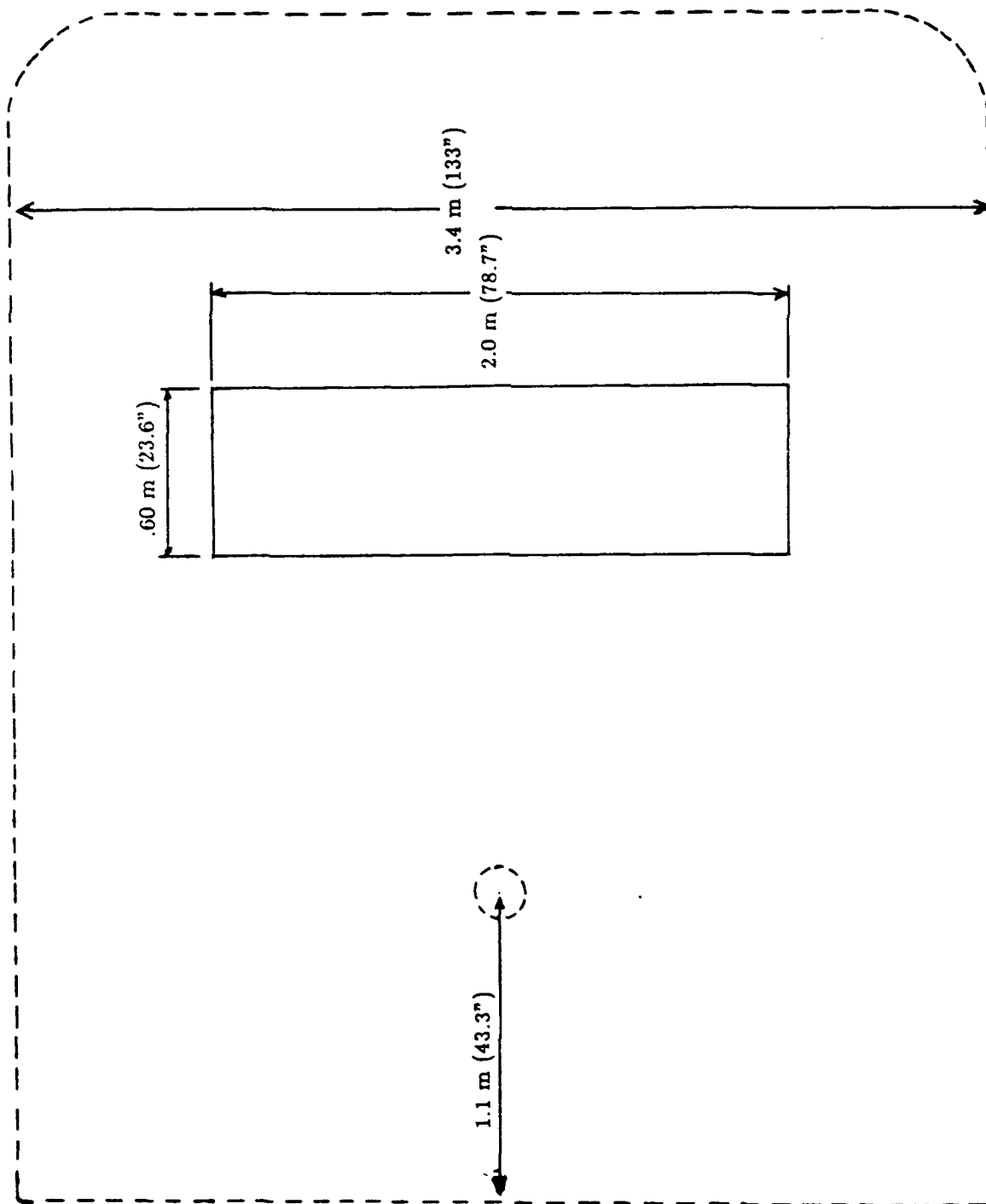
Figure 49. 1/5th Froude-Scale Testbed (Plan View).

3.4 m (133")

2.0 m (78.7")

.60 m (23.6")

1.1 m (43.3")

Figure 50. 1/5th Froude-Scale Testbed (Elevation View).

86
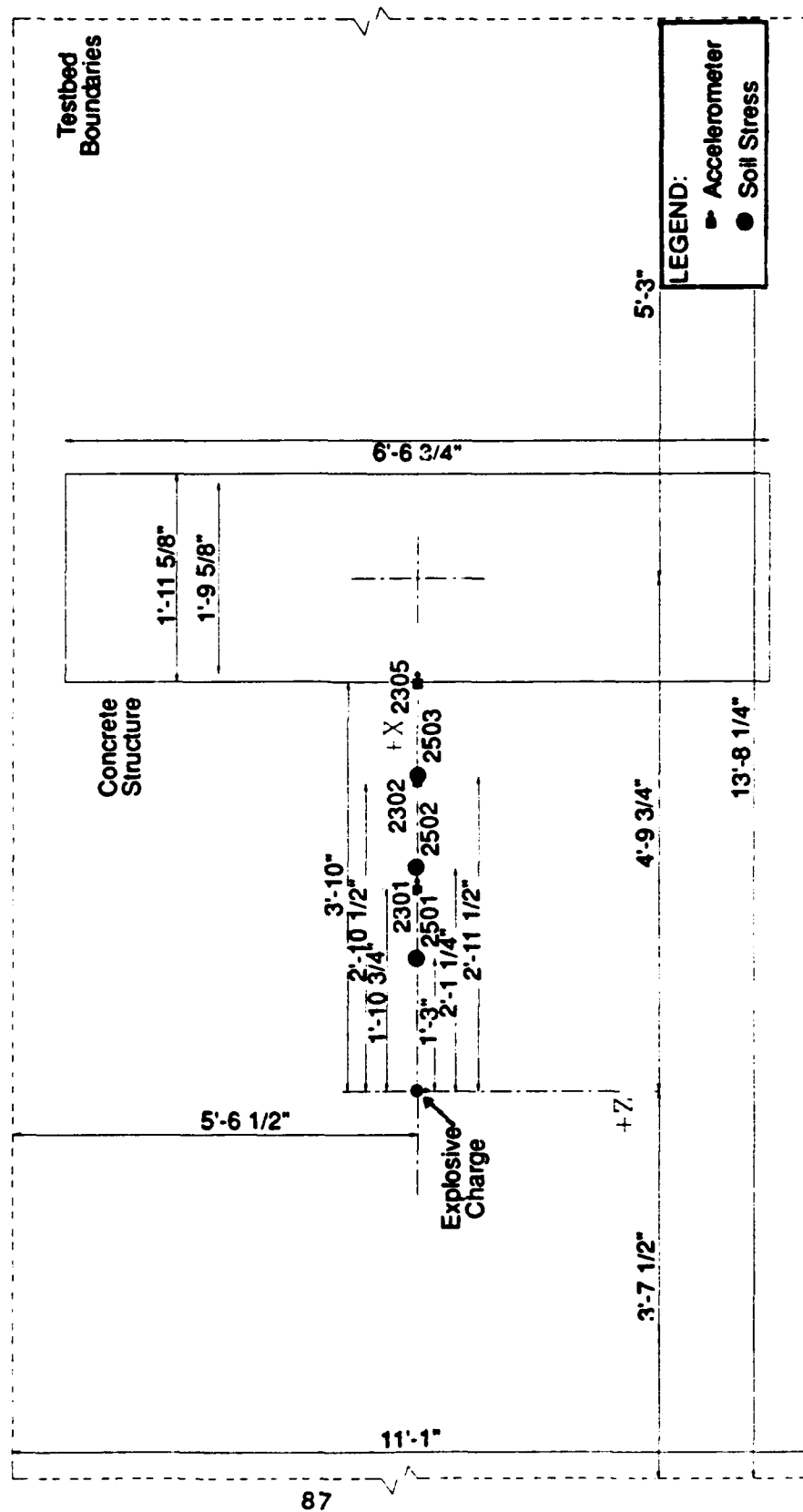
Figure 51. 1/5th Froude-Scale Test bed (Plan View).

SIDE VIEW

6'-6 3/4"

1'-9 5/8"

1'-10 5/8"

1'-11 5/8"

CONCRETE "GROUT"

REINFORCING
STEEL MESH

0.500

0.500

Detail

0.041

END VIEW

11 13/16"

11 5/16"

10 13/16"
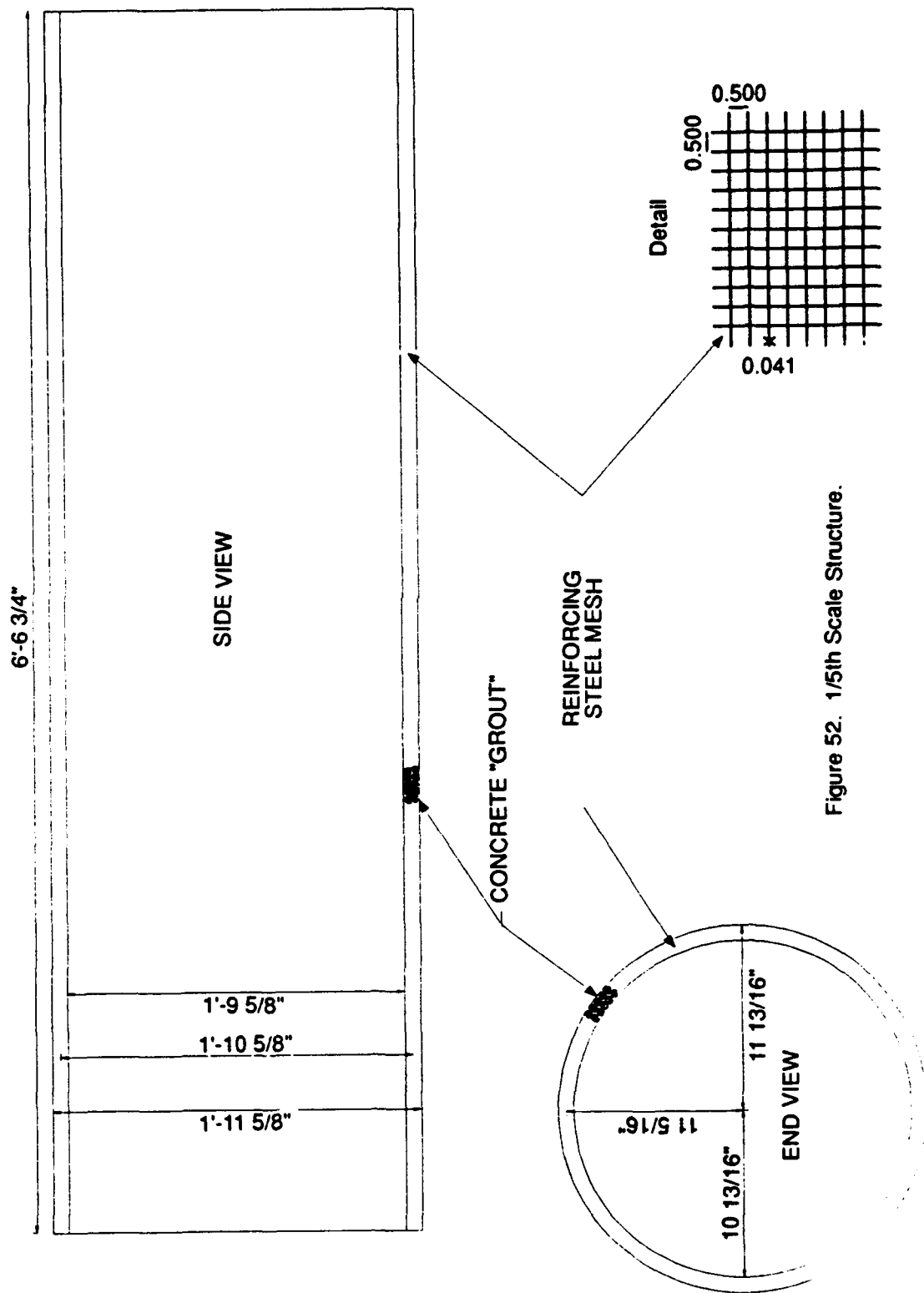
Figure 52. 1/5th Scale Structure.

88
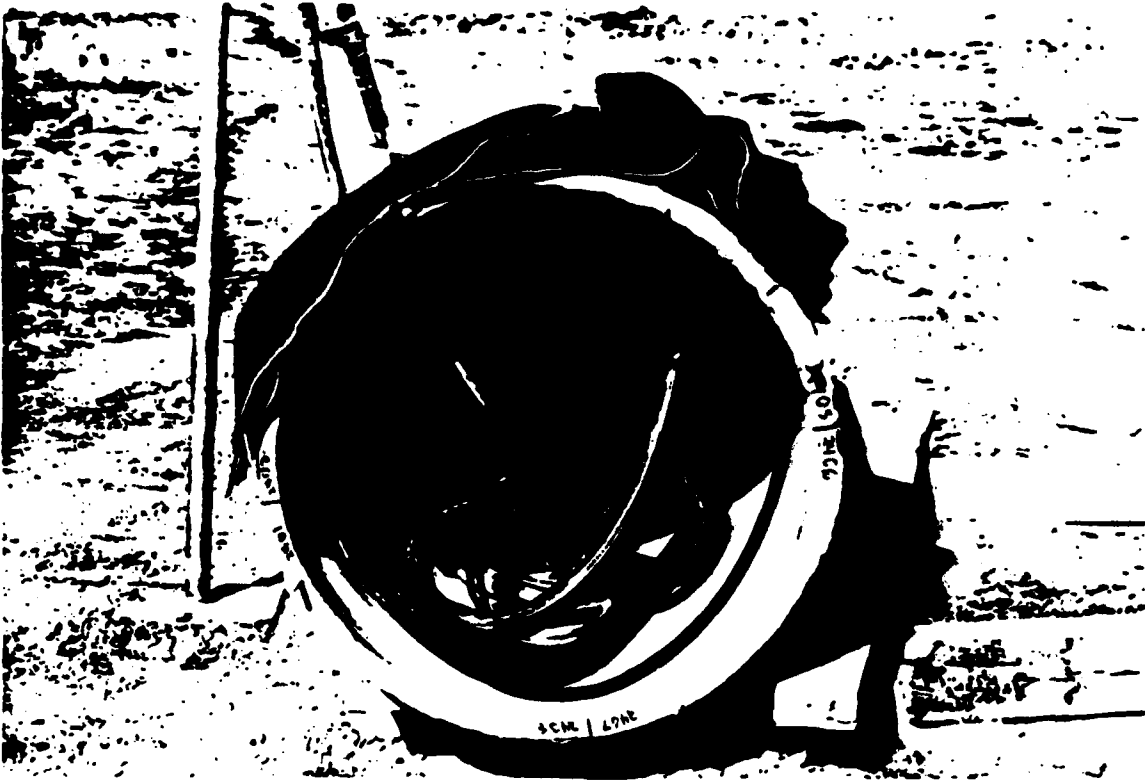
Figure 53. Test Cylinder Showing Cable Protection Scheme for Structural Accelerometers.
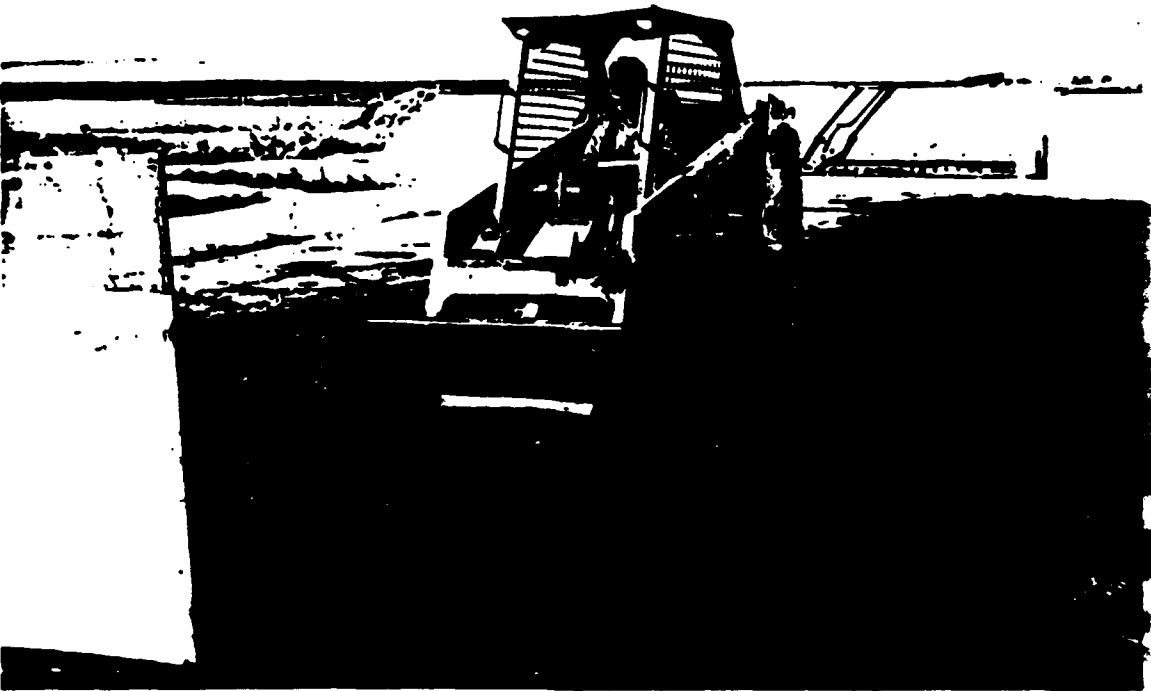
Figure 54. Crushing Coal Using Blade of Bobcat.

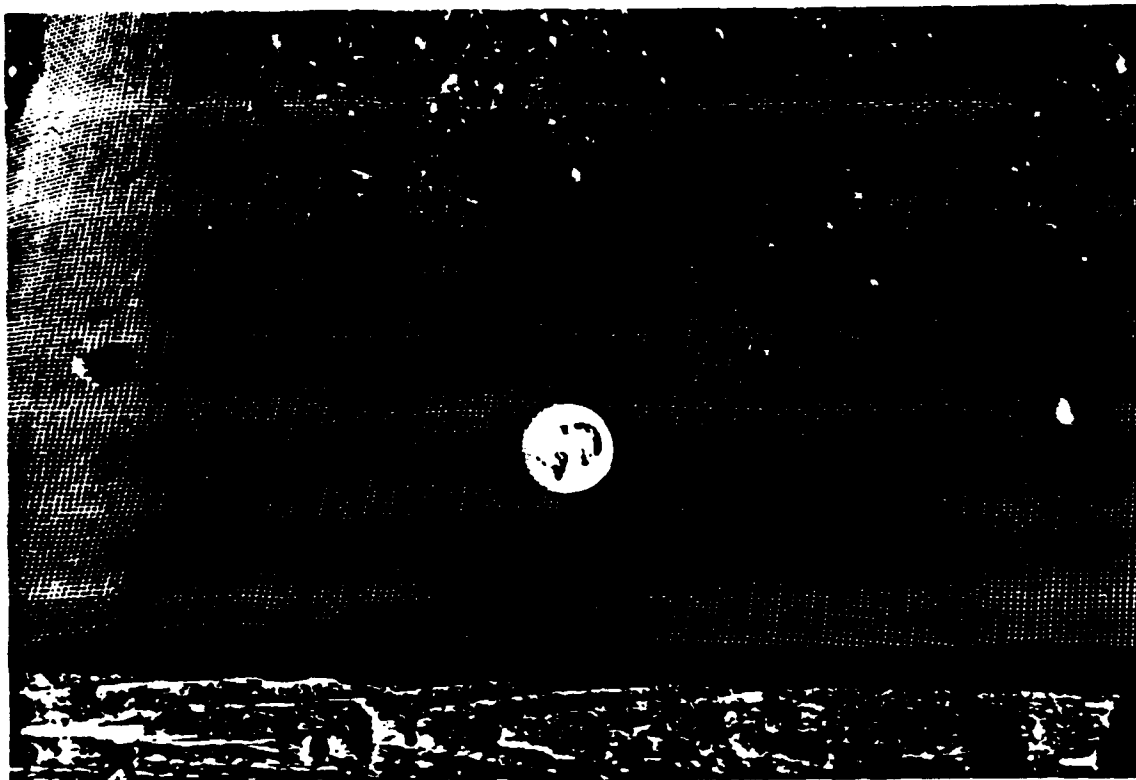Figure 55. Screening Crushed Coal to Obtain Correct Grain Size.
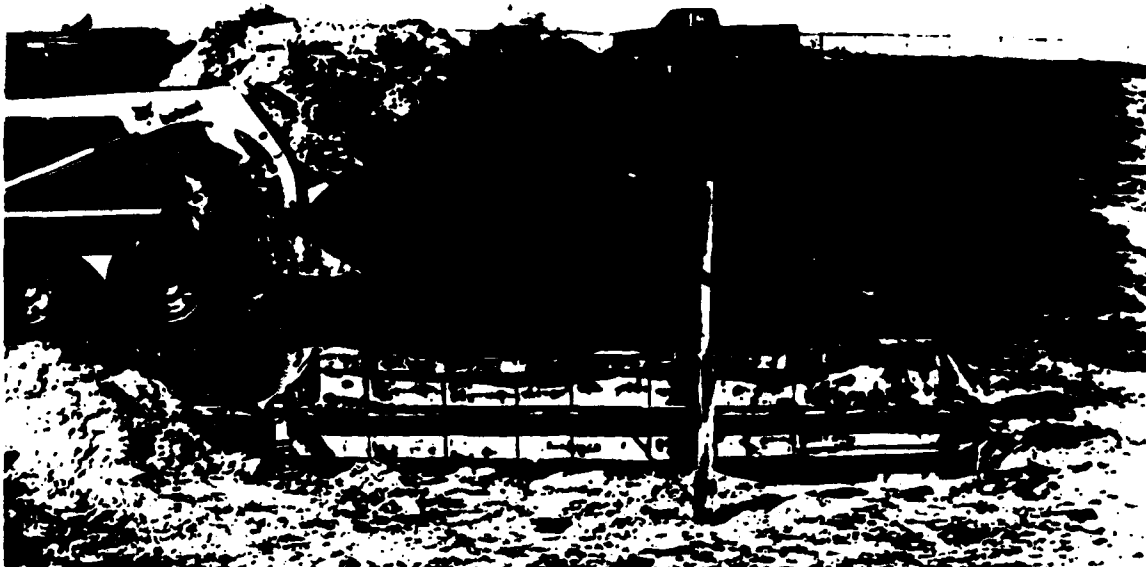

Figure 56. Detailed View of Screen

Figure 57. Backfilling of Coal into Testbed.

Figure 58. Testbed Preparation.
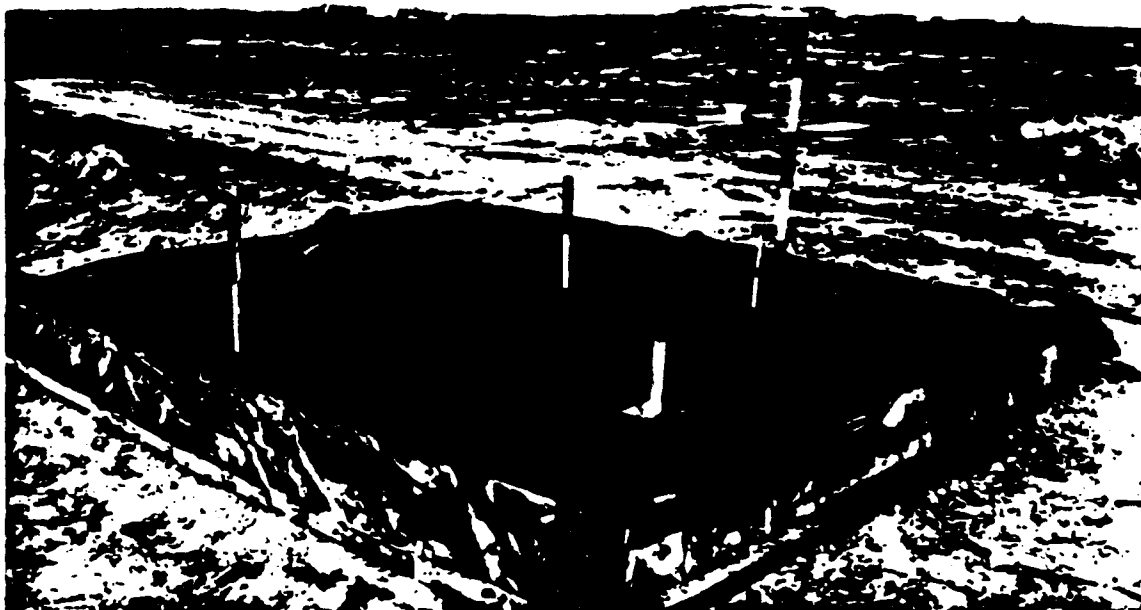
Figure 59. Explosive Charge Installation.

Figure 60. Completed Testbed.

Figure 61. Posttest View of Testbed.

Table 14 is a summary of the measured values of coal density, 850 kg/m^3 and recorded instrumentation values. The computed values of the coal porosity, 0.36, low stress wave propagation velocity of 120 m/s, and the constrained modules of 12.2 MPa are also presented.

Attenuation of peak values of acceleration, velocity and stress are presented in Figures 62-64. Time-of-arrival as a function of range is presented in Figure 65, as well as the computed wave propagation velocities.

As in the previous test, one measure of the validity of the instrumentation is to determine if the stress-time and velocity-time histories from gages at various ranges in a spherical flow field in a locking media and to all merge to a common value at later times. Investigation of Figures 66 and 67 show that after about 8 ms, some consistency exists for all stress measurements and some velocity traces indicating reasonable data quality for the desired simulation time of 18 ms. Two of the velocity traces with the earliest time-of-arrival obviously require additional interpretation.

Detailed time history plots of all the data are presented in Appendix E. Additional discussion of the results of this test will be delayed until a later section when comparisons can be made.

D. 1/10 FROUDE-SCALED EVENT - COAL/LEAD TEST BED

Elevation and plan views of the 1/10 Froude-scaled test are presented in Figures 68 and 69, and the instrumentation locations shown in Figures 70 and 71. The density scale factor for this test is about one so the structure shown in Figure 72 has dimensions based upon 1/10 scale of the prototype. Since the structure is constructed of reinforced concrete, it is ten times too stiff. However, since this test is intended to investigate only rigid body response this variation is considered acceptable.

The backfill for this test consists of a mixture of coal and lead. The coal is the same material used in the 1/5-Froude-scaled test. The lead is the same used in the laboratory Proof-of-Principle cone penetrometer test.

94

TABLE 14. SUMMARY OF 1/5 FROUDE-SCALED TEST RESULTS

Test Date: 19 October 1990

Test Bed Material: Coal
Measured Unit Weight = 53 lb/ft^3
Bulk Density = 850 kg/m^3
n = 0.36

Explosive Charge: 0.31 kg of C4
Theoretical Energy Released, W = 1.7 MN·m

Free Field Data					
Gage Number	Range, (m)	Time-of-arrival, t'(ms)	Acceleration, a(g)	Velocity, v (m/s)	Stress σ (MPa)
2501	0.45	1.3			1.6
2301	0.60	2.0	2200	5.8	
2303	0.60	2.0	2500	6.2	
2304	0.60	2.3	2000	6.0	
2502	0.75	3.6			0.6
2302	0.90	3.9	490	2.5	
2503	1.05	6.·			0.5
2305	1.17	6.·	130	1.3	
Structural Data					
2407	1.2	6.5	60	0.7	
2402	1.5	6.8	25	0.6	
2405	1.5	6.8	30	0.6	
2404	1.8	7.3	30	0.45	
2408	1.2	6.5	25	0	
2401	1.5	6.8	35	0.3	
2406	1.5	broke	--	--	
2403	1.8	7.3	30	0.1	

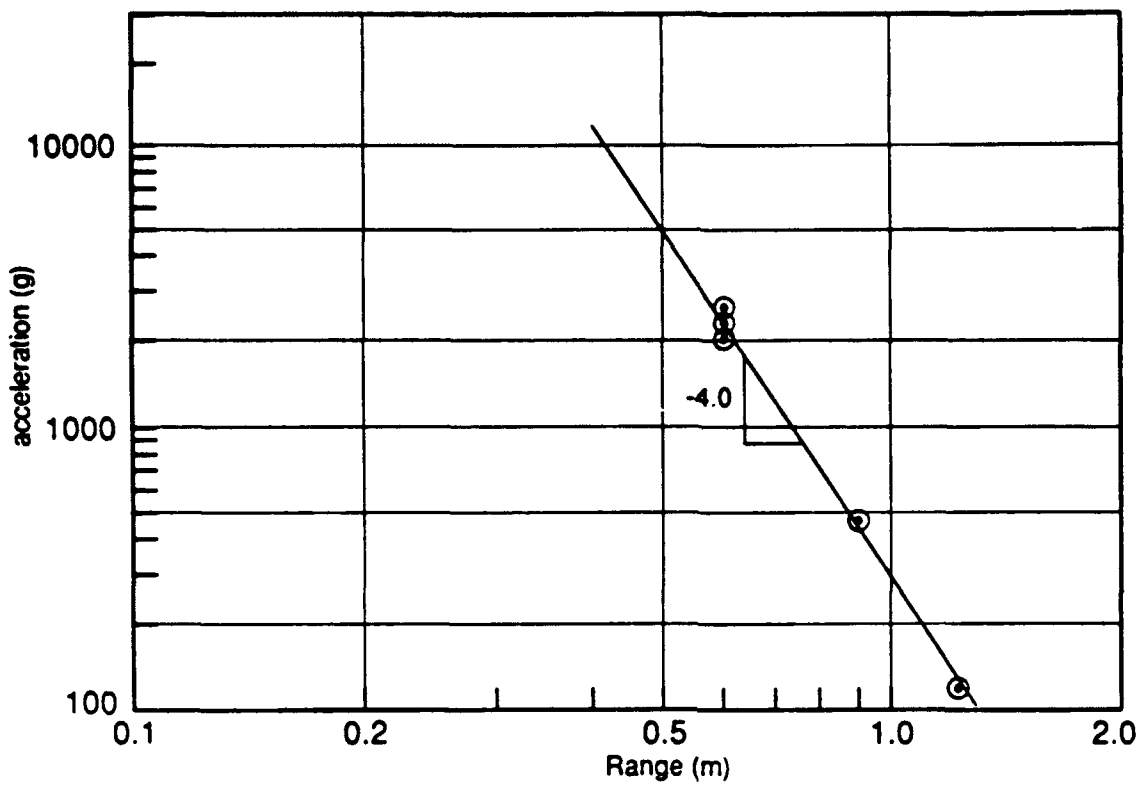Computed values: c = 120 m/s ρc^2 = 12.2 MPa

95

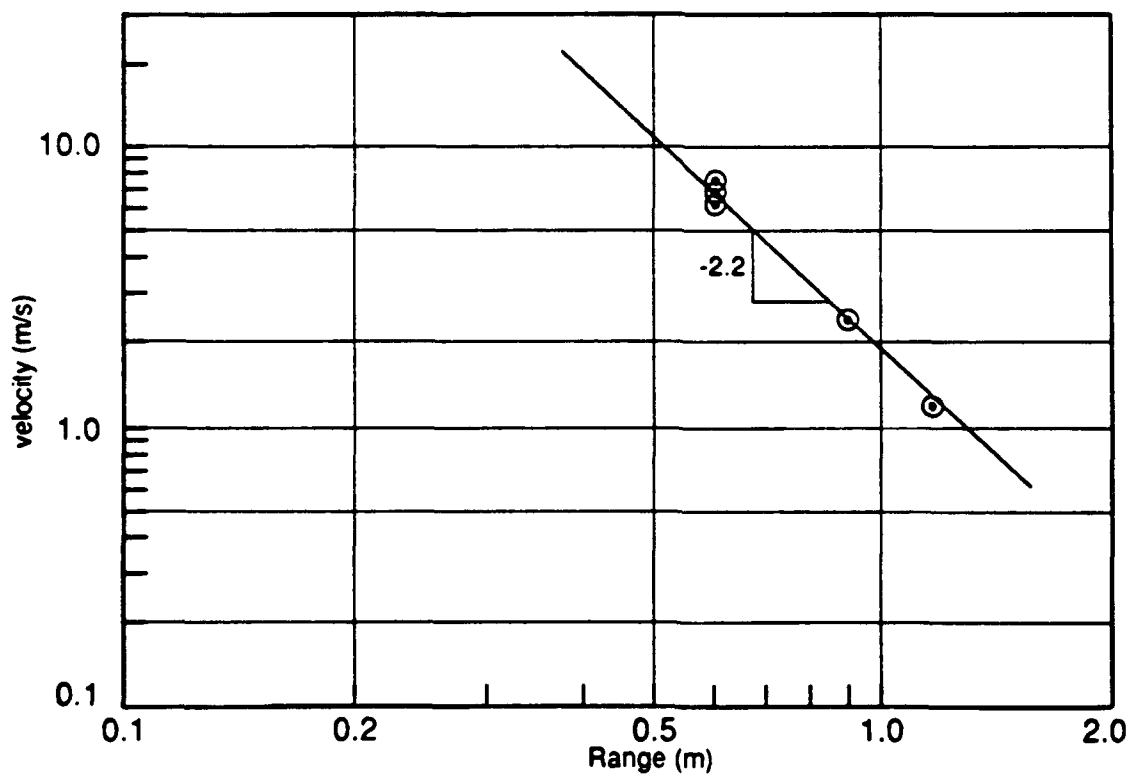Figure 62. 1/5th Froude-Scaled Test, Attenuation of Acceleration with Range.

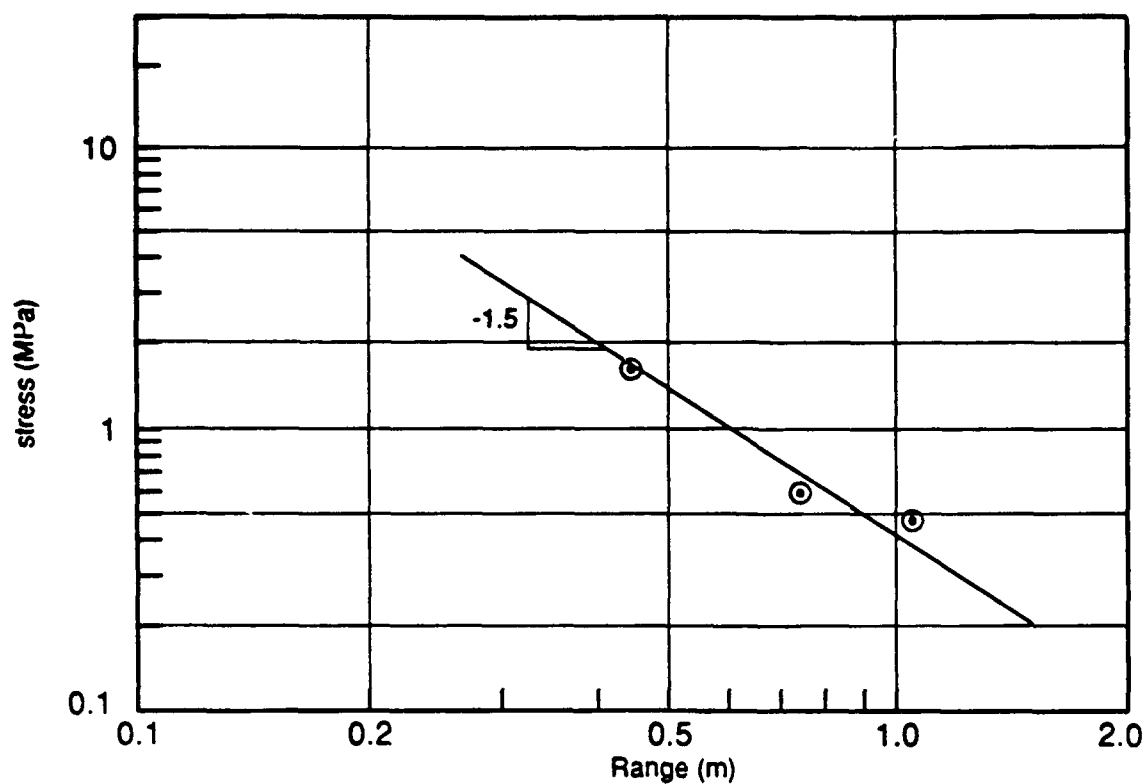Figure 63. 1/5th Froude-Scaled Test, Attenuation of Velocity with Range.

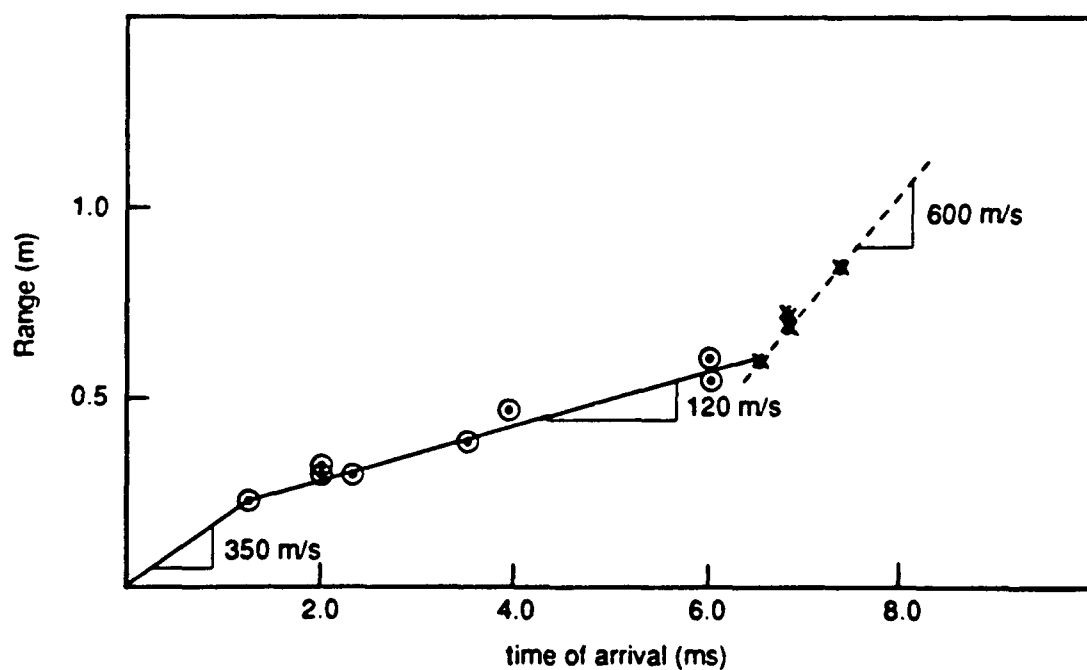Figure 64. 1/5th Froude–Scaled Test, Attenuation of Stress with Range.

Figure 65. 1/5th Froude–Scaled Test, Range vs. Time-of-arrival.
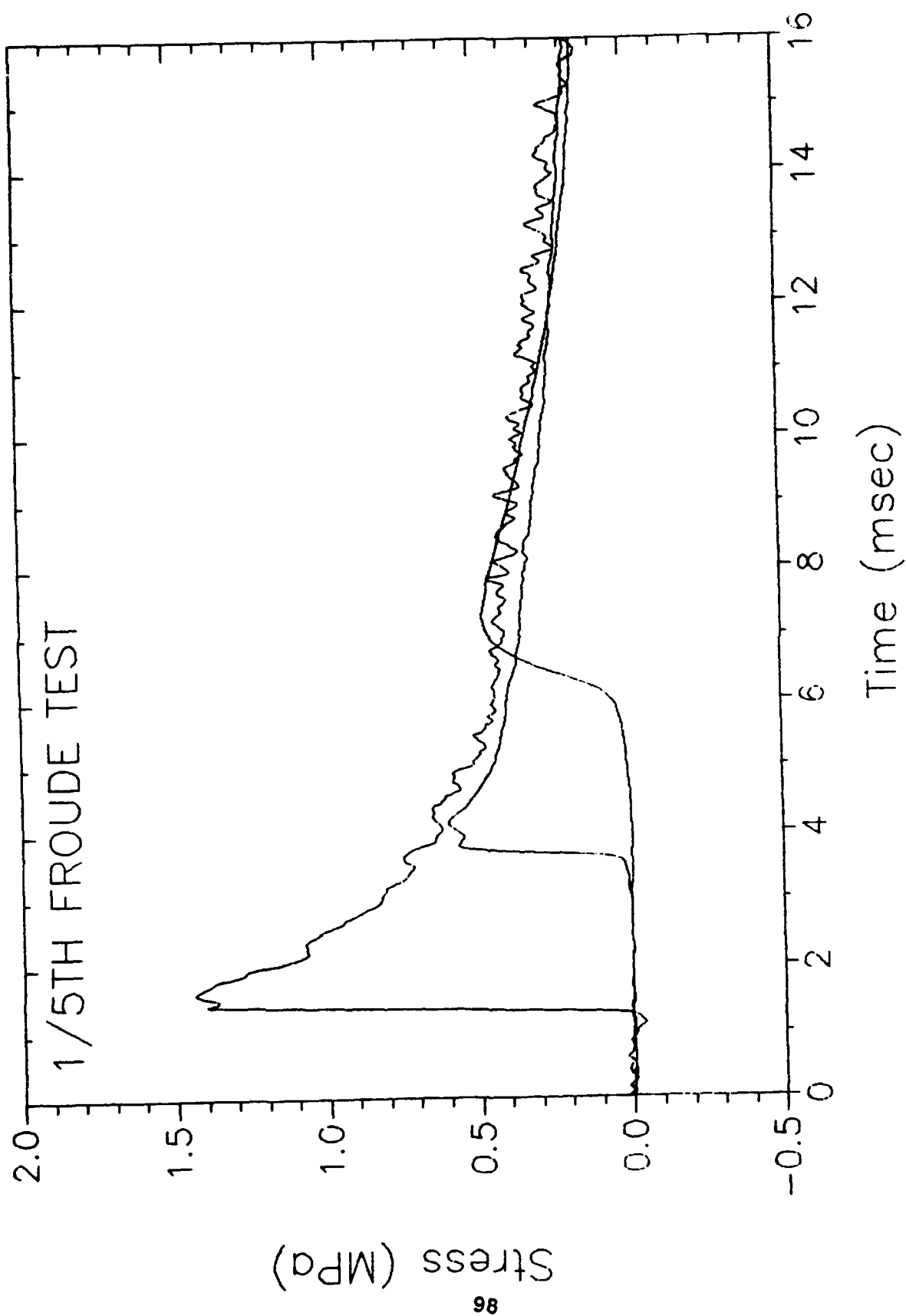
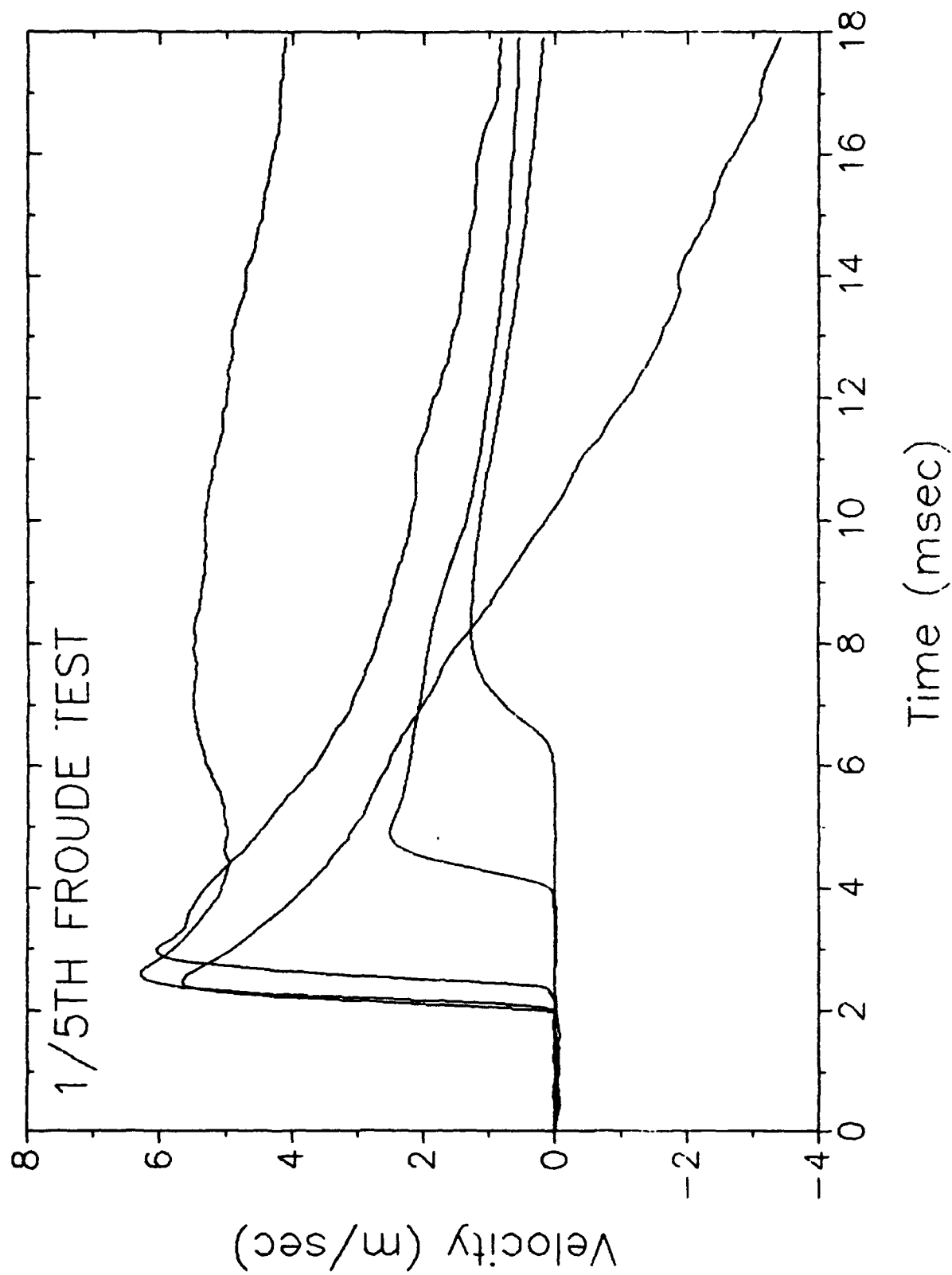Figure 66. Comparison of Free-Field Stress Waveforms.

1/5TH FROUDE TEST

Stress (MPa)

Time (msec)

Figure 67. Comparison of Free-Field Velocity Waveforms.

.12 m (4.72")

1.0 m (39.4") long
test article

.25 m (9.84")

.025 m (0.98")

.8 m (31.5")

.735 m (28.9")

.42 m (16.5")

.55 m (21.7")

2.1 m (82.7")

1.05 m (41.3")
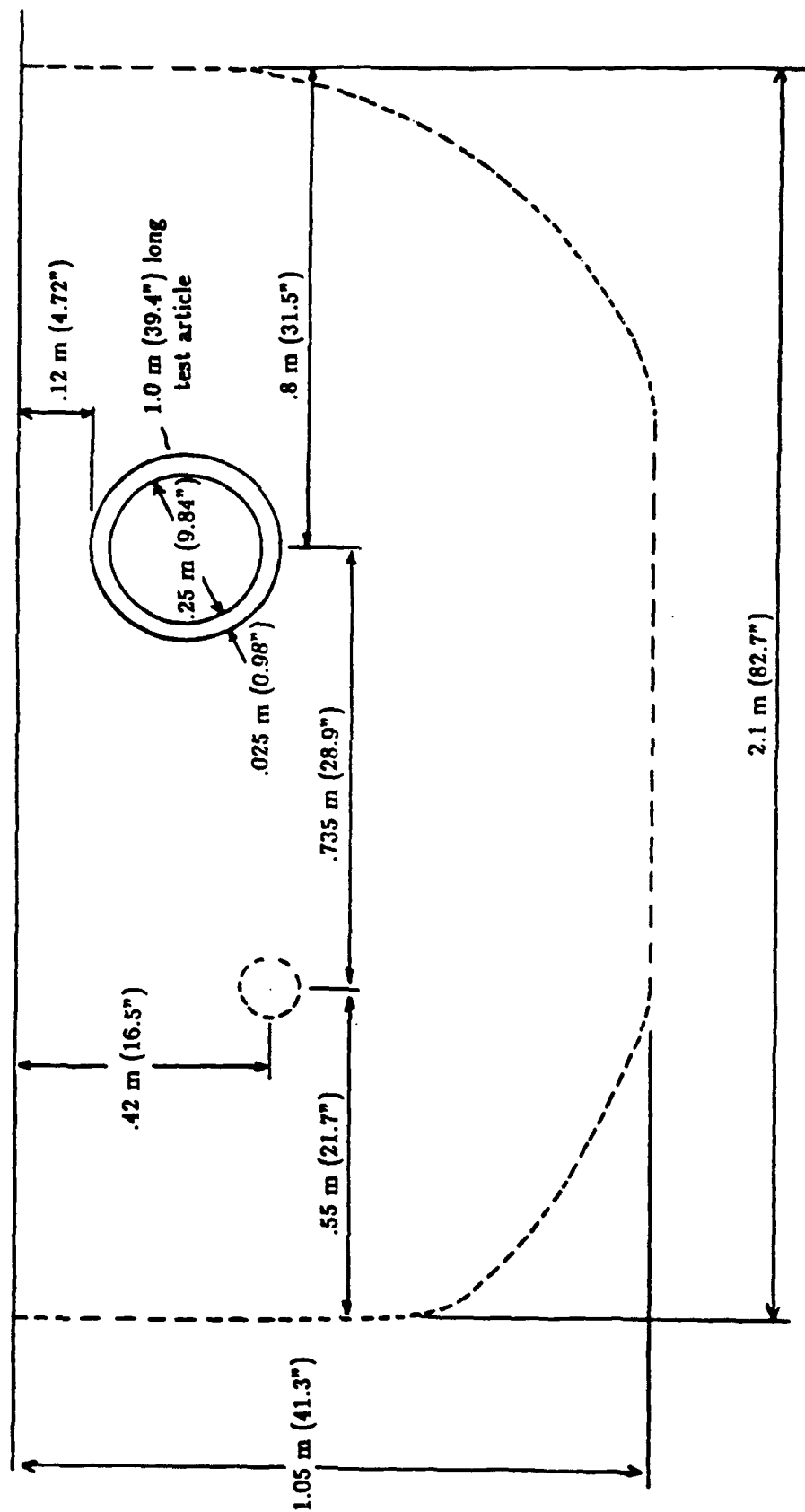
Figure 68. 1/10th Froude-Scale Testbed (Elevation View).

100
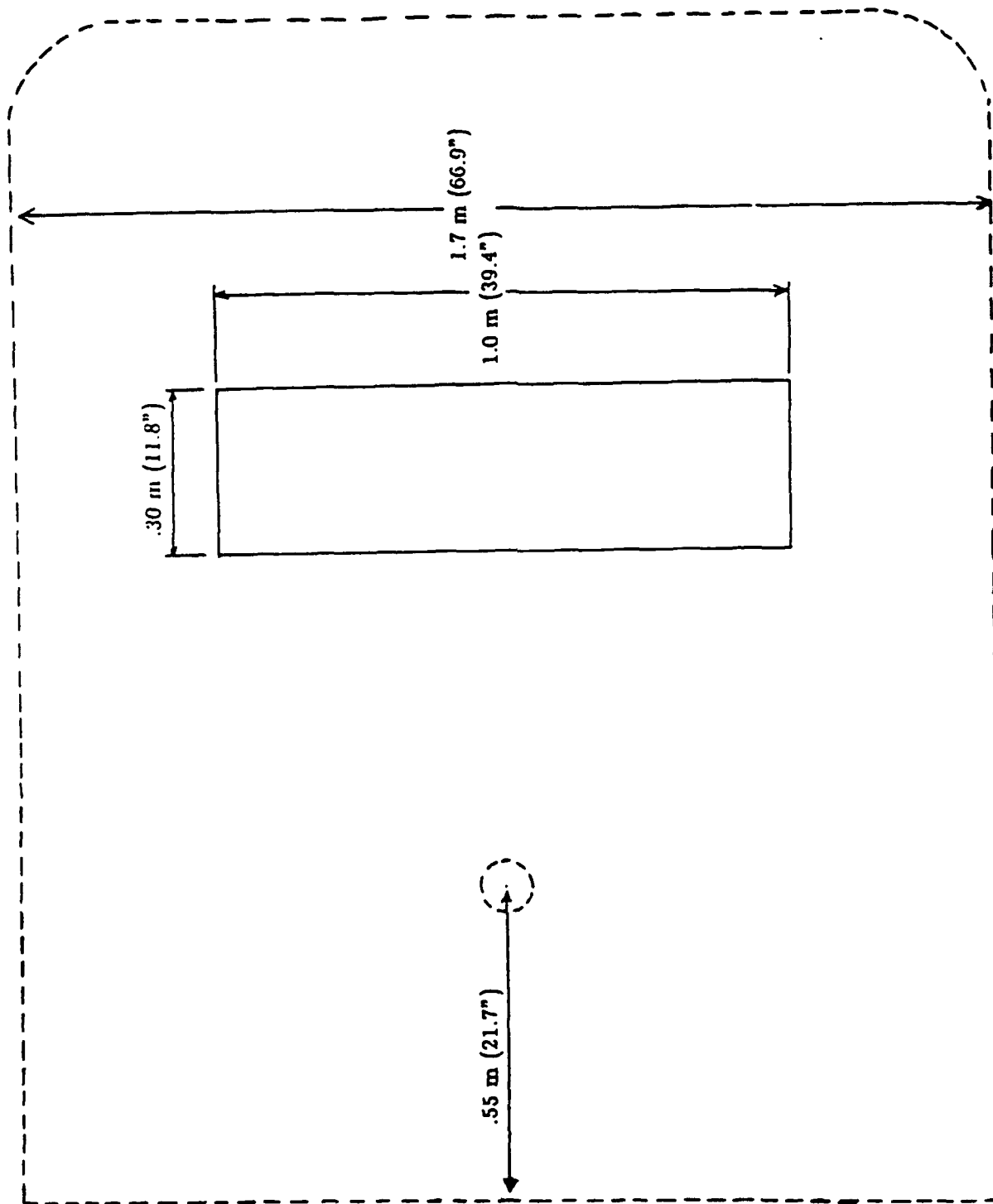
Figure 69. 1/10th Froude-Scale Testbed (Plan View).

1.7 m (66.9")

1.0 m (39.4")

.30 m (11.8")

.55 m (21.7")

101
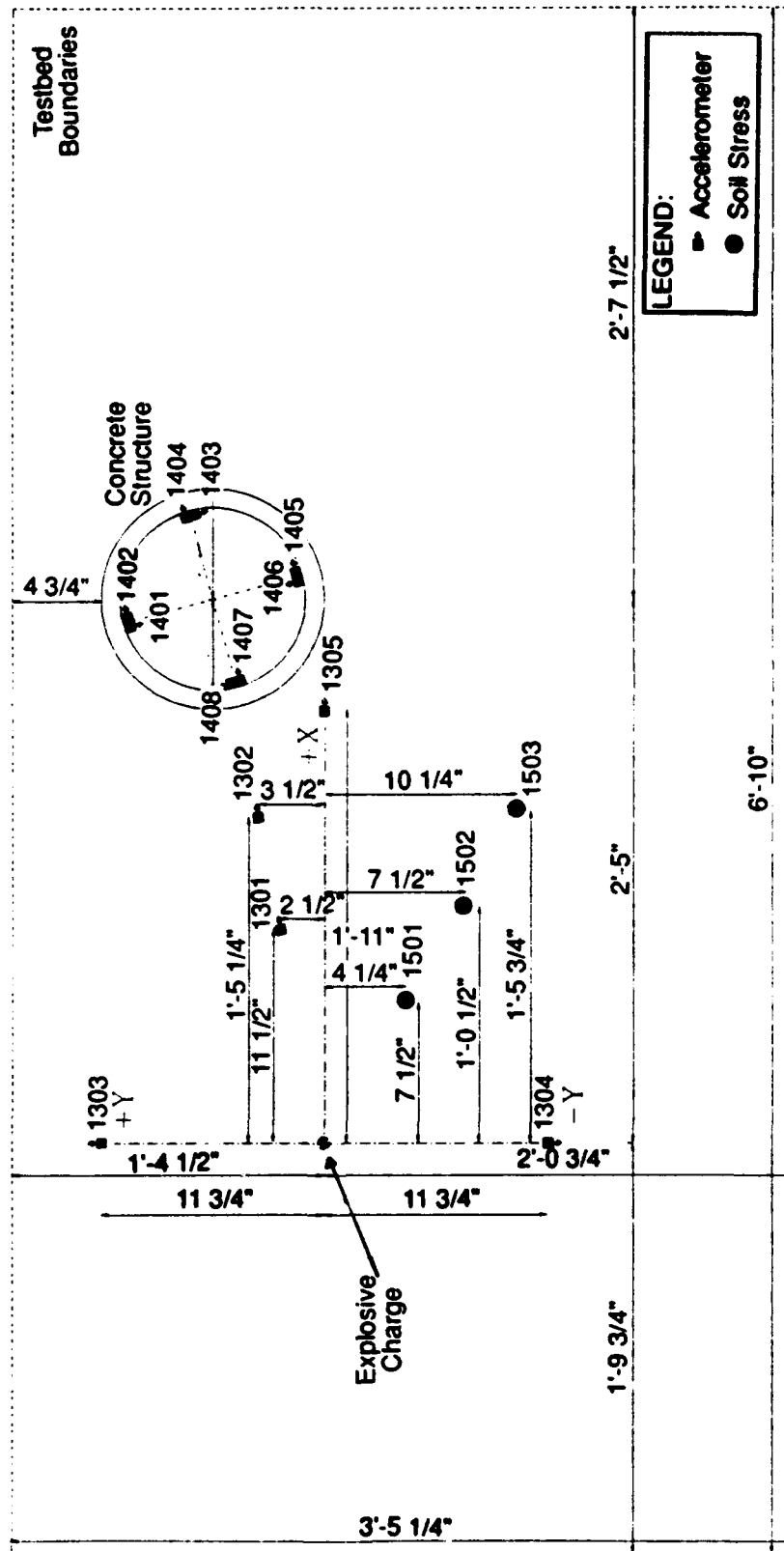
Figure 70. 1/10th Froude-Scale Testbed (Elevation View).
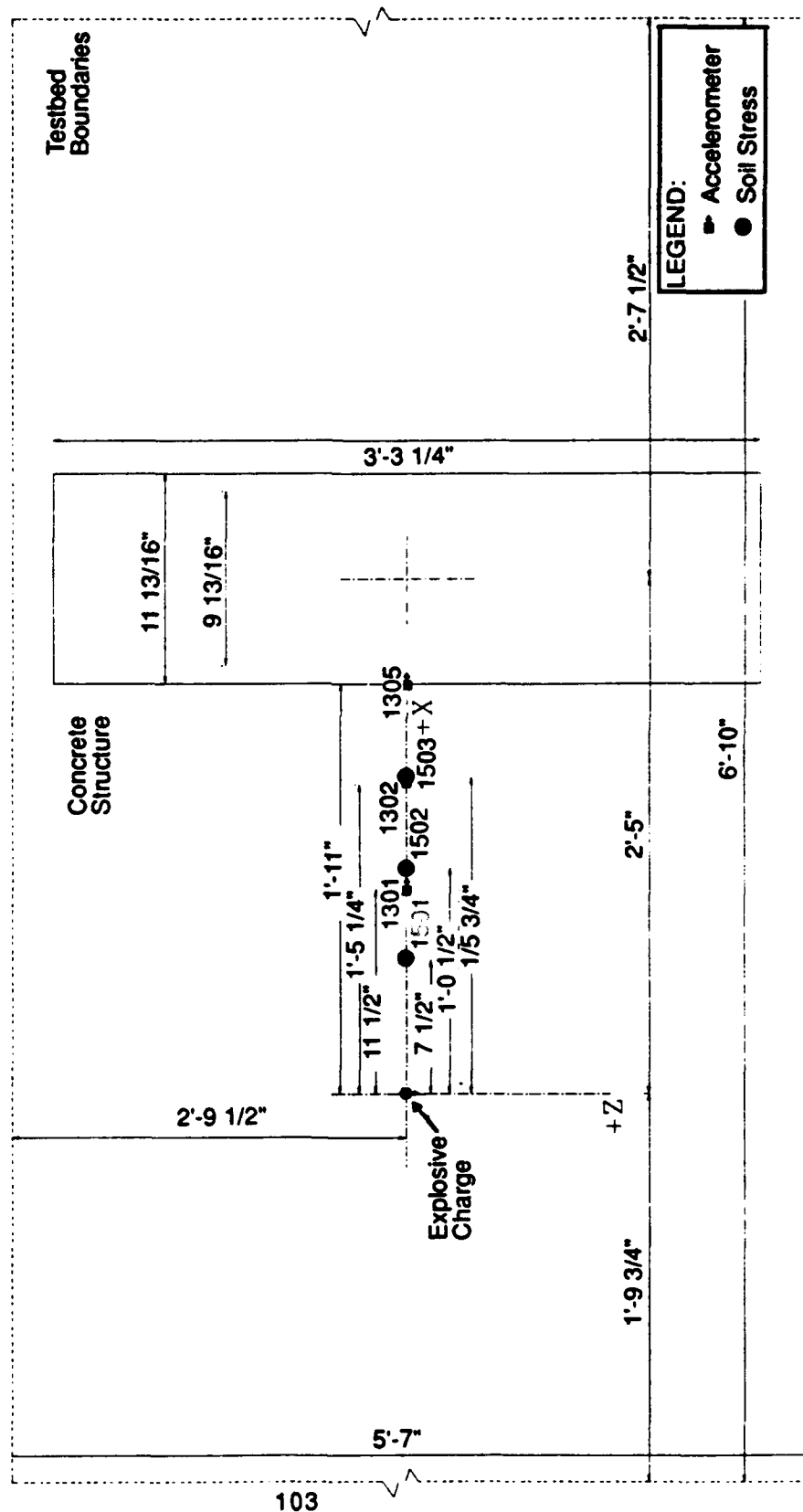
Figure 71. 1/10th Froude-Scale Testbed (Plan View).

3'-3 3/8"

SIDE VIEW

9 13/16"

10 13/16"

11 13/16"

1"

CONCRETE "GROUT"

REINFORCING STEEL MESH

Detail

0.500

0.500

0.041

END VIEW

5 29/32"

5 13/32"

4 29/32"
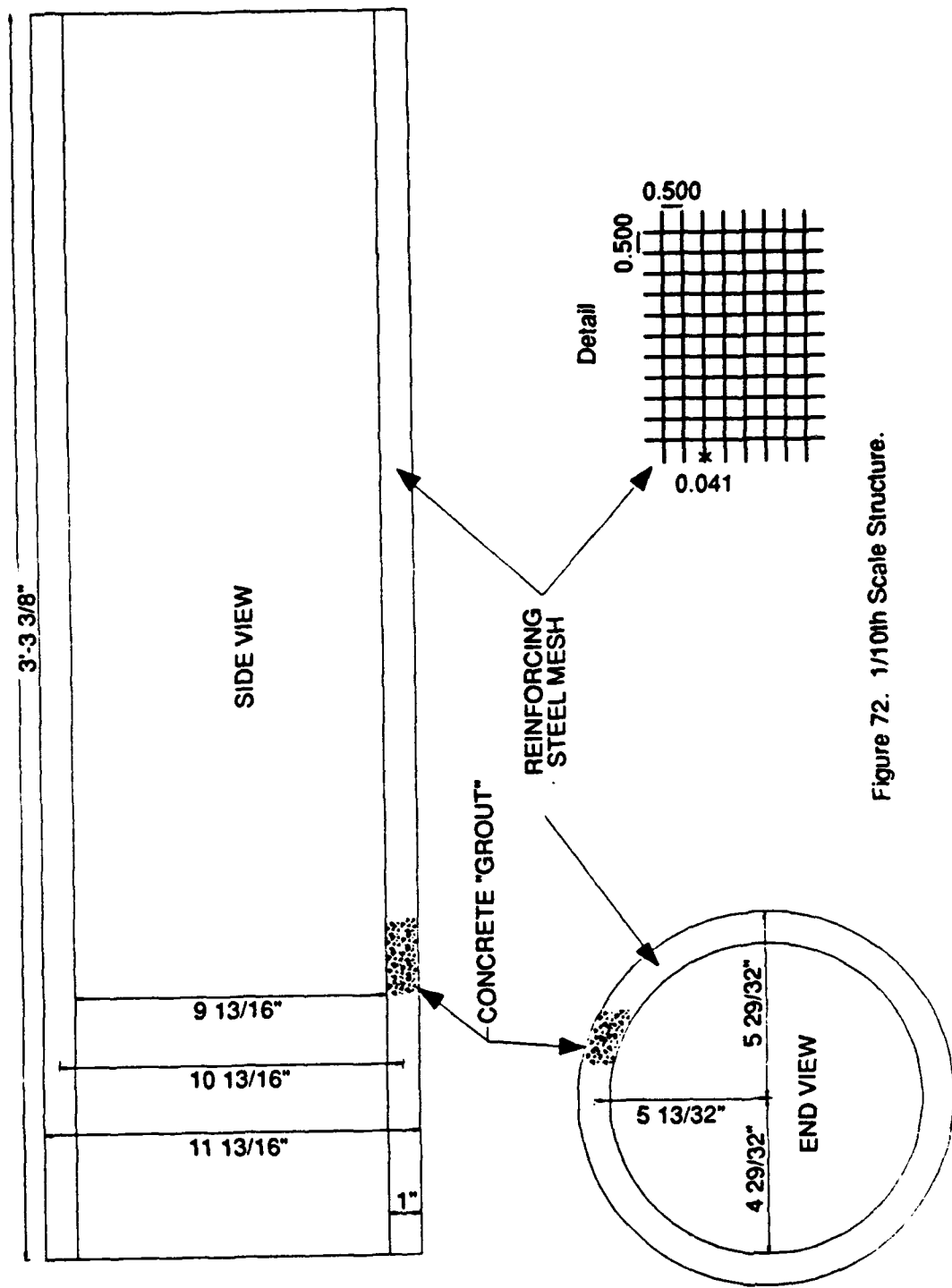
Figure 72. 1/10th Scale Structure.

Crushed coal and lead shot were mixed in the proportions of 60 percent lead and 40 percent coal by weight in a cement mixer as shown in Figure 73. This proportion can be expected to result in an average density for the mixture of 1880 kg/m^3 for a porosity of 0.34. Figure 74 shows the coal/lead mixture being placed into the test bed.

The size of the test bed required that the test bed be compacted by hand using a metal hand tamper. Figure 75 shows a stress gage being placed in the mixture and Figure 76 shows the test bed being constructed. Note the respiration masks worn by all personnel for safety precautions. Coal dust was everywhere!

The explosive charge, shown in Figure 77 consisted of a sphere of C-4, 0.039 kilograms in mass and having a radius of 18 mm. The charge was placed using the PVC pipe technique shown in Figure 78.

The completed test bed is shown in Figure 79 and Figure 80 depicts the test bed after detonation. The crater has a diameter of about 0.5 meter. Note the accelerometer and tubing which was ejected that were originally located just above the charge.

Table 15 is a summary of the measured values of the coal/lead mixture density of 1890 kg/m^3 and the recorded peak instrumentation values. The computed values of the mixture porosity is 0.34, the low stress wave propagation velocity of 84 m/s, and the constrained modules of 13.3 MPa.

Attenuation of peak values of acceleration, velocity and stress are presented in Figures 81-83. Figure 84 presents time-of-arrival as a function of range from which the wave propagation velocities can be computed.

Figure 85 and 86 again show that the data has a reasonable level of consistency, being similar after about 5 ms and well past the simulation time of 12.6 ms.

Detailed time history plots of all the data for this test are presented in Appendix E. Additional discussion of the results follows later in the section.
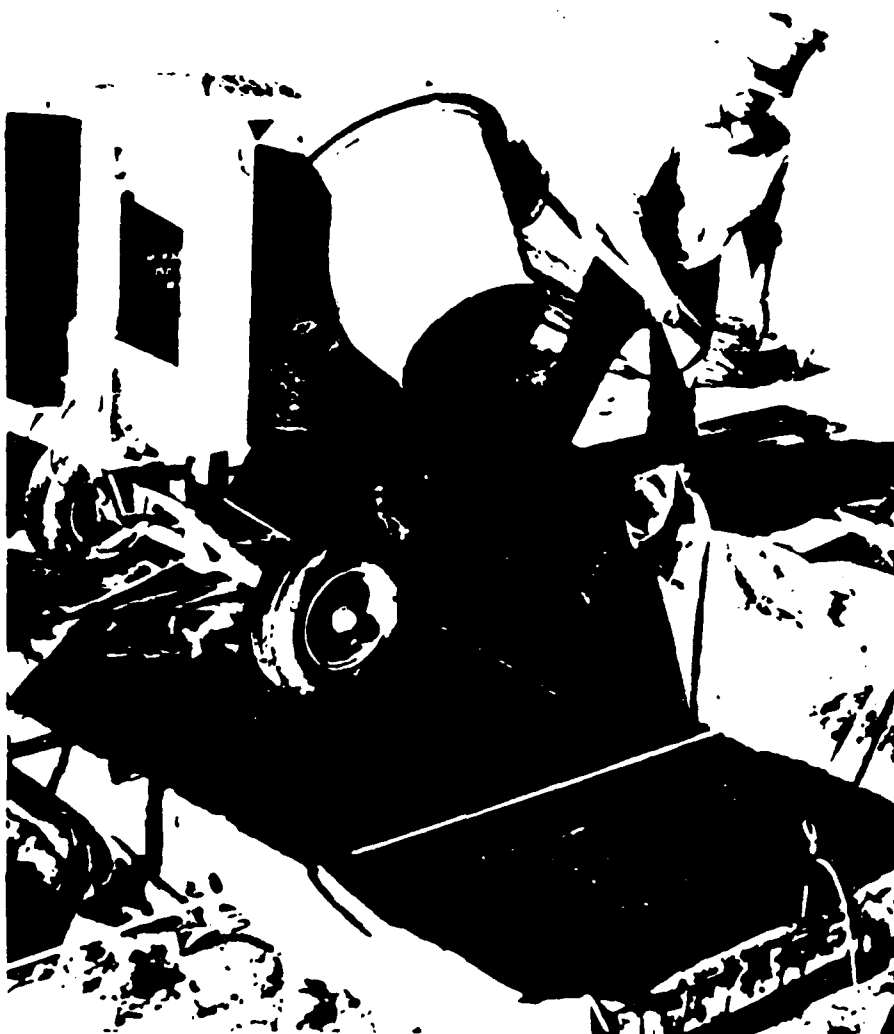
Figure 73. Mixing Lead and Coal.

Figure 74. Placing Lead/Coal Mixture into Testbed.

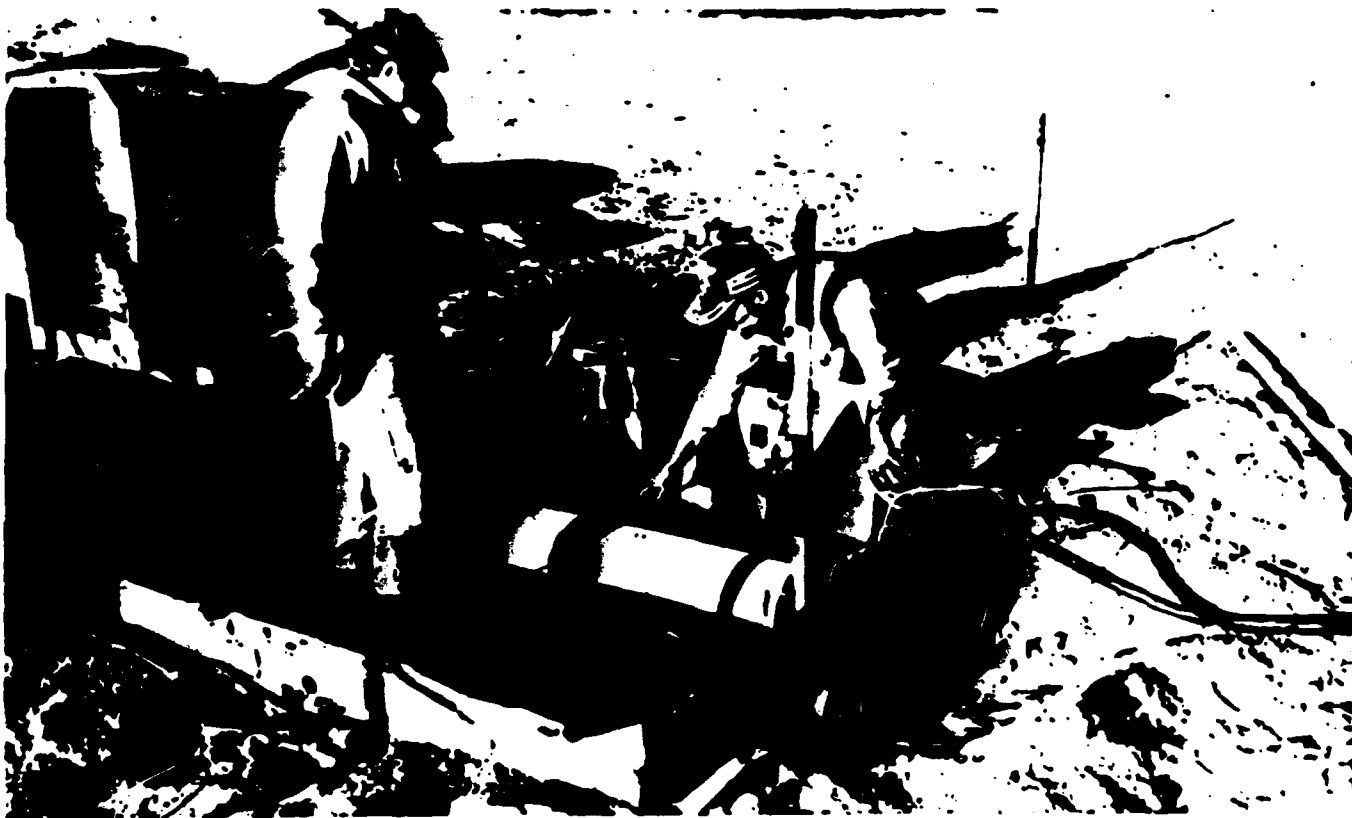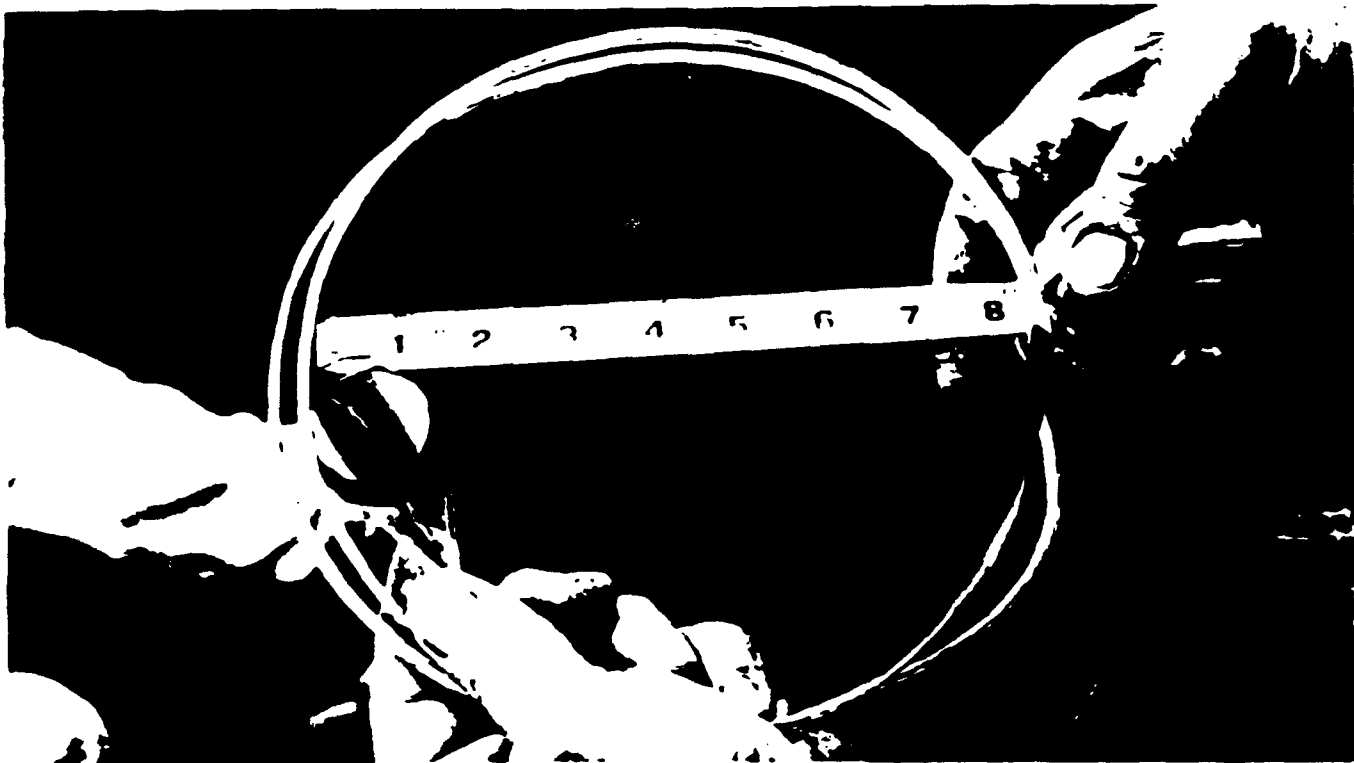Figure 75. Stress Gage Placement into Testbed.

Figure 76. Testbed Buildup.
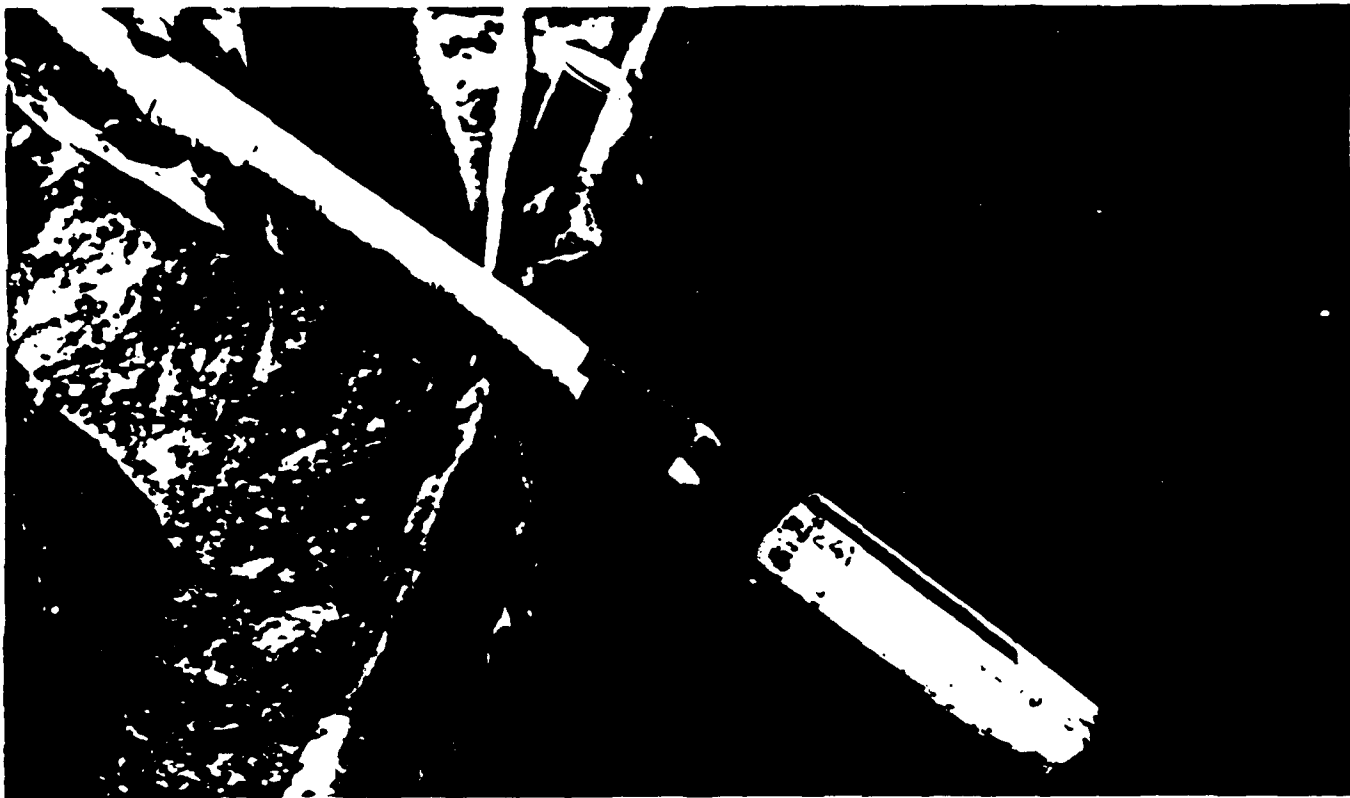
Figure 77. Charge for 1/10th Froude Scaled Test.

Figure 78. Charge Placement.

Figure 79. Completed Testbed.

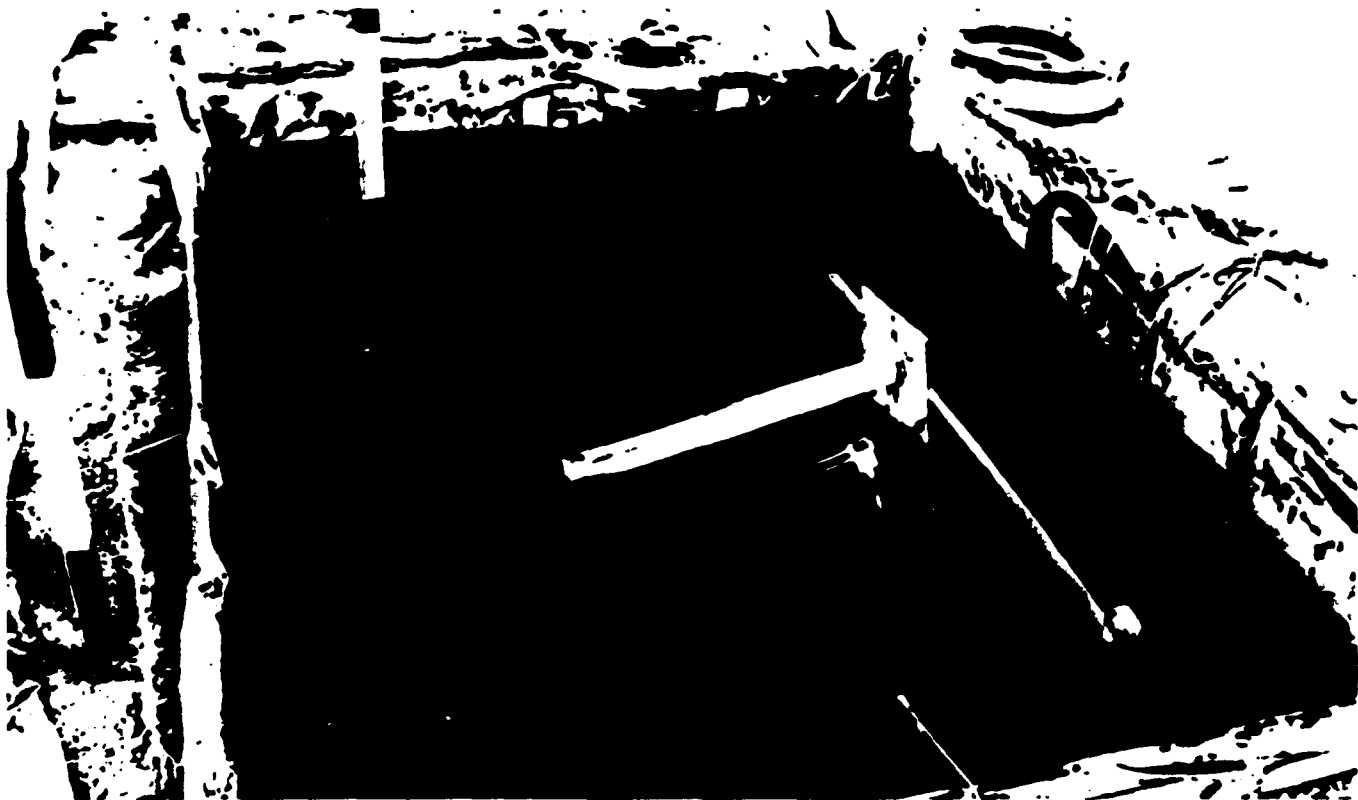
Figure 80. Posttest View of Testbed.

109

TABLE 15. SUMMARY OF 1/10 FROUDE-SCALED TEST RESULTS

Test Date: 1 November 1990

Test Bed Material: Lead/Coal Mixture
                    Measured Unit Weight = 118 lb/ft^3
                    Bulk Density = 1890 kg/m^3
                    n = 0.34, estimated

Explosive Charge: 0.039 kg of C4
                    Theoretical Energy Released, W = 0.21 MN·m

Free Field Data

Gage Number	Range, (m)	Time-of-arrival, t'(ms)	Acceleration, a(g)	Velocity, v (m/s)	Stress σ (MPa)
1501	0.225	.98	1000	3.5	1.45
1301	0.3	1.90	1800	4.1	
1303	0.3	1.52	2000	4.1	
1304	0.3	1.42			
1502	0.375	2.38	210	1.55	0.78
1302	0.45	3.82			
1503	0.525	3.98	150	1.01	0.44
1305	0.585	4.82			

Structural Data

1407	0.60	6.0	15.3	.31	
1402	0.75	6.5	13.6	.31	
1405	0.75	6.2	13.0	.37	
1404	0.90	7.0	14.1	.39	
1408	0.60	6.0	3	.0	
1401	0.75	6.5	4	.0	
1406	0.75	6.2	8	.0	
1403	0.90	7.0	14	.0	

Computed values: c = 84 m/s ρc^2 = 13.3 MPa
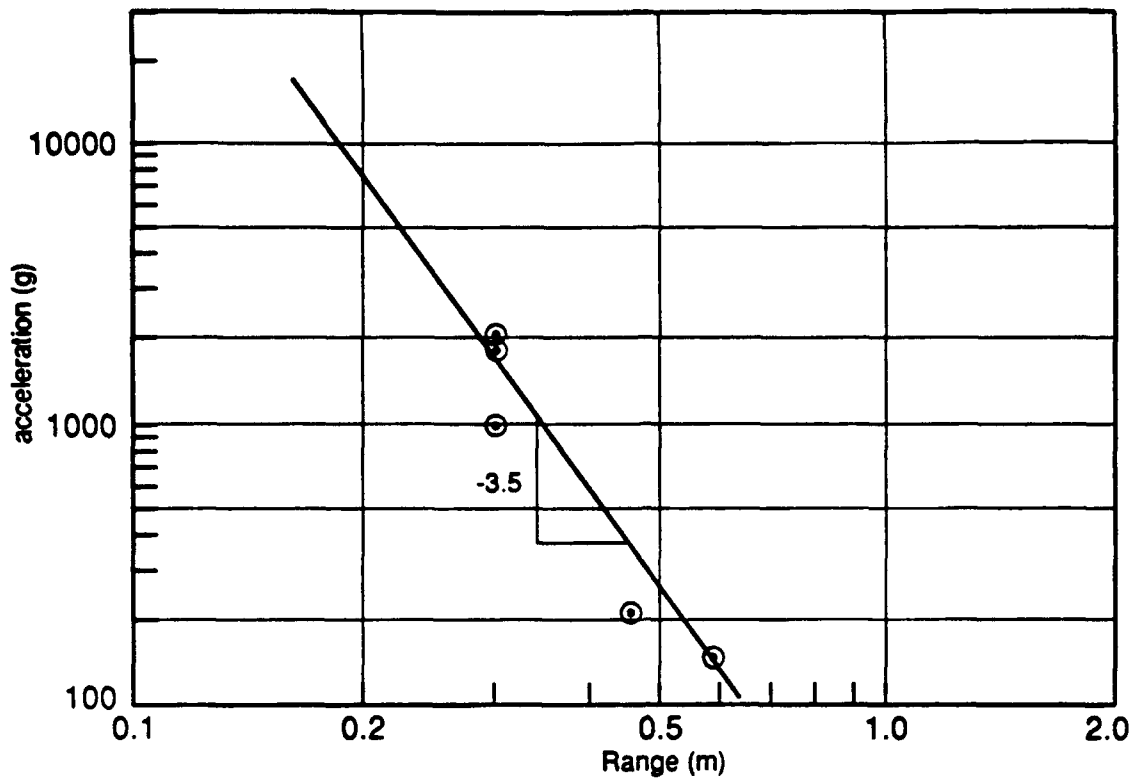
Figure 81. 1/10th Froude-Scaled Test, Attenuation of Acceleration with Range.
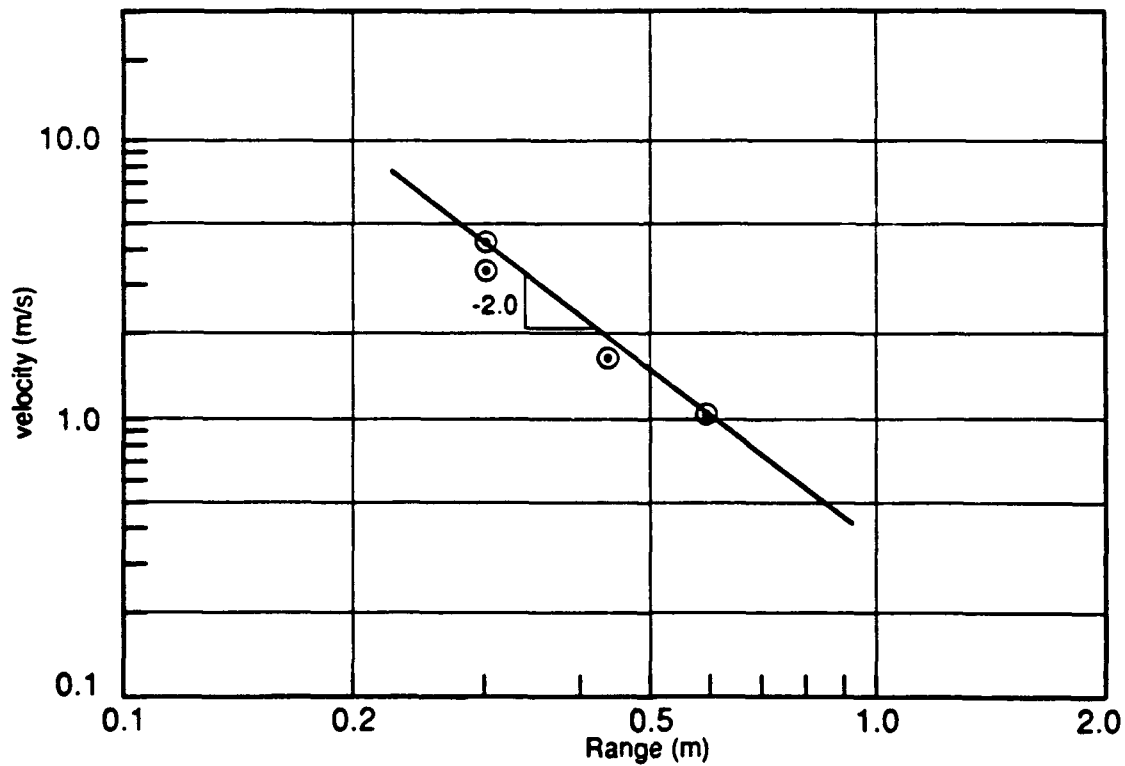

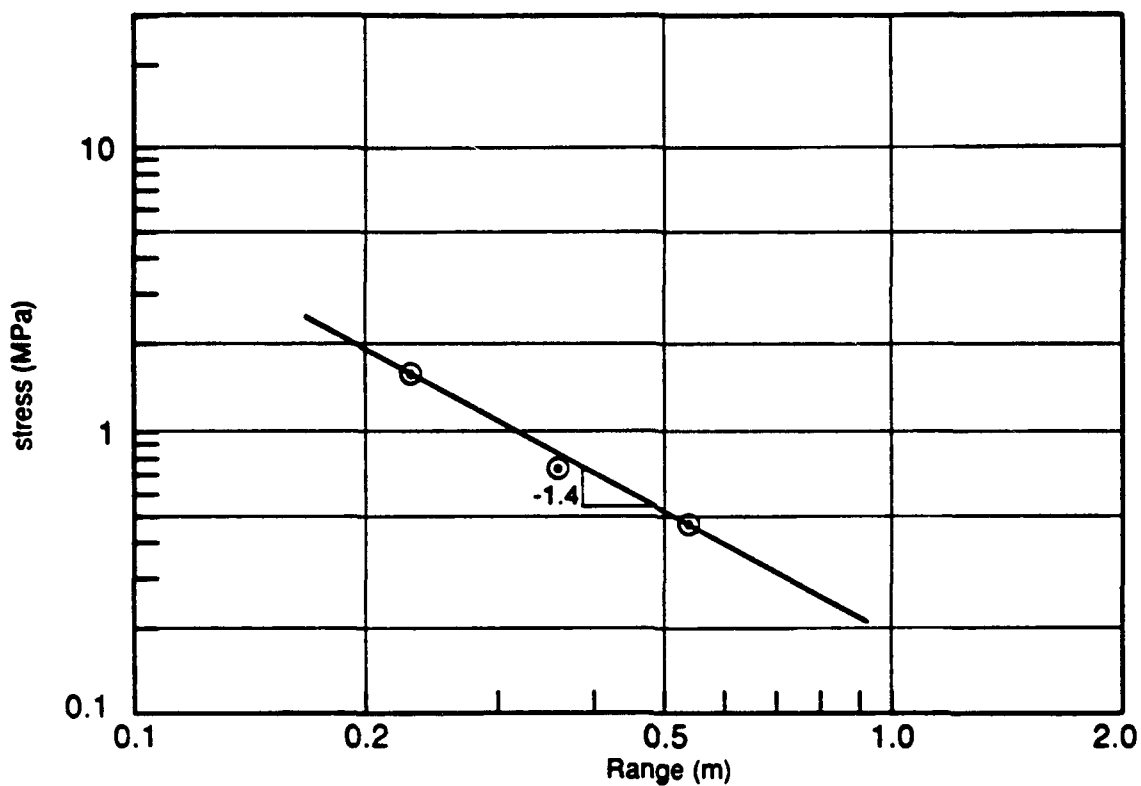Figure 82. 1/10th Froude-Scaled Test, Attenuation of Velocity with Range.

111

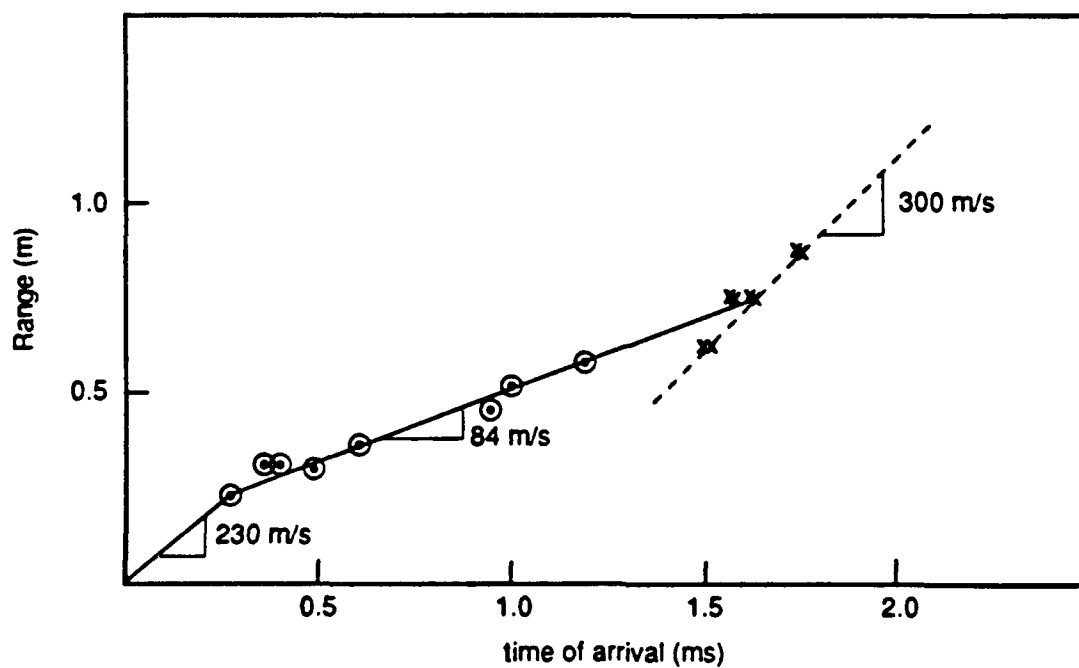Figure 83. 1/10th Froude-Scaled Test, Attenuation of Stress with Range.

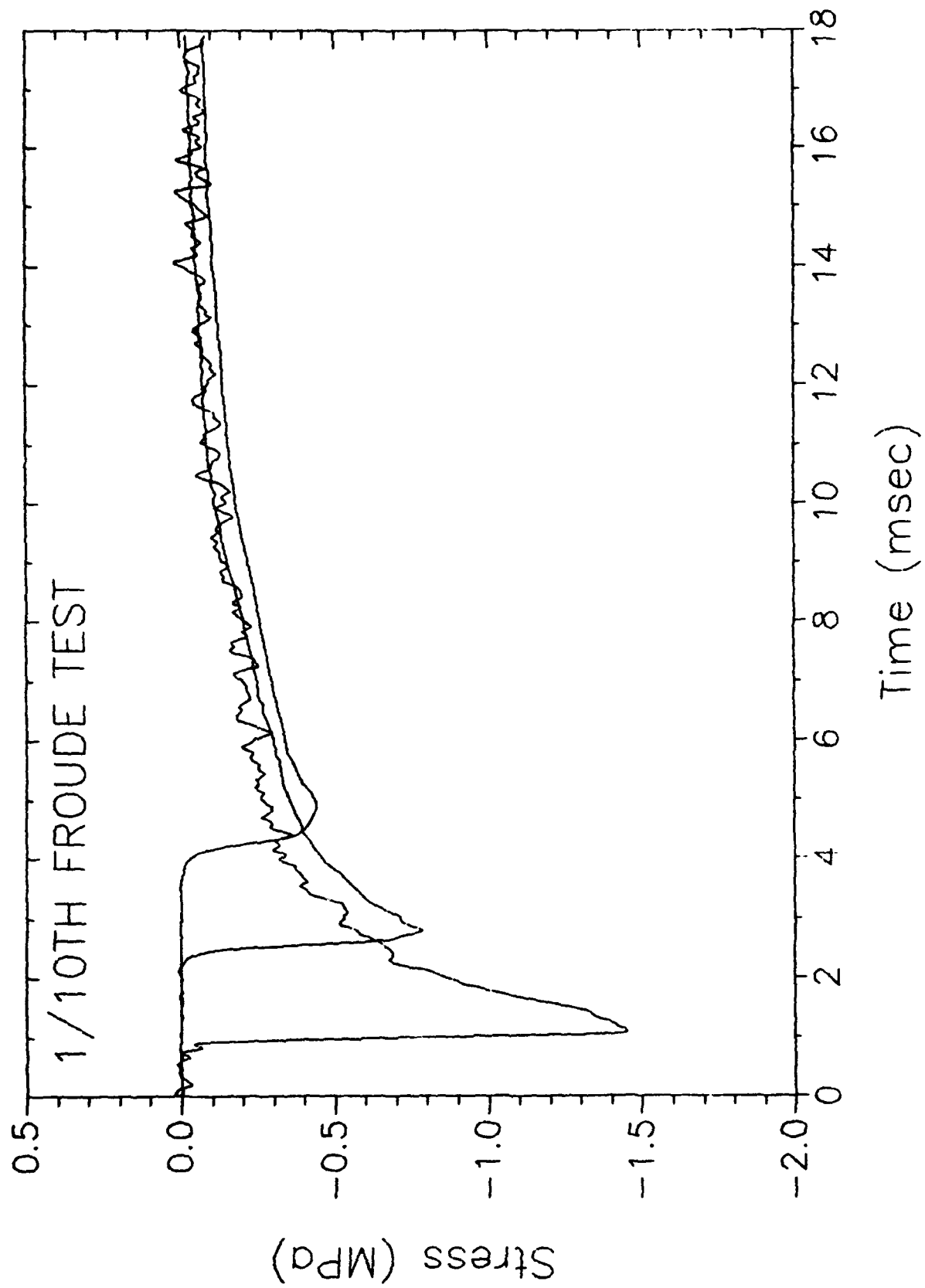Figure 84. 1/10th Froude-Scaled Test, Range vs. Time-of-arrival.

112

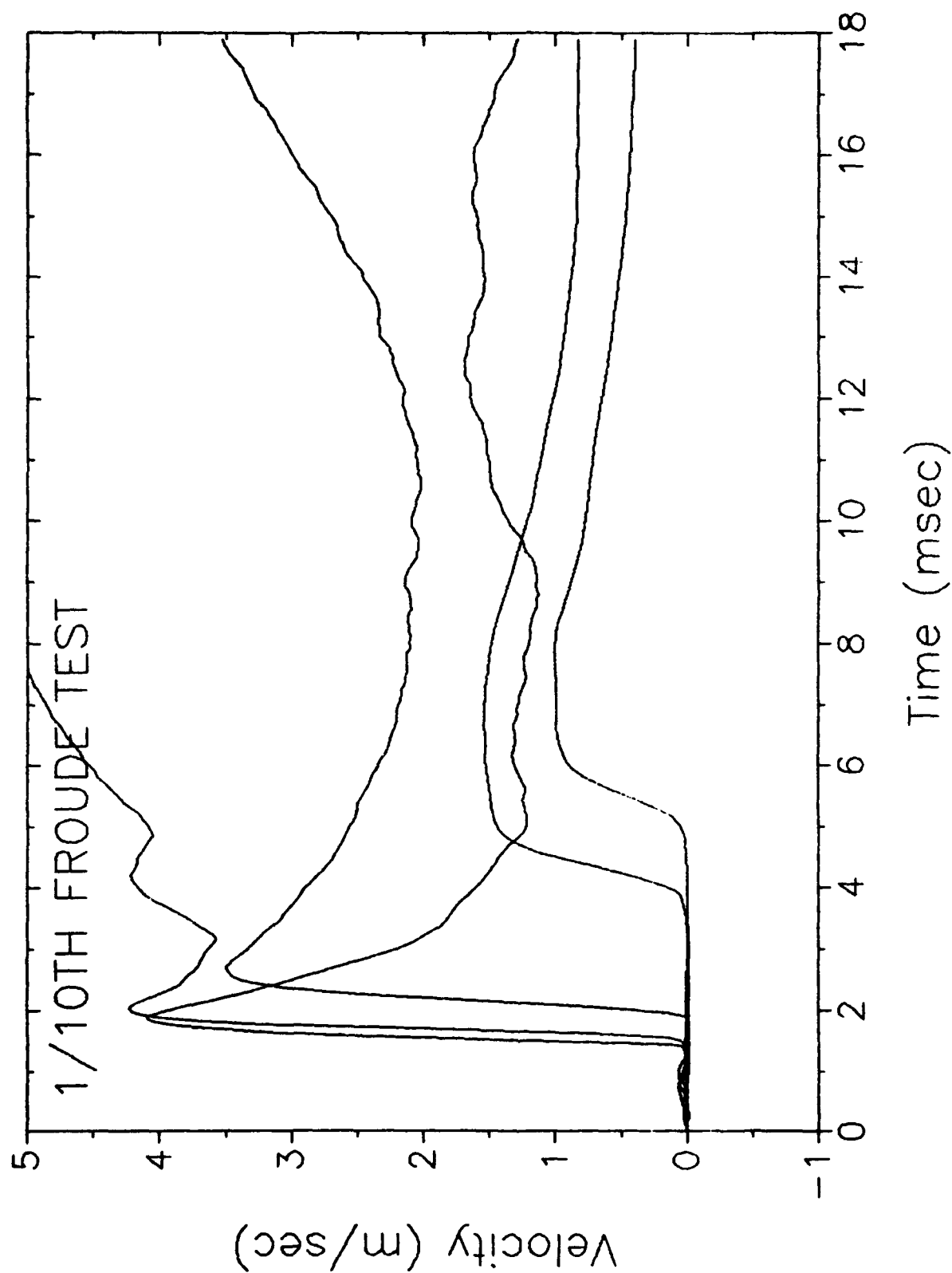Figure 85. Comparison of Free-Field Stress Waveforms.

113

Figure 86. Comparison of Free-Field Velocity Waveforms.

E. COMPARISONS OF TEST RESULTS

The objective of scale model testing was to obtain experimental information on models that can then be scaled to determine the desired information on larger prototype systems. Results of three scale model tests, (two Froude-scaled and one Replica-scaled) have been presented. These results have been scaled, nondimensionalized, and presented in Figures 87 through 90. If the scaling has been adequate, the results from all the tests should provide a single estimate for such parameters as variation of nondimensional peak acceleration, nondimensional peak velocity, nondimensional peak stress, and nondimensional time-of-arrival as a function of nondimensional range. Examination of Figures 87, 88 and 90 can lead to the conclusion that the spread of the data for acceleration, velo and time-of-arrival for the different tests could be of the same magnitude as that which would be expected from a single test thus validating both Replica scaling and Froude scaling for the free-field parameters measured and for the actual range of scales investigated. It does appear that the scaled stress data, Figure 89, would be best fit with two different curves, one passing through the Froude-scaled test data, another through the Replica-scaled data which would predict a much lower stress at a given range.

Comparison of the time histories of nondimensionalized acceleration in Figure 91, velocity in Figure 92, and stress in Figure 93 at common nondimensionalized ranges indicates good agreement among the three tests, (two were Froude-scaled and one Replica-scaled). Nondimensional time histories of all data are presented in Appendix F, while composite plots of nondimensional time histories are presented in Appendix G.

Tables 16 and 17 present the actual and nondimensional peak velocities of the structures tested in the three test events. The comparisons of the nondimensional radial (relative to the burst location) velocities show an average nondimensional value of 0.0048 with a variation of 15 percent on either side of the average value. The transverse bending velocities indicate that the 1/10 Replica-scaled test results and the 1/5 Froude-scaled results are in close agreement. The 1/10 Froude-scaled values for transverse bending velocity are smaller possibly because of the use of nonscaled concrete.

The observed difference in nondimensionalized peak stress as a function of range between the Froude-scaled tests and the Replica-scaled test, and the difference in the transverse bending structure velocity between the common value obtained in the 1/10 Replica test and 1/5 Froude test and the value obtained in the 1/10 Froude test may be explained by the failure to completely adhere to all the scaling laws. Strain rate and thermal effects are two parameters that were not considered in simulant material selection.
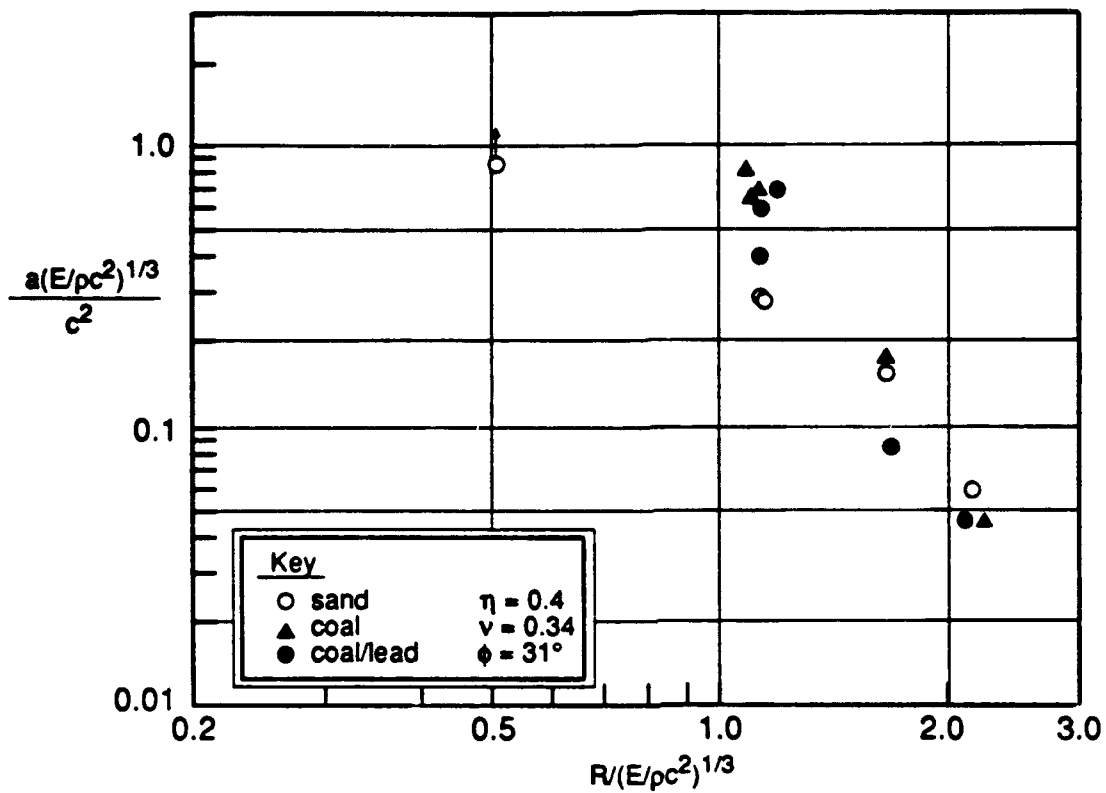
Figure 87. Nondimensional Acceleration vs. Nondimensional Range.
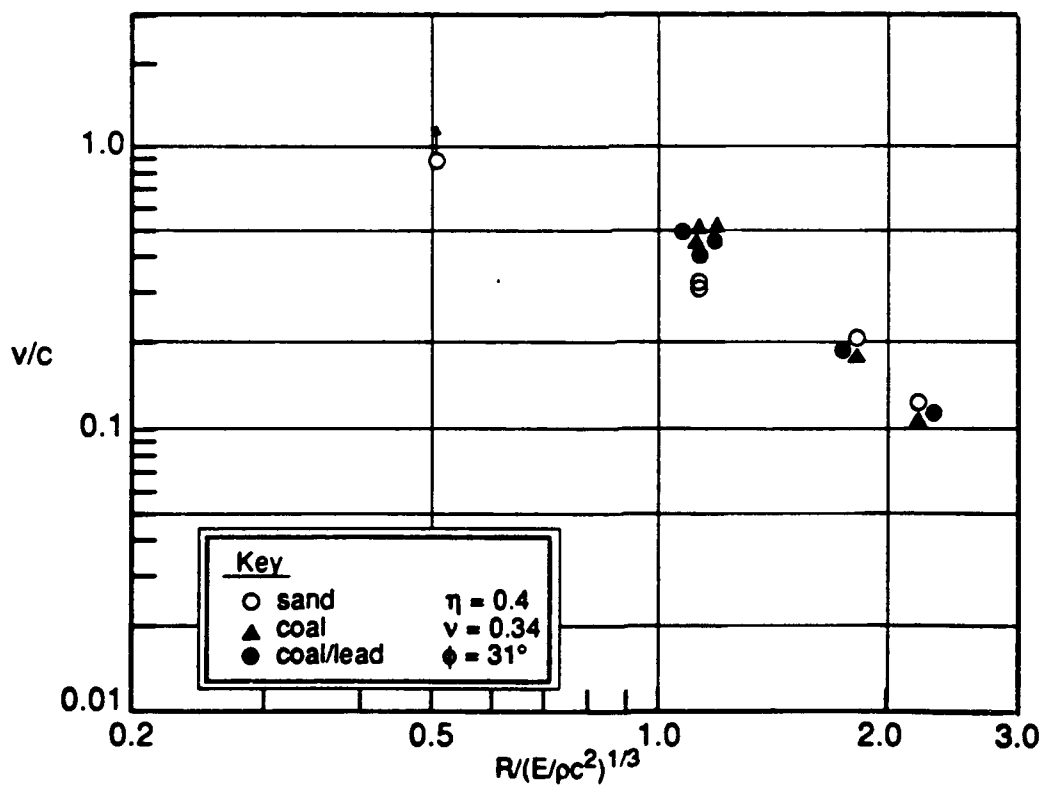
Figure 88. Nondimensional Velocity vs. Nondimensional Range.

116
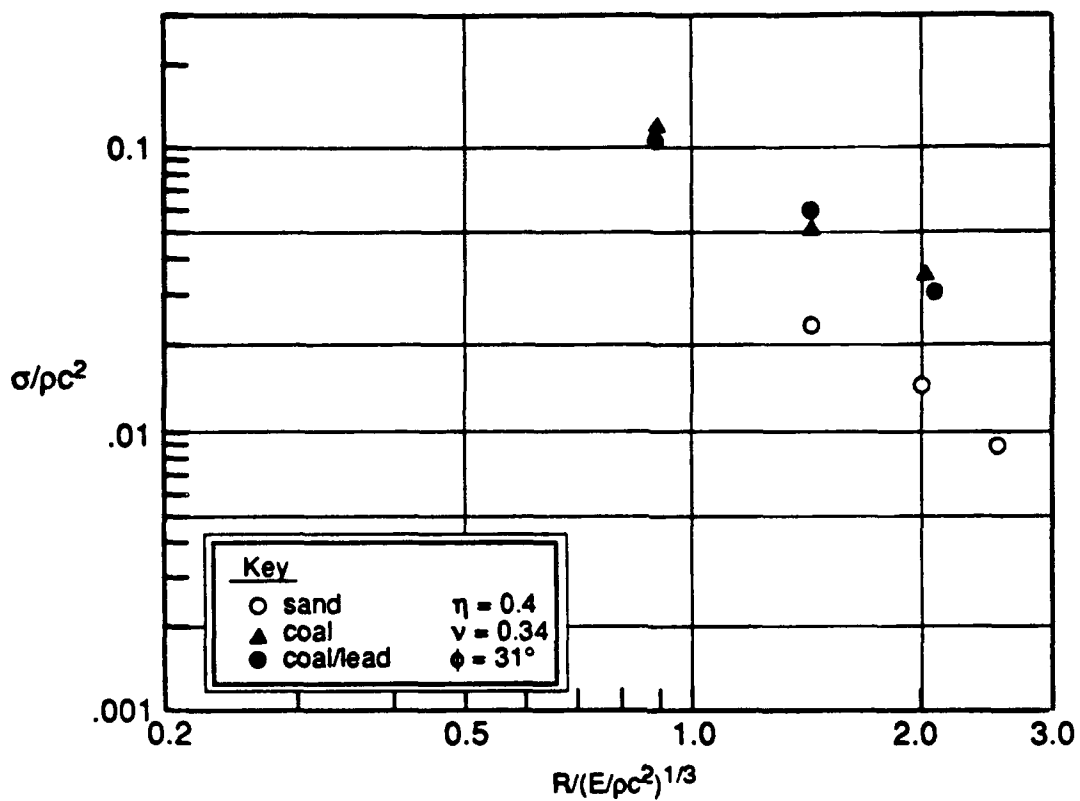
Figure 89. Nondimensional Stress vs. Nondimensional Range.
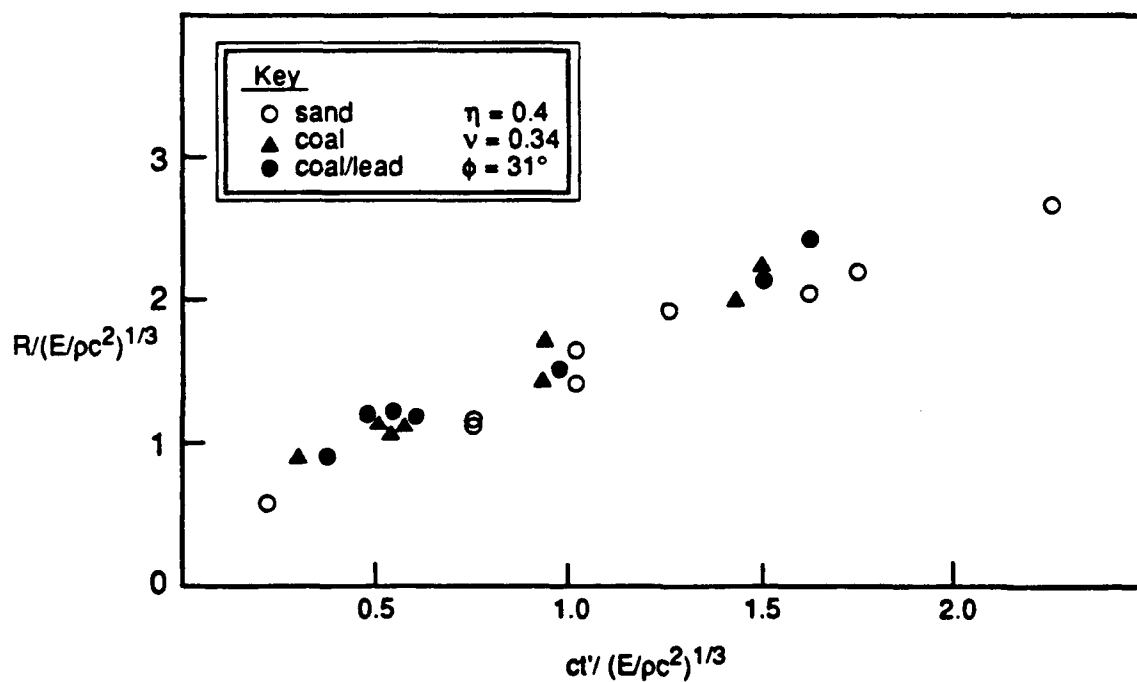
Figure 90. Nondimensional Range vs. Nondimensional Time of Arrival.

117

Figure 91. Comparison of Nondimensional Acceleration-time Waveforms at Same Nondimensional Range.

118
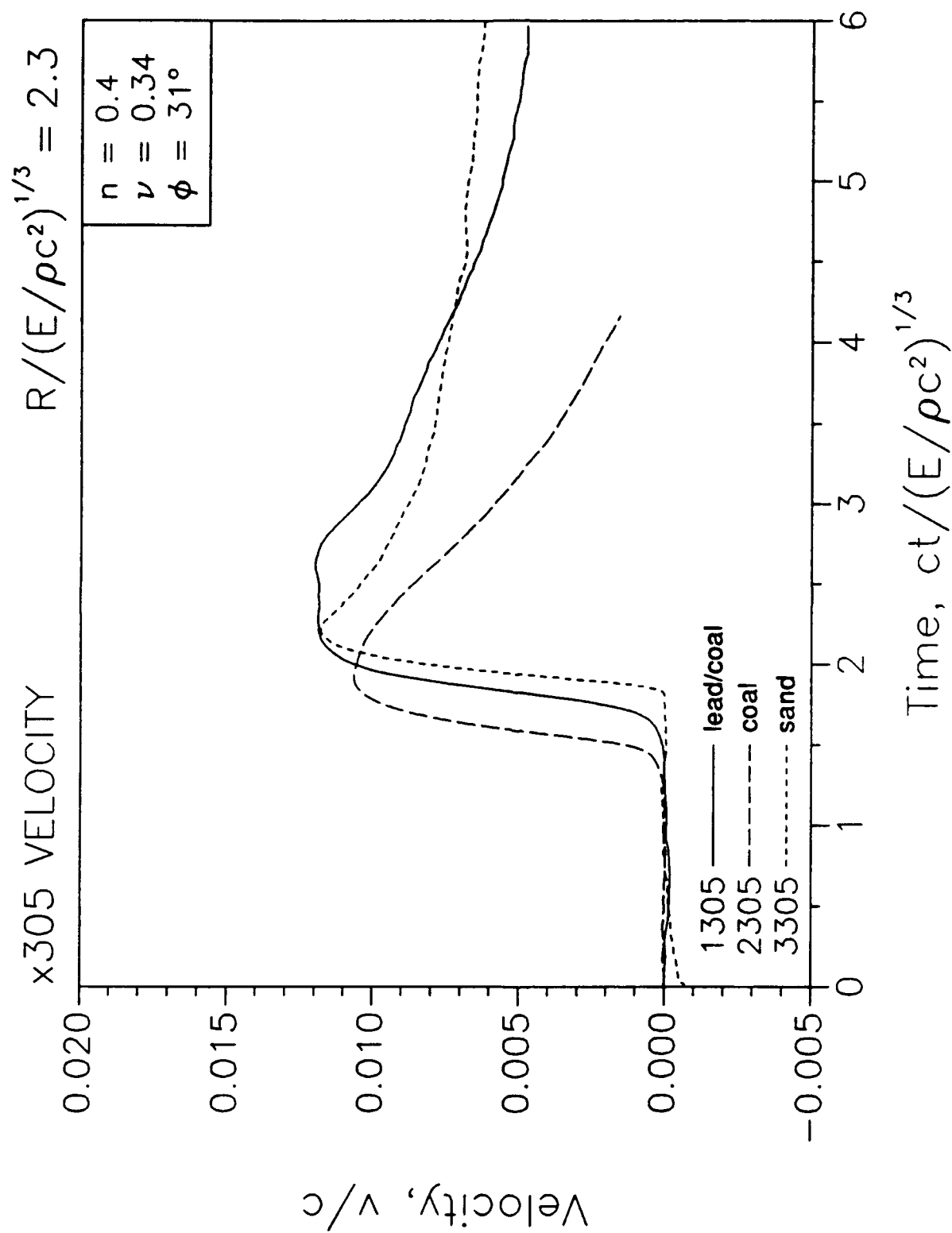
Figure 92. Comparison of Nondimensional Velocity-time Waveforms at Same Nondimensional Range.
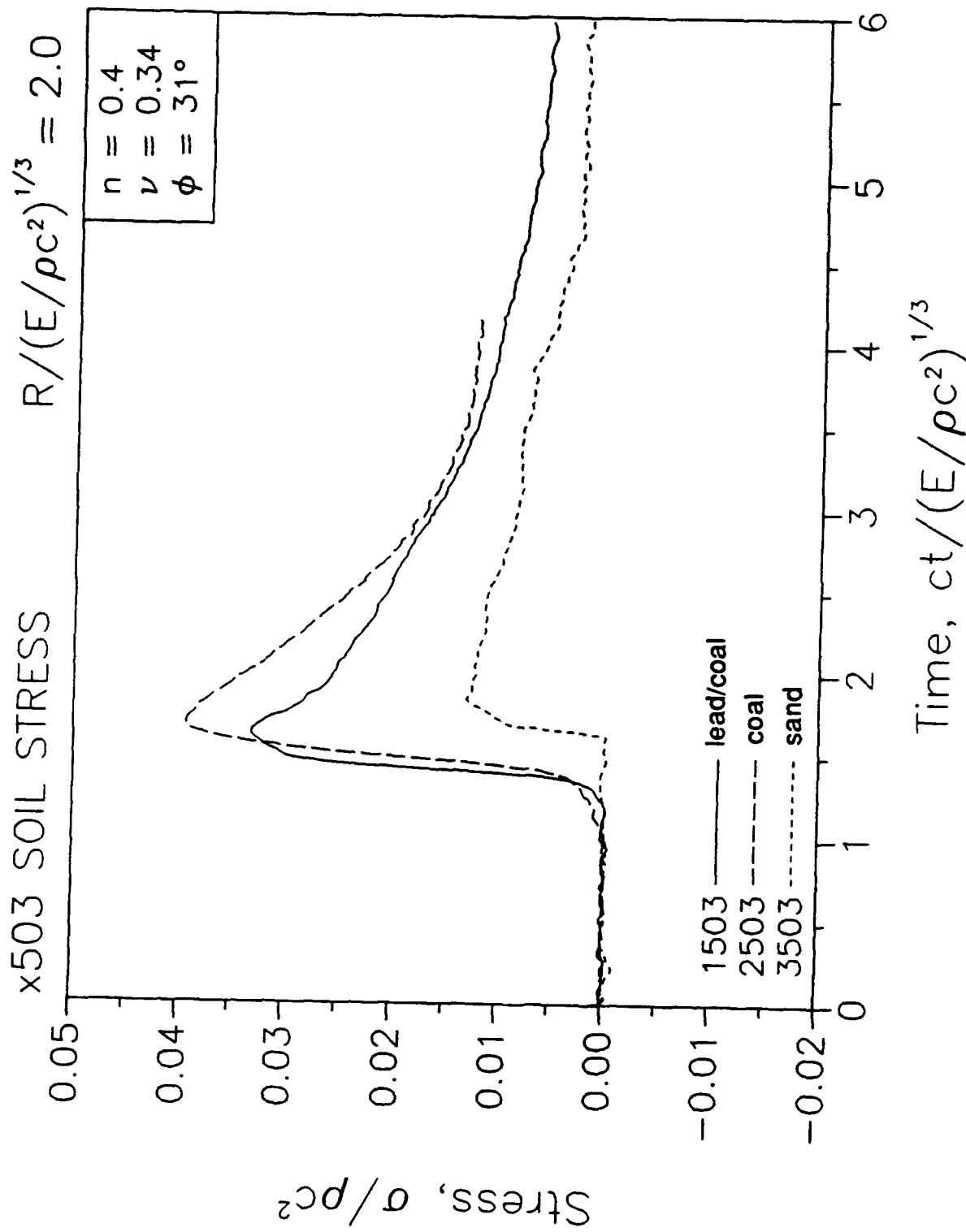
Figure 93. Comparison of Nondimensional Stress-time Waveforms at Same Nondimensional Range.

TABLE 16. MODEL STRUCTURE RADIAL RIGID BODY AND BENDING VELOCITY.

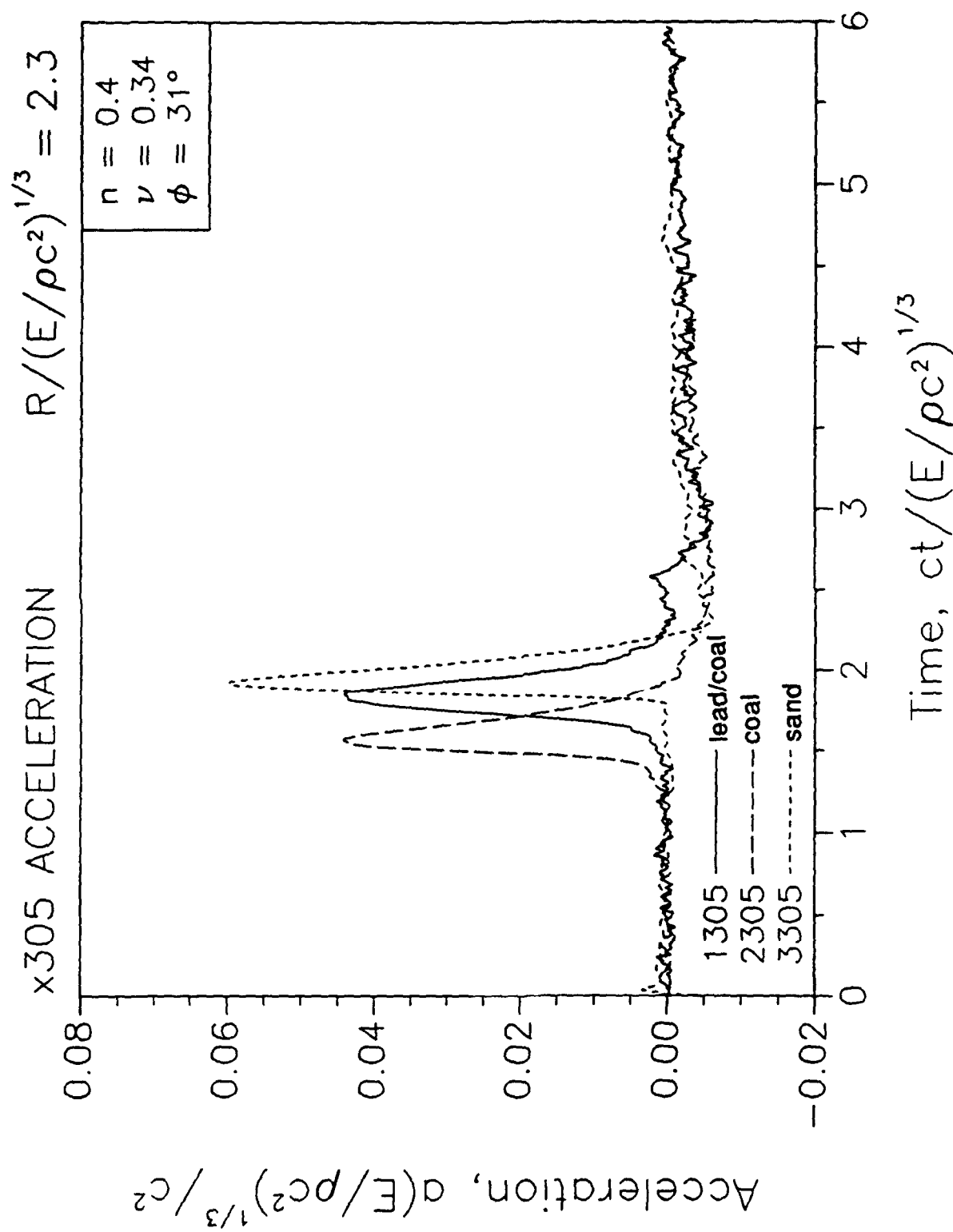| Radial Velocity	Test		
	1/10 Replica	1/5 Froude*	1/10 Froude **
Actual Values (m/s)	1.8	0.7	0.31
	1.6	0.6	0.37
	1.4	0.6	0.31
	1.2	0.45	0.39
Nondimensionalized by Soil/Simulant Properties (v/c)	0.0064	0.0058	0.0037
	0.0057	0.0050	0.0044
	0.0050	0.0050	0.0037
	0.0043	0.0038	0.0046

TABLE 17. MODEL STRUCTURE TRANSVERSE BENDING VELOCITY.

Bending Velocity	Test		
	1/10 Replica	1/5 Froude*	1/10 Froude **
Actual Values (m/s)	0.8	0.3	0.09
	1.0	--	0.05
Nondimensionalized by Soil/Simulant Properties (v/c)	0.0029	0.0025	.0011
	0.0035	--	.0006

*Mass and Bending stiffness approximately correct.
**Mass: 0.8X low and bending stiffness factor of 10X high for "exact" 1/10 Froude Scaling.

121

In the Replica-scaled test, the requirement that gravity be increased by the inverse of the scale factor was not followed. Failure to follow this requirement resulted in the stresses in the soil andstructure being less than the prototype. This distortion may have resulted in the observed lower stresses.

When damage to a small Replica-scaled structure is compared to damage to a full size structures loaded by Replica-scaled explosives the damage is less to the small structure. One possible explanation is that the stress reaching the smaller structure is lower than that which loads the larger structure. Other factors that do not scale such as strain rate effects could also explain some of the differences.

As noted previously, all of the structures were constructed of reinforced concrete. Froude scaling requires that the stiffness of the structure vary in the same manner as the stiffness of the soil simulant which was approximately 1/10. By adjusting the thickness of the 1/5 Froude-scaled structure by 1/2 of the proper value, the bending stiffness (which is proportional to the material stiffness and the thickness to the third power) was approximately correct. Thus, the reason for the agreement between the 1/10 Replica-scaled velocity and the 1/5 Froude-scaled velocity. The structure was ten times too stiff in bending (and hoop compression) although the mass was correct. This difference may explain the difference in velocity behavior .

It is apparent that other parameters were not precisely scaled in each of the tests. The inherently nondimensional parameters such as porosity, Poisson's ratio, and angle of internal friction could not be held constant among all three backfill materials as is required by either Replica or Froude scaling although they did match quite well. Also, some parameters such as strain rate cannot be scaled when using Replica or Froude scaling procedures.

The test configuration selected for the dynamic tests demonstrated that, for the range of scales investigated and the materials and simulants used, either Replica or Froude scaling will provide results that when nondimensionalized will predict nearly the same early time results. One obvious advantage of Froude scaling is that much smaller explosive charges can be used for a given scale factor. One obvious advantage of Replica scaling is that the same materials can be used in the model as in the prototype. For the case where gravity may become more important such as late time response or cratering phenomena, Froude scaling may be the preferred option.

SECTION VI
CONCLUSIONS AND RECOMMENDATIONS

A. CONCLUSIONS

Crushed coal can be used as a Froude-scaled simulant for sand. The density ratio of about 1/2 and stiffness ratio of about 1/10 leads to a length scale factor of about 1/5. The nondimensional values of initial porosity , Poission's ratio, and angle of internal friction for appropriately prepared coal and sand are very similar.

A mixture of crushed coal and lead can be used as simulant for sand. A small amount of lead shot by volume does not appreciably change the stiffness or nondimensional values of the coal. The lead, however, does increase the density. Length scale factors of about 1/10 can be obtained.

A combination of coal, lead, cement and water offers some promise for developing a Froude-scaled simulant for concrete.

The use of coal and a mixture of coal and lead as Froude-scaled simulants for sand leads to the same nondimensional results for the variation of stress at the tip of a cone penetrometer as a function of depth as was obtained from a full scale test in sand.

Comparison of the nondimensional dynamic response of the testbed and buried cylinder response from scaled tests involving 1/10 Replica-scaled, 1/5 Froude-scaled and 1/10 Froude-scaled parameters show considerable agreement among all the tests. The largest difference existed in nondimensional peak stress as a function of nondimensional range for the Replica test when compared with the two Froude tests. Peak scaled bending velocities of the buried structure in the transverse direction showed a wide variation. Both differences may be related to parameters that were not scaled or not scaled appropriately. Also the measurement of stress is difficult in dynamic tests. The crater size for the two Froude tests scaled while the Replica test crater size was much larger and did not scale.

Both Replica and Froude scaling of buried structure subjected to weapon effects offers cost effective means for investigating the response of prototype system. The choice of which scaling to use depends on the objectives of the test. Early time response of a structure where damage is of interest may be best investigated using Replica scaling. Later time response, cratering action or where elastic response is desired may be better addressed using Froude scaling.

B. RECOMMENDATIONS

A more thorough laboratory testing program defining the material properties of coal and coal/lead mixtures should allow for more precise simulant materials to be developed. The development of a simulant for concrete using coal, lead, cement, water and possibly other ingredients should be performed. Simulants for reinforcing steel should be developed so that failure of reinforced concrete structures may be addressed. Simulants for rock and clay and water should be developed to allow Froude scaling to be used for a wider variety of geologies.

Additional test programs should be developed that address the situations where the effects of gravity on the in situ earth stresses and strength and dead loads in the structure are important such as retaining walls and soil fabric systems. Deeply buried structures which have significant dead loading should be investigated using Froude scaling techniques.

Near surface protective system components such as foundations of aircraft shelters, floors and buried walls of C^3I facilities, and pavements subjected to cratering bursts could benefit from Froude-scaled tests.

The low velocity penetration of weapons into soil and structures could be investigated using Froude-scaled techniques.

The response of scaled structures to scaled earthquake motions could be investigated using Froude-scaled materials. The effects of gravity which are most important in the rocking frequency of structures and in the free fall accelerations of both structures and the earth material will be simulated. The current Replica scaling techniques severely distorts all gravity effects.

Coal could be investigated as a possible backfill material around protective structures. The low impedance of the material makes it a potential candidate for a energy absorbing material.

REFERENCES

1. Zahrah, T. F., Merkle, D. H., Auld, H. E., Gravity Effects in Small-Scale Structural Modeling, ESL-TR-88-57, Air Force Engineering and Services Laboratory, Tyndall Air Force Base, FL, December 1988.

2. Green, Mark L., Shear Friction Test Support Program. Report 1. Laboratory Test Results for WES Flume Sand Backfill, SL-86-20, Department of the Army Waterways Experiment Station, Corps of Engineers, Vicksburg, MS, September 1986.

3. Windham, J. E., Mechanical Property Recommendations for WES Flume Sand Backfill, Geomechanics Division, Structures Laboratory, U. S. Army Engineers Waterways Experiment Station, Vicksburg, MS, Revised 1990.

4. Modern Plastics Encyclopedia 88, Vol. 64, No. 10A., McGraw Hill, October 1987, .

5. Plastics Technology Manufacturing Handbook and Buyer's Guide 1988-89, Bill Communications, Inc., New York, August 1988, .

6. Shinn, James D., II, Smith, Elizabeth B., Timian, Steven M., McIntosh, Douglas E., Cone Penetration Investigation of the Misty Port III Test Site, DNA-TR-89-56, Defense Nuclear Agency, Washington, DC., January 1989.

7. Test Plan for the True Modeling of Gravity Test Series, Project 5582-4, Applied Research Associates, Inc., Lakewood, CO, 9 July 1990.

8. Dobratz, B. M., LLNL Explosive Handbook. Properties of Chemical Explosives and Explosive Simulants, Lawrence Livermore National Laboratory, Livermore, CA, 1981.

9. Drake, J. L.; Twisdale, L. A.; Frank, R. A.; Dass, W. C.; Rochefort, M. A.; Walker, R. E.; Britt, J. R.; Murphy, C. E.; Slawson, T. R.' Sues, R. H., Protective Construction Design Manual: Groundshock and Cratering (Section V), ESL-TR-87-57, Air Force Engineering and Services Laboratory, Tyndall AFB, Florida, November 1989.

10. Sweeney, B.P., and Clough, G.W., "Design of a Large Calibration Chamber," Geotechnical Testing Journal, GTJODJ, Vol. 13, No. 1, March 1990 pp. 36-44.